

BASIC HELICOPTER AERODYNAMICS

J. Seddon



BSP PROFESSIONAL BOOKS

Basic Helicopter Aerodynamics

Basic Helicopter Aerodynamics

An account of first principles in the fluid mechanics
and flight dynamics of the single rotor helicopter

J. Seddon

PhD, DSc, CEng, CFF, FRAeS

BSP PROFESSIONAL BOOKS

OXFORD LONDON EDINBURGH

BOSTON MELBOURNE

Copyright © J. Seddon 1990

All rights reserved. No part of this publication may be reproduced, stored in a retrieval system, or transmitted, in any form or by any means, electronic, mechanical, photocopying, recording or otherwise without the prior permission of the copyright owner.

First published 1990

British Library
Cataloguing in Publication Data
Seddon, J.
Basic helicopter aerodynamics.
1. Aircraft. Aerodynamics
I. Title
629.132'3

ISBN 0-632-02032-6

BSP Professional Books
A division of Blackwell Scientific
Publications Ltd
Editorial Offices:
Osney Mead, Oxford OX2 0EL
(Orders: Tel. 0865 240201)
8 John Street, London WC1N 2ES
23 Ainslie Place, Edinburgh EH3 6AJ
3 Cambridge Center, Suite 208, Cambridge,
MA 02142, USA
107 Barry Street, Carlton, Victoria 3053,
Australia

Set by Setrite Typesetters Limited
Printed and bound in Great Britain by
Mackays of Chatham plc, Chatham, Kent

Contents

<i>Preface</i>	ix
<i>Notation List</i>	xii
<i>Units</i>	xvi
<i>List of Abbreviations</i>	xviii
Chapter 1: Introduction	1
Chapter 2: Rotor in Vertical Flight: Momentum Theory and Wake Analysis	5
2.1 Momentum theory for hover	5
2.2 Figure of merit	8
2.3 Momentum theory for vertical climb	9
2.4 Vertical descent	11
2.5 Complete induced-velocity curve	13
2.6 Autorotation	14
2.7 Summary remarks on momentum theory	15
2.8 Complexity of real wake	16
2.9 Wake analysis methods	20
2.10 Ground effect	21
Chapter 3: Rotor in Vertical Flight: Blade Element Theory	23
3.1 Basic method	23
3.2 Thrust approximations	27

3.3	Non-uniform inflow	28
3.4	Ideal twist	29
3.5	Blade mean lift coefficient	31
3.6	Power approximations	32
3.7	Tip loss	34
3.8	Example of hover characteristics	35

Chapter 4: Rotor Mechanisms for Forward Flight

4.1	The edgewise rotor	37
4.2	Flapping motion	42
4.3	Rotor control	44
4.4	Equivalence of flapping and feathering	49

Chapter 5: Rotor Aerodynamics in Forward Flight

5.1	Momentum theory	51
5.2	Wake analysis	54
5.3	Blade element theory	55
5.3.1	Factors involved	55
5.3.2	Thrust	58
5.3.3	In-plane H force	60
5.3.4	Torque and power	61
5.3.5	Flapping coefficients	64
5.3.6	Typical numerical values	66

Chapter 6: Aerodynamic Design

6.1	Introductory	70
6.2	Blade section design	71
6.3	Blade tip shapes	76
6.4	Parasite drag	78
6.5	Rear fuselage upsweep	83
6.6	Higher harmonic control	87
6.7	Aerodynamic design process	88

Chapter 7: Performance		95
7.1	Introductory	95
7.2	Hover and vertical flight	97
7.3	Forward level flight	99
7.4	Climb in forward flight	102
7.5	Optimum speeds	103
7.6	Maximum level speed	103
7.7	Rotor limits envelope	105
7.8	Accurate performance prediction	106
7.9	A world speed record	107
7.10	Speculation on the really-low-drag helicopter	108
7.11	An exercise in high-altitude operation	113

Chapter 8: Trim, Stability and Control

Chapter 8: Trim, Stability and Control		117
8.1	Trim	117
8.2	Treatment of stability and control	121
8.3	Static stability	122
8.3.1	Incidence disturbance	123
8.3.2	Forward speed disturbance	124
8.3.3	Angular velocity disturbance	124
8.3.4	Sideslip disturbance	125
8.3.5	Yawing disturbance	125
8.3.6	General conclusion	125
8.4	Dynamic stability	125
8.4.1	Analytical process	125
8.4.2	Special case of hover	126
8.5	Hingeless rotor	127
8.6	Control	128
8.7	Autostabilization	130
<i>Index</i>		133

Preface

During the past decade and a half, several noteworthy textbooks have been published in the previously neglected field of helicopter aerodynamics, spurred no doubt by a growing acceptance worldwide of the importance of the helicopter in modern society. One may cite in this context Bramwell's *Helicopter Dynamics* (1976), Johnson's *Helicopter Theory* (1980) and *Rotary wing aerodynamics* (1984) by Stepniewski and Keys. The appearance now of another book on the subject requires some explanation, therefore. I have three specific reasons for writing it.

The first reason is one of brevity. Bramwell's book runs to 400 pages, that of Stepniewski and Keys to 600 and Johnson's extremely comprehensive treatment to over 1000. The users I have principally in mind are University or Polytechnic students taking a short course of lectures – say one year – in the subject, probably as an ‘optional’ or ‘elective’ in the final undergraduate or early post-graduate year. The object in that time is to provide them with a grounding while hopefully stimulating an interest which may carry them further in the subject at a later date. The amount of teaching material required for this purpose is only a fraction of that contained in the standard textbooks and a monograph of around 150 pages is more than sufficient to contain what is needed and hopefully may be produced at a price not beyond the individual student's pocket.

My second reason, which links with the first, concerns the type of approach. This book does not aim at a comprehensive treatment but neither is it content to consign problems to the digital computer at the earliest opportunity. In between lies an analytical route to solutions, taken far enough to produce results of usable accuracy for many practical purposes, while at the same time providing a physical understanding of the phenomena involved, which rapid recourse to the computer often fails to do. It is this route that the

book attempts to follow. The analytical approach is usually terminated when it is thought to have gone far enough to serve the stated purpose, the reader being left with a reference to one of the standard textbooks in case he should wish to pursue the topic further.

The third reason is one of content. Despite the need for brevity, I have thought it worthwhile to include, in addition to treatments of the standard topics – momentum theory, blade element theory, basic performance, stability and control – a strong flavour of research and development activity (Chapter 6) and of forward-looking, if speculative, calculations (Chapter 7). It might be considered that these items are of such a transitory nature as not to be suitable for a textbook, but my criterion of stimulating the student's interest is what has determined their inclusion. Certainly they have proved to be interesting in classroom presentation and there seems no reason why that should not be so for the written word.

In addition to meeting the needs of students, to whom it is primarily addressed, the book should have an appeal as background material to short courses held in or on behalf of industry: such courses are increasing in popularity. Companies and research establishments may also find it useful for new entrants and for more established workers requiring a 'refresher' text.

Reverting to the matter of brevity, the recent publication *Helicopter Aerodynamics* by Prouty is a most admirable short exposition, well worth studying as an adjunct to any other textbook: however it shuns the mathematics completely and therefore will not suffice alone for the present purposes. Saunders' *Dynamics of Helicopter Flight* is not greatly beyond the target length but as the title implies it is concerned more with flight dynamics than with aerodynamics and is adapted more to the needs of pilots than to those of engineering students already equipped with a general aerodynamic background.

I have taken it as a starting point that my readers have a knowledge of the aerodynamics of lifting wings as they exist in fixed-wing aircraft. A helicopter rotor blade performs the same function as a lifting wing but in a very different environment; and to note the similarities on the one hand and the distinctions on the other can be a considerable fillip to the learner's interest, one which I have tried to nurture by frequent references back to fixed-wing situations. This again is a somewhat non-standard approach. Substantial omissions from the book are not hard to find. A

historical survey might have been included in Chapter 1 but was thought not necessary despite its undoubtedly interest. To judge by the work effort it attracts, wake analysis ('Vortex theory') deserves a more extensive treatment than it gets (Chapters 2 and 5) but here it was necessary to refrain from opening a Pandora's box of different approaches. Among topics which could have been included in Chapter 5 are autorotation in forward flight, pitch-flap coupling and blade flexibility but these were seen as marginally 'second-line' topics. The forward look in Chapter 6 might have contained a discussion of the potential of circulation control, the only system which is capable of attacking all the three non-uniformities of rotor blade flow, chordwise, spanwise and azimuthal; but the subject is too big and too distinct from the main line of treatment. The reference to autostabilization in Chapter 8 is brief in the extreme but again the choice was between this and a much lengthier exposition in which aerodynamics would have been largely submerged beneath system mechanics and electronics.

In compiling the book I have been greatly helped by discussions with Mr D.E.H. ('Dave') Balmford, Head of Advanced Engineering at Westland Helicopters, to whom my thanks are expressed. Other Westland staff members whose assistance I wish to acknowledge in specific contexts are Dr M.V. Lowson (now Professor of Aerospace Engineering at Bristol University) for Section 7.10, Mr F.J. Perry for Section 6.6, Mr R.V. Smith for Section 7.11 and Mr B. Pitkin for Chapter 8. Naturally the standard textbooks, particularly those mentioned earlier, have been invaluable in places and I trust that this fact is duly recognized in the text and diagrams.

Formal acknowledgement is made to Westland Helicopters for permission to reproduce the photographs at Figs 2.11, 4.10, 4.11, 7.6 and 7.7; to Edward Arnold, Publishers, for the use of Figs 2.10, 2.13, 5.1, 5.3, 6.3, 8.5 and 8.6 from A.R.S. Bramwell's book *Helicopter Dynamics* (1976); to Mr P.G. Wilby of the Royal Aircraft Establishment for Figs 6.2 and 6.5, which are reproduced with the permission of the Controller of Her Majesty's Stationery Office; and to Dr J.P. Jones for the use of Figs 2.12, 4.2 and 4.4.

My thanks are due to Molly Gibbs of Bristol University who copy-typed the manuscript and to my grandson Daniel Cowley who drew the figures.

Notation List

General

a	lift curve slope $dC_L/d\alpha$
a_0	first term in Fourier expansion of β
a_1	coefficient of second term in Fourier expansion of β
a_2	coefficient of fourth term in Fourier expansion of β
A	area of rotor disc
A_b	total blade area (N blades)
A_1	coefficient of second term in Fourier expansion of θ
A_2	coefficient of fourth term in Fourier expansion of θ
A_p	projected frontal area of rotorhead (Chapter 6)
A_s	flow spoiling factor (Chapter 6)
A_z	boundary layer shielding factor (Chapter 6)
b_1	coefficient of third term in Fourier expansion of β
b_2	coefficient of fifth term in Fourier expansion of β
B	tip loss factor in $r = BR$
B_1	coefficient of third term in Fourier expansion of θ
B_2	coefficient of fifth term in Fourier expansion of θ
c	blade chord
C_D	drag coefficient
C_L	lift coefficient
C_H	H -force coefficient
C_P	power coefficient
C_Q	torque coefficient
C_T	thrust coefficient
d	differential operator

D	aerodynamic drag
e	hinge offset ratio
f	equivalent flat-plate area
H	H -force
I	moment of inertia
k	empirical constant in expression for profile power
K	empirical constant in Glauert expression for induced velocity
ℓ	moment arm of tail rotor thrust about main shaft
L	aerodynamic lift
m	blade mass per unit span
M	figure of merit
M	Mach number
M	moment (Figs. 8.4, 8.5)
M_T	aerodynamic moment about flapping axis
n	inertia number (Chapter 8)
N	number of blades
p	static pressure
P	power
q	torque coefficient (Bramwell definition)
q	dynamic pressure, $\frac{1}{2}\rho V^2$
Q	torque
r	fraction of blade span from axis ($= y/R$)
R	blade radius
S	stiffness number
t_c	thrust coefficient (Bramwell definition)
T	thrust
u	component velocity (non-dimensional, $U/\Omega R$)
U	component velocity (dimensional)
v	induced velocity
V	stream velocity (flight speed)
V'	hypothetical velocity in Glauert formula for forward flight
V_c	climbing speed
w	disc loading, T/A

<i>W</i>	aircraft weight
<i>y</i>	distance along blade span from axis
<i>z</i>	height of rotor plane above ground

Greek

α	incidence (angle of attack) of blade, positive nose-up
α	incidence of fuselage (Chapter 6), positive nose-up
α_t	angle of attack of tip path plane to flight direction, positive nose-down
β	flapping angle (blade span to reference plane)
β	compressibility factor $\sqrt{1-M^2}$ (Chapter 6)
γ	Lock number
δ	relative density of air, ρ/ρ_0
Δ	prefix denoting increment, thus ΔP
θ	blade pitch angle
κ	empirical constant in expression for induced power
λ	inflow factor (non-dimensional induced velocity)
λ	blade natural flapping frequency (Chapter 8)
μ	advance ratio, $V/\Omega R$
π	pi
ρ	absolute density of air
σ	blade solidity factor
ϕ	angle of resultant velocity at blade to reference plane
ψ	angle of azimuth in blade rotation
Ω	blade rotational speed, radians per sec

Suffixes

<i>av</i>	available
<i>b</i>	blade
<i>c</i>	suffix for thrust coefficient (Bramwell definition)
<i>C</i>	in climb
<i>D</i>	drag
<i>h</i>	hover value

<i>H</i>	<i>H</i> -force
<i>i</i>	induced
<i>L</i>	lift
max	maximum
<i>o</i>	basic or constant value
<i>p</i>	parasite
<i>P</i>	power
<i>Q</i>	torque
req	required
<i>t</i>	blade tip
tw	blade twist
<i>T</i>	thrust
∞	conditions ‘at infinity’, i.e. where flow is undisturbed

Units

The metric system is taken as fundamental, this being the educational basis in the UK. Imperial units are still used extensively, however, particularly in the USA but also by industry and other organizations in the UK. For dimensional examples in the text and diagrams, therefore, those units are used which it is felt have stood the test of time and may well continue to do so. Often units in both systems are quoted: in other cases reference may need to be made to the conversion tables set out below. In either system, units other than the basic one are sometimes used, depending on the context; this is particularly so for velocity, where for example aircraft flight speed is more conveniently expressed in kilometres/hour or in knots than in metres/second or in feet/second. The varieties used in the book are included in the table.

Quantity	Metric unit and symbol	Imperial equivalent
<i>Primary quantities</i>		
Mass	kilogram (kg)	0.0685 slug
Weight	newton (N)	0.2248 pound (lb)
Length	metre (m)	3.281 feet (ft)
Time	second (s)	1.0 second (sec)
Temperature	kelvin (K)	Celsius ($^{\circ}$ C) $\text{Temp}(K) = \text{temp} (^{\circ}\text{C}) + 273.15$
<i>Derived quantities</i>		
Weight (force)	kilogram force 9.807 N (kG)	2.2046 lb 0.00194 slug/ ft^3
Density	kg/m^3	
Pressure	N/m^2 0.1020 kG/m ²	0.0209 lb/ ft^2
Velocity	m/s 3.600 km/h	3.281 ft/sec 196.86 ft/min 1.941 knots
Acceleration	m/s ²	3.281 ft/sec ²
Accel. of gravity	9.807 m/s ² (g)	32.2 ft/sec ²
Power	watt, N m/s (W)	0.7376 ft.lb/sec
Metric horsepower	75 kG m/s (mhp)	0.9863 HP
English horsepower	76.04 kG m/s	550 ft.lb/sec

List of Abbreviations

Aero. Jour.	Journal of the Royal Aeronautical Society
AGARD	Advisory Group for Aeronautical Research and Development
AIAA	American Institute for Aeronautics and Aerospace
ARC	Aeronautical Research Council
CG	Centre of gravity
IGE	In ground effect
JAHS	Journal of the American Helicopter Society
NACA	National Advisory Committee for Aeronautics (now NASA)
NFA	No-feathering axis
NFP	No-feathering plane
OGE	Out of ground effect
RLD	Really-low-drag (helicopter)
R & M	Reports and Memoranda of the ARC
SAE	Society of Automotive Engineers
SA	Shaft axis
SNP	Shaft normal plane
TPA	Tip-path axis
TPP	Tip-path plane
UK	United Kingdom
USA	United States of America
WHL	Westland Helicopters Ltd

1 Introduction

'It is easy to invent a flying machine;
more difficult to build one;
to make it fly is everything'

Otto Lilienthal, 1848–1896

One may doubt whether Lilienthal, the pioneer *par excellence* of gliding flight, had the helicopter in mind when he wrote the above but his words could not have been more appropriate to our subject. To take the quotation line by line, the concept of a lifting rotor constitutes the essential invention. Making it large is simply taking advantage of Newton's Second and Third Laws, which guarantee that blowing a large quantity of air at low speed is an efficient way of producing a thrust. When it comes to building a machine, the problems of directing it around the sky have to be thought out and translated into hardware: ultimately, however, the solutions for the helicopter are both straightforward and impressive. Upward lift is obtained with the rotor shaft essentially vertical; forward (or backward or sideways) propulsion is achieved by tilting the shaft in the desired direction; and moments for manoeuvring are produced by tilting the rotor plane relative to the shaft. Here is a system more elegant in principle than that of a fixed-wing aircraft, where such integration of functions is not possible. And to pursue its virtues one stage further, when the direction of airflow through the rotor becomes reversed in descent, blade lift can be produced without power ('autorotation'), allowing a controlled landing in the event of engine failure. These points were made by J.P. Jones in the 1972 Cierva Memorial Lecture¹ to the Royal Aeronautical Society. To quote him at this juncture:

'Can we wonder that the conventional rotor has been a success? At this stage one might think the real question is why the fixed-wing aircraft has not died out'

But back to Lilienthal and there's the rub. Making the helicopter fly has involved wrestling with a long catalogue of problems, of

which some have been solved and others continue to be lived with. Thus it was necessary to invent the use of a tail rotor to stop the helicopter spinning round on the main rotor axis. It took the genius of Juan de la Cierva to devise a system of articulated blades to prevent the aircraft rolling over continuously. The helicopter can never fly fast judged by fixed-wing aircraft standards, the restriction, surprisingly enough, being one of blade stalling. Climbing is straightforward aerodynamically but descending involves a deliberate venture into an aerodynamicist's nightmare of vortices, turbulence and separated flow. Blade articulation leads to sluggish control, which can be improved by going to the more modern system of a hingeless rotor, but only at the expense of worsening the aircraft stability. With any practical combination of stability and control characteristics the helicopter remains a difficult and taxing aircraft to fly and generally requires autostabilization to restrict the pilot workload to a safe and comfortable level.

It would seem that we have on our hands a veritable box of tricks. What is certain, however, is that the modern world cannot do without it. The helicopter has become an invaluable asset in many fields of human activity and the variety of its uses continues to increase. Moreover, to come close to the purpose of this book, the problems that have been solved, or if only partly solved, at least understood, make good science, high in interest value. This the book purports to show.

The period since World War II has seen a proliferation of different types of rotary-wing aircraft. The single-rotor helicopter (with tail rotor), established firmly by Sikorsky during the war years, has been joined by versions having tandem rotors, side-by-side rotors, coaxial rotors and tip-driven rotors. A second group, heading back increasingly towards fixed wings, includes compound systems, tilt rotors and tilt wings. The tilt rotor, in which as the name implies the rotors face upwards for vertical take-off and hover and forwards for horizontal flight, offers considerable promise and may in the future become the type which releases the helicopter from its inhibiting speed restriction. Up to the present, however, the single-rotor helicopter remains by far the most numerous worldwide and in this book we concentrate exclusively on that type. Its familiar profile, sketched in Fig. 1.1, is the result of practical considerations not readily varied. The engines and gearbox require to be grouped tightly around the rotor shaft and

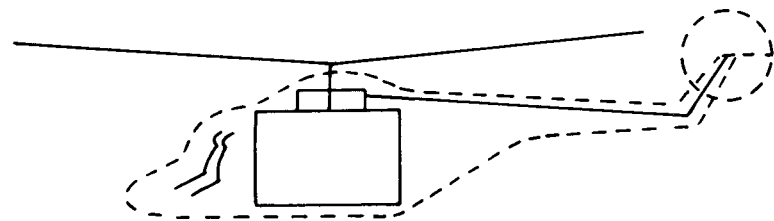


Fig. 1.1 The single-main-rotor helicopter in essence.

close below the rotor. Below them the payload compartment is centrally placed fore and aft to minimize centre of gravity movements away from the shaft line. In front of the payload compartment is the flight cabin. The transmission line from gearbox to tail rotor needs to be as straight and uninterrupted as possible. Put a fairing around these units so defined and the characteristic profile emerges.

It will be helpful to explain certain logistics of the presentation. Symbols are defined when first introduced but for ease of reference are also collected in a table at the start of the book. As concerns units, where there is complete freedom of choice the metric system is preferred: since, however, much use continues to be made of imperial units, particularly in the USA, I have also employed these units freely in numerical examples, sometimes giving both. Again there are tables at the start defining primary and derived units and listing the conversion factors. Lastly, on the question of references, these are numbered in each chapter and listed at the end of the chapter in the usual way. Exception is made, however, in the case of three standard textbooks, which are referred to repeatedly, usually for further information on a topic where the present short treatment is deemed to have gone far enough. The three books are:

- (1) Bramwell, A.R.S. (1976) *Helicopter dynamics*. Edward Arnold.
- (2) Johnson, Wayne (1980) *Helicopter theory*. Princeton University Press.
- (3) Stepniewski, W.Z. and Keys, C.N. (1984) *Rotary-wing aerodynamics*, Vols I and II. Dover Publications Inc.

In the text, these are called upon by author's name and no further reference is given.

With this brief introduction we are poised to move into the main treatment of our subject.

Reference

- 1 Jones, J.P. (1980) 'The rotor and its future'. *Aero. Jour.*, July 1973.

2 Rotor in Vertical Flight: Momentum Theory and Wake Analysis

2.1 Momentum theory for hover

The helicopter rotor produces an upward thrust by driving a column of air downwards through the rotor plane. A relationship between the thrust produced and the velocity communicated to the air can be obtained by the application of Newtonian mechanics – the laws of conservation of mass, momentum and energy – to the overall process. This approach is commonly referred to as the momentum theory for helicopters. It corresponds essentially to the theory set out by Glauert¹ for aircraft propellers, based on earlier work by Rankine and Froude for marine propellers.

The rotor is conceived as an 'actuator disc', across which there is a sudden increase of pressure, uniformly spread. In hover the column of air passing through the disc is a clearly defined streamtube above and below the disc: outside this streamtube the air is undisturbed. No rotation is imparted to the flow. The situation is illustrated in Fig. 2.1. As air is sucked into the disc from above, the pressure falls. An increase of pressure Δp occurs at the disc, after which the pressure falls again in the outflow, eventually arriving back at the initial or atmospheric level p_∞ . Velocity in the streamtube increases from zero at 'upstream infinity' to a value v_i at the disc and continues to increase as pressure falls in the outflow, reaching a value v_∞ at 'downstream infinity'. Continuity of mass flow in the streamtube requires that the velocity is continuous through the disc.

Energy conservation, in the form of Bernoulli's equation, can be applied separately to the flows before and after the disc. Using the assumption of incompressible flow, we have in the inflow:

$$p_\infty = p_i + \frac{1}{2}\rho v_i^2$$

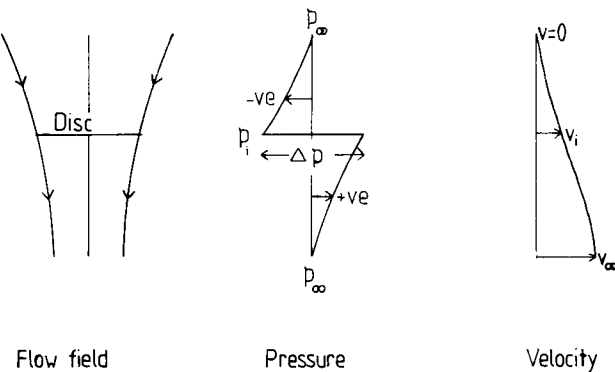


Fig. 2.1 Actuator disc concept for rotor in hover.

ρ being the air density, and in the outflow:

$$p_i + \Delta p + \frac{1}{2}\rho v_i^2 = p_\infty + \frac{1}{2}\rho v_\infty^2$$

It follows from these that:

$$\Delta p = \frac{1}{2}\rho v_\infty^2$$

Now by momentum conservation, the thrust T on the disc is equal to the overall rate of increase of axial momentum of the air, that is to say:

$$T = \rho A v_i v_\infty$$

A being the disc area, hence $\rho A v_i$ is the mass flow through it. Since Δp is the thrust per unit area of the disc we have:

$$\Delta p = \frac{T}{A} = \rho v_i v_\infty$$

From the two expressions for Δp it is seen that:

$$v_\infty = 2v_i \quad (2.1)$$

Thus half the velocity communicated to the air occurs above the disc and half below it, and the relationship between thrust and the velocity v_i is:

$$T = 2\rho A v_i^2 \quad (2.2)$$

or if the thrust is known,

$$v_i = \sqrt{\frac{T}{2\rho A}} = \sqrt{\frac{w}{2\rho}} \quad (2.3)$$

where $w = T/A$ is termed the ‘disc loading’. v_i is the ‘induced velocity’ or alternatively the ‘downwash’, using an analogy with aircraft wing flow which becomes more obvious when the helicopter is in forward flight (Chapter 5).

In practice the level of disc loading for a piston-engined helicopter will normally be around 10 kG/m^2 . Piston engines are heavy and a large rotor diameter must be used to minimize the engine size needed for vertical lift; hence the disc loading is relatively low. The gas turbine engine, used much the more extensively in modern helicopters, has a higher power-to-weight ratio, so smaller rotors can be used, which in turn lead to shorter fuselages, all this giving savings on weight, drag and cost (though the engine itself is a more costly item). With gas turbine engines, helicopter disc loadings are generally in the region of $30-40 \text{ kG/m}^2$.

The work done on the air, represented by its change in kinetic energy per unit time, is $\frac{1}{2}(\rho A v_i) v_\infty^2$, which by Equation (2.1) is $2\rho A v_i^3$ or simply, by Equation (2.2), $T v_i$. This is known as the induced power of the rotor written as

$$P_i = T v_i = T^{3/2} / \sqrt{2\rho A} \quad (2.4)$$

To non-dimensionalize the above relationships, we use as representative velocity the rotor tip speed ΩR , where Ω is the angular velocity and R the rotor radius. Then the coefficients are:

$$\text{thrust: } C_T = T / \rho A (\Omega R)^2$$

$$\text{power: } C_P = P / \rho A (\Omega R)^3$$

$$\text{induced velocity: } \lambda_i = v_i / \Omega R$$

and the relationships of simple momentum theory for a rotor in hover become

$$\lambda_i = \sqrt{C_T / 2} \quad (2.5)$$

$$C_{pi} = \lambda_i C_T = C_T^{3/2} / \sqrt{2} \quad (2.6)$$

More rigorous forms of the momentum theory can be developed – see standard full length texts – to take account of swirl energy in the wake, non-uniformity of the induced velocity and so on.

Generally the corrections emerging amount to a few per cent only and are not always of the same sign. So for much performance work, the simple momentum theory, combined with blade element theory (Chapter 3) gives adequate results.

When more exact rotor analyses are required, calculation of the induced velocity involves assembling a realistic picture of the complex pattern of vortices which in actuality exists in the flow below the rotor. A short description of this approach by ‘vortex theory’ is contained later in the present chapter.

2.2 Figure of merit

The induced power P_i is the major part of the total power absorbed by a rotor in hover. A further power component is needed, however, to overcome the aerodynamic drag of the blades: this is the profile power P_o , say. Since it is the induced power which relates to the useful function of the rotor – that of producing lift – the ratio of induced power to total power is a measure of rotor efficiency in the hover. This ratio is called the *figure of merit*, commonly denoted by M . Using the results of simple momentum theory, M may be variously expressed as:

$$M = \frac{P_i}{(P_i + P_o)} = \left(1 + \frac{P_o}{P_i}\right)^{-1} = \left(1 + \frac{C_{P_o} \sqrt{2}}{C_T^{3/2}}\right)^{-1} \quad (2.7)$$

C_{P_o} being the profile power coefficient $P_o/\rho A(\Omega R)^3$. Now for a given rotor blade the drag, and hence the profile power, may be expected not to vary greatly with the level of thrust, provided the blade does not stall nor experience high compressibility drag rise. Equation (2.7) shows therefore that the value of M for a given rotor will generally increase as C_T increases. This feature means that care is needed in using the figure of merit for comparative purposes. A designer may have scope for producing a high value of M by selecting a low blade area such that the blades operate at high lift coefficient approaching the stall but he needs to be sure that the blade area is sufficient for conditions away from hover, such as in high speed manoeuvre. Again, a comparison of different blade designs – section shape, planform, twist etc, – for a given application must be made at constant thrust coefficient.

A good figure of merit is around 0.75, the profile drag accounting for about one quarter of total rotor power. We may note that for the helicopter as a whole, some power is also required to drive the tail rotor, to overcome transmission losses and to drive auxiliary

components: as a result the induced power in hover amounts to only 60–65% of the total power absorbed.

2.3 Momentum theory for vertical climb

A flow diagram for the rotor in vertical climb, with upward velocity V_c , is shown in Fig. 2.2. Applying Bernoulli's equation as before, we now have in the inflow:

$$p_\infty + \frac{1}{2}\rho V_\infty^2 = p_i + \frac{1}{2}\rho(V_c + v_i)^2$$

and in the outflow:

$$p_i + \Delta p + \frac{1}{2}\rho(V_c + v_i)^2 = p_\infty + \frac{1}{2}\rho(V_c + v_\infty)^2$$

Also the thrust, by momentum conservation, is:

$$T = \rho A(V_c + v_i)v_\infty$$

It is readily seen that these equations lead, as in the hover case, to the relation:

$$v_\infty = 2v_i$$

whence the expression for thrust becomes:

$$T = 2\rho A(V_c + v_i)v_i \quad (2.8)$$

If we write v_h for the value of v_i in hover at the same thrust, the

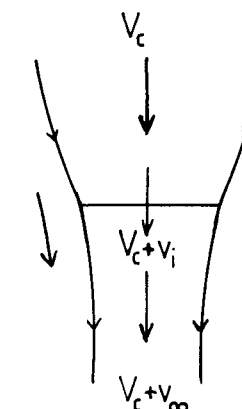


Fig. 2.2 Flow field in vertical climb.

relationship between induced velocities in hover and vertical climb is given by:

$$v_h^2 = (V_c + v_i)v_i \quad (2.9)$$

which for v_i in terms of v_h has the solution:

$$\frac{v_i}{v_h} = -\frac{V_c}{2v_h} + \sqrt{\left\{ \left(\frac{V_c}{2v_h} \right)^2 + 1 \right\}} \quad (2.10)$$

Thus the induced velocity decreases as climbing speed increases (Fig. 2.3), falling asymptotically towards zero for high rates of climb. For low rates of climb v_i approximates to $(v_h - V_c/2)$.

The power consumption, or total work done by the thrust, is

$$P_i = T(V_c + v_i),$$

of which TV_c is the work done on the rotor and Tv_i is that done on the air, represented by the kinetic energy in the induced velocity. Relating P_i to the value in hover and using Equation (2.10) gives:

$$\frac{P_i}{P_h} = \frac{P_i}{Tv_h} = \frac{V_c}{v_h} + \frac{v_i}{v_h} = \frac{V_c}{2v_h} + \sqrt{\left\{ \left(\frac{V_c}{2v_h} \right)^2 + 1 \right\}} \quad (2.11)$$

Thus the induced power increases with climb speed, the manner of this being shown in Fig. 2.4. At high rates of climb P_i approximates to the climb work TV_c only. For small rates we have approximately:

$$P_i \approx P_h + TV_c/2$$

Here momentum theory, because of its over-simplified picture of

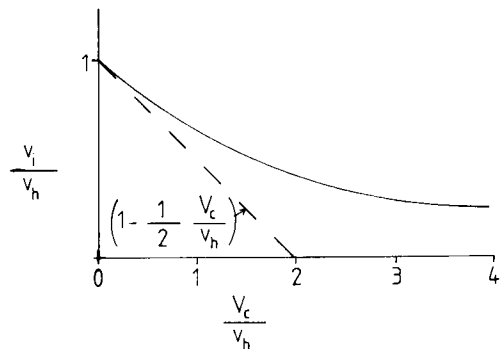


Fig. 2.3 Induced velocity as function of climbing speed.

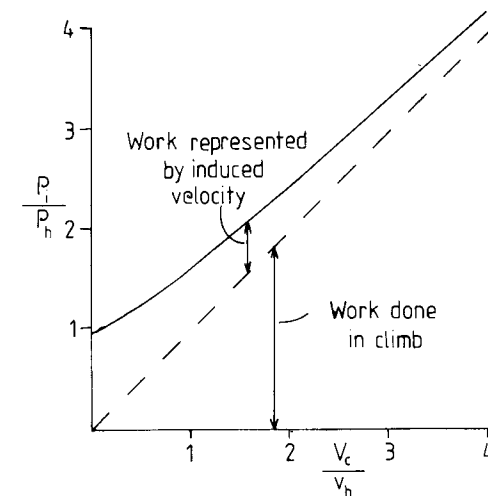


Fig. 2.4 Induced power as function of climbing speed.

the nature of the outflow below the rotor, fails to reveal a power benefit in climb which has been shown to be significant, at least on some helicopters. The position of the tip vortex from a blade (Section 2.8) when the next blade passes by is found to be lower in climb than in hover. This changes the upwash at the blade tips in such a way that for small rates of climb the power required is actually less than for the hover.

2.4 Vertical descent

In vertical descent the nature of flow through the rotor undergoes significant changes. The stream velocity V_c is now negative while the induced velocity v_i remains positive as the rotor continues to maintain lift. Becoming evident when V_c reaches a level about half v_i , an interaction takes place between the upward flow around the disc and the downward flow through it, resulting in the formation of a vortex ring encircling the rim of the disc, doughnut fashion. The situation is illustrated in Fig. 2.5. As this *vortex-ring state* develops the flow becomes very unsteady and the rotor exhibits high levels of vibration. It appears that the ring vortex builds up

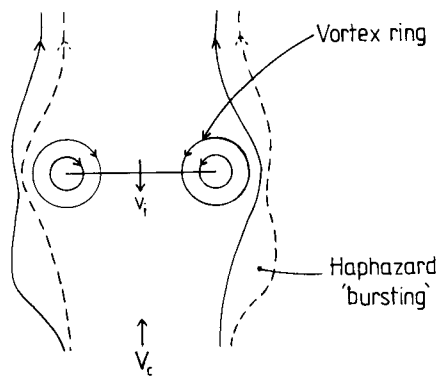


Fig. 2.5 Vortex-ring state in vertical descent.

strength and periodically breaks away from the disc, spilling haphazardly into the flow and causing fluctuations in lift and also in helicopter pitch and roll. Flight in the developed vortex-ring state, which reaches its worst condition when the descent rate is about three quarters of the hover induced velocity, is unpleasant and potentially dangerous. Because of the dissipation of energy in the unsteady flow, simple momentum theory cannot be applied.

As the descent rate approaches the level of the induced velocity, a modified state is observed in which, corresponding to the near equality, there is little or no net flow through the disc. Now the flow is characterized by vortices shed into the wake in the manner of the flow around a solid bluff body. In this *turbulent-wake state* (Fig. 2.6) flight is still rough but less so than in the vortex-ring state. Simple momentum theory is again not applicable, since energy is dissipated in the eddies of the wake.

At large descent rates, when V_c is numerically greater than about $2v_i$, the flow is everywhere upwards relative to the rotor, producing a *windmill-brake state*, in which power is transferred from the air to the rotor. With a flow pattern as in Fig. 2.7, simple momentum theory gives a reasonable approximation: thus with V_c negative and v_i positive the thrust is:

$$T = -2\rho A(V_c + v_i)v_i \quad (2.12)$$

and the induced velocity relates to v_h by:

$$v_i(V_c + v_i) = -v_h^2 \quad (2.13)$$

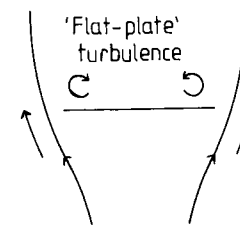


Fig. 2.6 Turbulent-wake state in vertical descent.

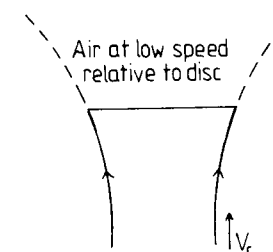


Fig. 2.7 Windmill-brake state in vertical descent.

The power required to maintain thrust in vertical descent generally falls as the rate of descent increases, except that in the vortex-ring state an increase is observed (Fig. 2.8). The effect appears to be caused by stalling of the blade sections during the violent vortex-shedding action. The increase can be embarrassing when making a near-vertical landing approach under conditions in which the engine power available is relatively low, as would be the case under high helicopter load in a high ambient temperature.

2.5 Complete induced-velocity curve

It is of interest to know how the induced velocity varies through all the phases of axial flight. For the vortex-ring and turbulent-wake states, where momentum theory fails, information has been obtained from measurements in flight, supported by wind tunnel tests (Gustafson (1945), Gessow (1948), Brotherhood (1949), Castles and Gray (1951) and others). Obviously the making of flight tests (measuring essentially the rate of descent and control angles) is

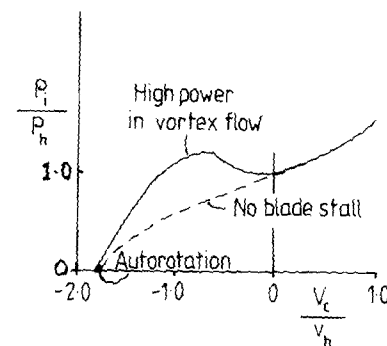


Fig. 2.8 Variation of induced power in climb and descent.

both difficult and hazardous, especially where the vortex-ring state is prominent, and not surprisingly the results show some variation: nevertheless the main trend has been ascertained and what is effectively a universal induced-velocity curve can be defined. This is shown in Fig. 2.9, using the simple momentum-theory results of Equations (2.10) and (2.13) in the regions to which they apply. We see that moving from hover into descent the induced velocity increases more rapidly than momentum theory would indicate. The value rises, in the vortex-ring state, to about twice the hover value, then falls steeply to about the hover value at entry to the windmill-brake state.

2.6 Autorotation

The point of intersection of the induced-velocity curve with the line $V_c + v_i = 0$ is of particular interest because it defines the state of *ideal autorotation*, (IA in Fig. 2.9), in which since there is no mean flow through the rotor, the induced power is zero. Autorotation is an extremely important facility because in a case of power failure the rotor can continue to produce a thrust approximately equal to the aircraft weight, allowing a controlled descent to ground to be made. The term ideal autorotation is used because in practice power is still needed to overcome the drag of the blades. This profile power, P_o say, means that *real autorotation* occurs at a somewhat higher descent rate, given by

$$V_c + v_i = -P_o/T$$

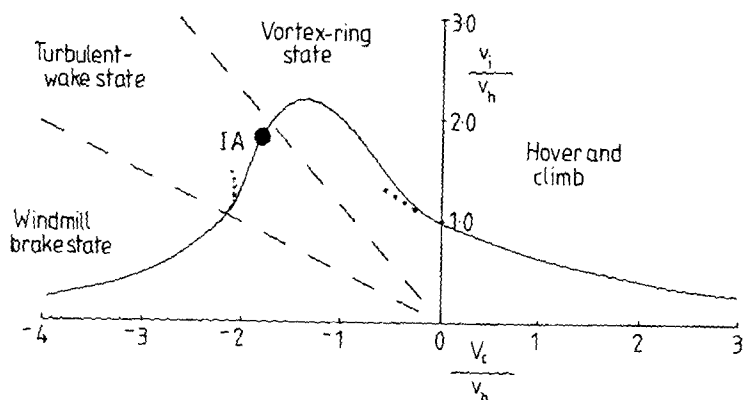


Fig. 2.9 General induced velocity characteristic (after Johnson).

so that total power is

$$P_i + P_o = T(V_c + v_i) \sim T(V_c + v_i) = 0$$

In round terms, values of V_c/v_h for ideal and real autorotation are about -1.8 and -1.7, respectively. Pursuing the analogy of flow past a solid plate (turbulent-wake state, Section 2.4), the plate drag may be written

$$D = \frac{1}{2}\rho V_c^2 A C_D$$

and if this is equated to rotor thrust we have

$$\frac{1}{2}\rho V_c^2 A C_D = 2 \rho A v_h^2$$

from which

$$C_D = 4 \left(\frac{V_c}{v_h} \right)^2$$

With $V_c/v_h = -1.8$, C_D has the value 1.23 which is close to that for a solid plate. A slightly better analogy is obtained by taking the real value $V_c/v_h = -1.7$, which yields a C_D value 1.38, close to the effective drag coefficient of a parachute. Thus in autorotative vertical descent the rotor behaves very like a parachute.

2.7 Summary remarks on momentum theory

The place of momentum theory is that it gives a broad understanding of the functioning of the rotor and provides basic relationships

for the induced velocity created and the power required in producing a thrust to support the helicopter. The actuator disc concept, upon which the theory is based, is most obviously fitted to flight conditions at right angles to its plane, that is to say the hover and vertical flight states we have discussed. Nevertheless further reference to the theory will be made when discussing forward flight (Chapter 5).

Momentum theory brings out the importance of disc loading as a gross parameter: it cannot however look into the detail of how the thrust is produced by the rotating blades and what design criteria are to be applied to them. For such information we need additionally a blade element theory, corresponding to aerofoil theory in fixed-wing aerodynamics: to this we shall turn in Chapter 3.

2.8 Complexity of real wake

The actuator disc concept, taken together with blade-element theory, serves well for the purposes of helicopter performance calculation. When, however, blade loading distributions or vibration characteristics are required for stressing purposes it is necessary to take into account the real nature of flow in the rotor wake. This means abandoning the disc concept and recognizing that the rotor consists of a number of discrete lifting blades, carrying vorticity corresponding to the local lift at all points along the span. Corresponding to this bound vorticity a vortex system must exist in the wake (Helmholtz's theorem) in which the strength of wake vortices is governed by the rate of change of circulation along the blade span. If for the sake of argument this rate could be made constant, the wake for a single rotor blade in hover would consist of a vortex sheet of constant spanwise strength, descending in a helical pattern at constant velocity, as illustrated in Fig. 2.10. The situation is analogous to that of elliptic loading with a fixed wing, for which the induced drag (and hence the induced power) is a minimum. This ideal distribution of lift, however, is not realizable for the rotor blade, because of the steadily increasing velocity from root to tip.

The most noticeable feature of the rotor-blade wake in practice is the existence of a strong vortex emanating from the blade tip, where because the velocity is highest the rate of change of lift is

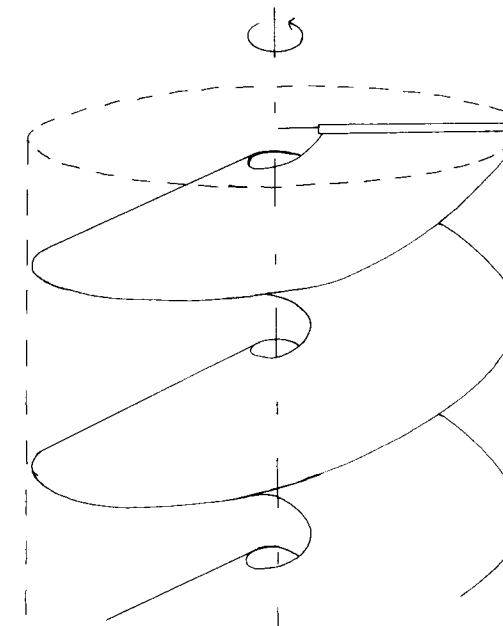


Fig. 2.10 Idealized wake of single rotor blade in hover (after Bramwell).

greatest. In hover the tip vortex descends below the rotor in a helical path. It can be visualized in a wind tunnel using smoke injection (Fig. 2.11) or other means and is often observable in open flight under conditions of high load and high humidity. An important feature which can be seen in Fig. 2.11 is that on leaving the blade the tip vortex initially moves inwards towards the axis of rotation and stays close under the disc plane: in consequence the next tip to come round receives an upwash, increasing its effective incidence and thereby intensifying the tip vortex strength. Figure 2.12 due to J.P. Jones² shows a calculated spanwise loading for a Wessex helicopter blade in hover and indicates the tip vortex position on successive passes. The kink in loading distribution at 80% span results from this tip vortex pattern, particularly from the position of the immediately preceding blade.

The concentration of the tip vortex can be reduced by design changes such as twisting the tip nose-down, reducing the blade tip area or special shaping of the planform, but it must be borne in mind that the blade does its best lifting in the tip region where the velocity is high.

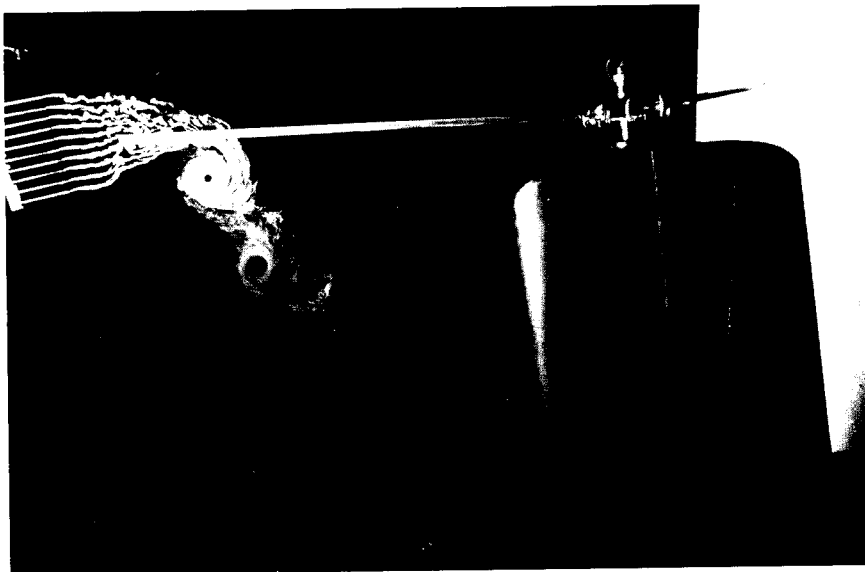


Fig. 2.11 Wind tunnel visualization of tip vortex. (Reproduced courtesy of Westland Helicopters Ltd.)

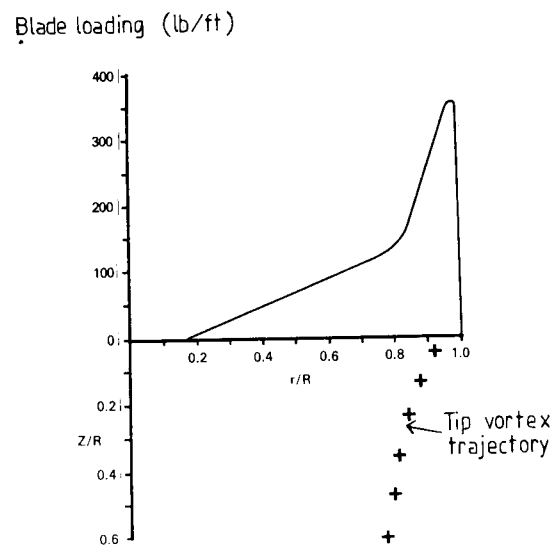


Fig. 2.12 Calculated spanwise loading for Wessex blade (after J.P. Jones).

Since blade loading increases from the root to near the tip (Fig. 2.12), the wake may be expected to contain some inner vorticity in addition to the tip vortex. This might appear as a form of helical sheet akin to that of the illustration in Fig. 2.10, though generally not of uniform strength. Definitive experimental studies by Gray³, Landgrebe⁴ and their associates have shown this to be the case. Thus the total wake comprises essentially the strong tip vortex and an inner vortex sheet, normally of opposite sign. The situation as established by Gray and Landgrebe is pictured, in a diagram which has become standard, by Bramwell (p. 117) and other authors. Figure 2.13 is a modified version of this diagram, intended to indicate vortex lines making up the inner sheet, emanating from the bound vorticity on the inner part of the blade.

The Gray/Landgrebe studies show clearly the contraction of the wake immediately below the rotor disc. Other features which have

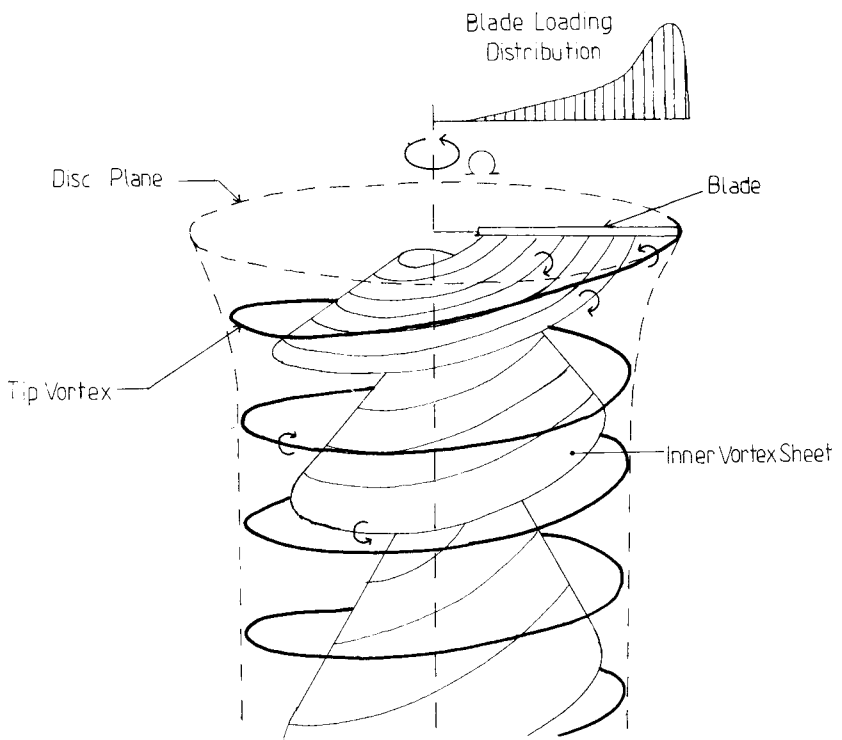


Fig. 2.13 Nature of total wake in hover, deduced from smoke studies (after Gray and Landgrebe).

been observed are that the inner sheet moves downward faster than the tip vortex and that the outer part of the sheet moves faster than the inner part, so the sheet becomes increasingly inclined to the rotor plane.

2.9 Wake analysis methods

By analysis of his carefully conducted series of smoke-injection tests, Landgrebe⁵ reduced the results to formulae giving the radial and axial coordinates of a tip vortex in terms of azimuth angle, with corresponding formulae for the inner sheet. From these established vortex positions the induced velocities at the rotor plane may be calculated. The method belongs in a general category of *prescribed-wake analysis*, as do earlier analyses by Prandtl, Goldstein and Theodorsen, descriptions of which are given by Bramwell. These earlier forms treated either a uniform vortex sheet as pictured in Fig. 2.10 or the tip vortex in isolation, and so for practical application are effectively superseded by Landgrebe's method.

More recently, considerable emphasis has been placed on *free-wake analysis*, in which modern numerical methods are used to perform iterative calculations between the induced velocity distribution and the wake geometry, both being allowed to vary until mutual consistency is achieved. This form of analysis has been described for example by Clark and Leiper⁶. Generally the computing requirements are very heavy, so considerable research effort also goes into devising simplified free-wake models which will reduce the computing load.

Calculations for a rotor involve adding together calculations for the separate blades. Generally this is satisfactory up to a depth of wake corresponding to at least two rotor revolutions. A factor which helps this situation is the effect on the tip vortex of the upwash ahead of the succeeding blade – analogous to the upwash ahead of a fixed wing. The closer the spacing between blades, the stronger is this effect from a succeeding blade on the tip vortex of the blade ahead of it; thus it is observed that when the number of blades is large, the tip vortex remains approximately in the plane of the rotor until the succeeding blade arrives, when it is convected downwards. In the ‘far’ wake, that is beyond a depth corresponding to two rotor revolutions, it is sufficient to represent the vorticity in simplified fashion; for example free-wake calculations can

be simplified by using a succession of vortex rings, the spacing of which is determined by the number of blades and the mean local induced velocity. Eventually in practice both the tip vortices and the inner sheets from different blades interact and the ultimate wake moves downward in a confused manner.

There we leave this brief description of the real wake of a hovering rotor and the methods used to represent it. This branch of the subject is often referred to as *vortex theory*. It will be touched on again in the context of the rotor in forward flight (Chapter 5). For more detailed accounts, the reader is referred to the standard textbooks and the more specific references which have been given in these past two sections.

2.10 Ground effect

The induced velocity of a rotor in hover is considerably influenced by near presence of the ground. At ground surface the downward velocity in the wake is of course reduced to zero and this effect is transferred upwards to the disc through pressure changes in the wake, resulting in a lower induced velocity for a given thrust. The induced power is therefore lower, which is to say that a helicopter at a given weight is able to hover at lower power thanks to ‘support’ given by the ground. Alternatively put, for a given power output, a helicopter ‘in ground effect’ is able to hover at a greater weight than when it is away from the ground. As Bramwell has put it, ‘the improvement in performance may be quite remarkable; indeed some of the earlier, underpowered, helicopters could hover only with the help of the ground.’

The theoretical approach to ground effect is, as would be expected, by way of an image concept. A theory by Knight and Hafner⁷ makes two assumptions about the normal wake, (1) that circulation along the blade is constant, thus restricting the vortex system to the tip vortices only, and (2) that the helical tip vortices form a uniform vortex cylinder reaching to the ground. The ground plane is then represented by a reflection of this system, of equal dimensions below the plane but of opposite vorticity, ensuring zero normal velocity at the surface. The induced velocity at the rotor produced by the total system of real and image vortex cylinders is calculated and hence the induced power can be derived as a function of rotor height above the ground.

It is found that the power, expressed as a proportion of that required in absence of the ground, is as low as 0.5 when the rotor height to rotor radius is about 0.3, a typical value for the point of take-off. Since induced power is roughly two thirds of total power (Section 2.2), this represents a reduction of about one third in total power. By the time the height to radius ratio reaches 2.0, the power ratio is close to 1.0, which is to say the ground effect has virtually disappeared. The results are only slightly dependent on the level of thrust coefficient.

Similar results have been obtained from tests on model rotors, measuring the thrust that can be produced for a given power. A useful expression emerges from a simple analysis made by Cheeseman and Bennett⁸, who give the approximate relationship:

$$\frac{T}{T_\infty} = \frac{1}{1 - (R/4Z)^2}$$

Z being the rotor height above ground, R the rotor radius. This shows good agreement with experimental data.

References

- 1 Glauert, H. (1937) *The elements of aerofoil and airscrew theory*. Cambridge University Press.
- 2 Jones, J.P. (1973) 'The rotor and its future'. *Royal Aeronautical Society Journal*, July 1973.
- 3 Gray, R.B. (1956) 'An aerodynamic analysis of a single-bladed rotor in hovering and low speed forward flight as determined from smoke studies of the vorticity distribution in the wake'. *Princeton University Aeronautical Engineering Report 356*.
- 4 Landgrebe, A.J. (1972) 'The wake geometry of a hovering helicopter rotor and its influence on rotor performance'. *JAHS* **17**, no. 4, October 1972.
- 5 Landgrebe, A.J. (1971) 'Analytical and experimental investigation of helicopter rotor hover performance and wake geometry characteristics'. *USAAMRDL Technical Report*, 71-24.
- 6 Clark, D.R. and Leiper, A.C. (1970) 'The free wake analysis – a method for the prediction of helicopter rotor hovering performance'. *JAHS* **15**, no. 1, January 1970.
- 7 Knight, M. and Hefner, R.A. (1941) 'Analysis of ground effect on the lifting airscrew'. *NACA TN 835*.
- 8 Cheeseman, I.C. and Bennett, W.E. (1955) 'The effect of the ground on a helicopter rotor'. *ARC R & M 3021*.

3 Rotor in Vertical Flight: Blade Element Theory

3.1 Basic method

Blade element theory is basically the application of the standard process of aerofoil theory to the rotating blade. Although in reality flexible, the blade is assumed throughout to be rigid, justification for this lying in the fact that at normal rotation speeds the outward centrifugal force is the largest force acting on a blade and in effect is sufficient to hold the blade in rigid form. In vertical flight, including hover, the main complication is the need to integrate the elementary forces along the blade span. Offsetting this, useful simplification occurs because the blade incidence and induced flow angles are normally small enough to allow small-angle approximations to be made.

Figure 3.1 is a plan view of the rotor disc, viewed from above. Blade rotation is anticlockwise (the normal system in Western-world countries) with angular velocity Ω . The blade radius is R , the tip speed therefore being ΩR , alternatively written as V_t . An elementary blade section is taken at radius y , of chord length c and spanwise width dy . Forces on the blade section are shown in Fig. 3.2. The flow seen by the section has velocity components Ωy in the disc plane and $(v_i + V_c)$ perpendicular to it. The resultant of these is

$$U = [(v_i + V_c)^2 + (\Omega y)^2]^{1/2} \quad (3.1)$$

The blade pitch angle, determined by the pilot's collective control setting (see Chapter 4), is θ . The angle between the flow direction and the plane of rotation, known as the *inflow angle* is ϕ , given by

$$\phi = \tan^{-1} [(V_c + v_i)/\Omega y] \quad (3.2)$$

or for small angles, which we shall assume,

$$\phi = (V_c + v_i)/\Omega y \quad (3.3)$$

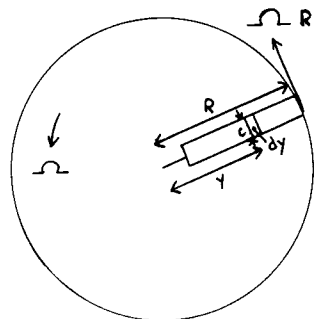


Fig. 3.1 Rotor disc viewed from above.

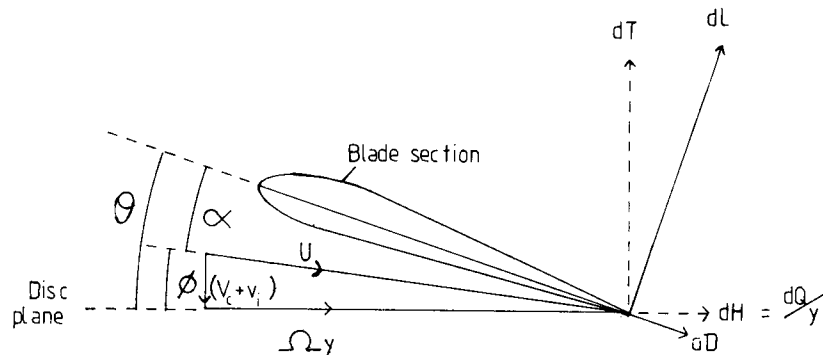


Fig. 3.2 Blade section flow conditions in vertical flight.

The angle of incidence of the blade section, denoted by α , is seen to be

$$\alpha = \theta - \phi \quad (3.4)$$

The elementary lift and drag forces on the section are

$$dL = \frac{1}{2} \rho U^2 c dy C_L$$

and

$$dD = \frac{1}{2} \rho U^2 c dy C_D$$

Resolving these normal and parallel to the disc plane gives an element of thrust

$$dT = dL \cos \phi - dD \sin \phi$$

and an element of blade torque

$$dQ = (dL \sin \phi + dD \cos \phi) y$$

The inflow angle ϕ may generally be assumed small: from Equation (3.3) this may be questionable near the blade root where Ω_y is small, but there the blade loads are themselves small also. The following approximations can therefore be made:

$$\begin{aligned} U &\approx \Omega y \\ dT &\approx dL \\ dQ &\approx (\phi dL + dD) y \end{aligned}$$

It is convenient to introduce dimensionless quantities at this stage. The development then follows in principle the exposition given by Johnson. We write

$$r = y/R \quad (3.5)$$

$$\frac{U}{\Omega R} = \frac{\Omega y}{\Omega R} = r \quad (3.6)$$

$$dC_T = dT / \rho A (\Omega R)^2 \quad (3.7)$$

$$dC_Q = dQ / \rho A (\Omega R)^2 R \quad (3.8)$$

$$\lambda = \frac{(V_c + v_i)}{\Omega R} = r\phi \quad (3.9)$$

λ is known as the *inflow factor* and was previously used in Chapter 2. Now the element of thrust becomes

$$dC_T = \frac{1}{2} \frac{\rho}{\pi R^2} \frac{U^2 c}{(\Omega R)^2} dy C_L = \frac{1}{2} \frac{c}{\pi R} C_L r^2 dr$$

This is for a single blade. For N blades we have

$$dC_T = \frac{1}{2} \frac{Nc}{\pi R} C_L r^2 dr$$

and introducing a solidity factor σ which for constant blade chord c is given by

$$\sigma = \frac{\text{blade area}}{\text{disc area}} = \frac{NcR}{\pi R^2} = \frac{Nc}{\pi R} \quad (3.10)$$

we are led to

$$dC_T = \frac{1}{2} \sigma C_L r^2 dr \quad (3.11)$$

Integrating along the blade span gives the rotor thrust coefficient

$$C_T = \frac{1}{2} \sigma \int_0^1 C_L r^2 dr \quad (3.12)$$

The element of torque, non-dimensionalized, becomes

$$dC_Q = \frac{1}{2} \frac{c}{\pi R} (\phi C_L + C_D) r^3 dr$$

for a single blade; and for N blades of constant chord,

$$dC_Q = \frac{1}{2} \sigma (\phi C_L + C_D) r^3 dr \quad (3.13)$$

Integrating along the span gives the torque coefficient

$$\begin{aligned} C_Q &= \frac{1}{2} \sigma \int_0^1 (\phi C_L + C_D) r^3 dr \\ &= \frac{1}{2} \sigma \int_0^1 (\lambda C_L r^2 + C_D r^3) dr \end{aligned} \quad (3.14)$$

The rotor power requirement is given by

$$P = \Omega Q \quad (3.15)$$

so that, defining the power coefficient as

$$C_P = P/\rho A(\Omega R)^3 \quad (3.16)$$

we see that C_P and C_Q are identical.

We are using here and throughout this book the American forms of thrust and torque coefficient. Other forms are also in use: thus Bramwell uses

$$t_c = T/\rho A(\Omega R)^2 \quad \text{and} \quad q_c = Q/\rho A \Omega^2 R^3 \quad (3.17)$$

These are seen to be related to the present C_T and C_Q by

$$t_c = C_T/\sigma, \quad q_c = C_Q/\sigma \quad (3.18)$$

Another possibility is the use of a factor $\frac{1}{2}$ in the denominator, thus

$$C_T = T/\frac{1}{2}\rho A(\Omega R)^2, \quad C_Q = Q/\frac{1}{2}\rho A \Omega^2 R^3 \quad (3.19)$$

which is sometimes called the British definition.

To evaluate Equations (3.12) and (3.14) it is necessary to know the span-wise variation of blade incidence α and to have blade section data which give C_L and C_D as a functions of α . The equations can then be integrated numerically. Since α is given by $(\theta - \phi)$, its distribution depends upon the variations of θ , the blade pitch, and $(V_c + V_i)$, the induced velocity, represented by the inflow factor λ . Useful approximations can be made, however, which allow analytical solutions with, in most cases, only small loss of accuracy.

3.2 Thrust approximations

If the blade incidence α is measured from the no-lift line and stall and compressibility effects can be neglected, the section lift coefficient can be approximated by the linear relation,

$$C_L = a\alpha = a(\theta - \phi) \quad (3.20)$$

where the two-dimensional lift slope factor 'a' has a value about 5.7. Equation (3.12) then takes the form

$$\begin{aligned} C_T &= \frac{1}{2} \sigma a \int_0^1 (\theta - \phi) r^2 dr \\ &= \frac{1}{2} \sigma a \int_0^1 (\theta r^2 - \lambda r) dr \end{aligned} \quad (3.21)$$

For a blade of zero twist, θ is constant. For uniform induced velocity – as assumed in simple momentum theory – the inflow factor λ is also constant. In these circumstances Equation (3.21) integrates readily to

$$C_T = \frac{1}{2} \sigma a \left[\frac{1}{3} \theta - \frac{1}{2} \lambda \right] \quad (3.22)$$

Conventionally, modern blades have a degree of negative twist, decreasing the pitch angle towards the tip so as to compromise on the blade loading distribution. Thus θ takes a form such as

$$\theta = \theta_0 + r \theta_{tw} \quad (3.23)$$

with θ_{tw} negative. Using this form the thrust coefficient becomes

$$C_T = \frac{1}{2} \sigma a \left[\frac{1}{3} \theta_0 + \frac{1}{4} \theta_{tw} - \frac{1}{2} \lambda \right] \quad (3.24)$$

If the reference pitch angle is taken to be that at three-quarters radius, that is to say

$$\theta = \theta_{0.75} + (r - 0.75) \theta_{tw} \quad (3.25)$$

, then it is readily seen that the relation in Equation (3.22) is restored, namely

$$C_T = \frac{1}{2} \sigma a \left[\frac{1}{3} \theta_{0.75} - \frac{1}{2} \lambda \right] \quad (3.26)$$

Thus a blade with linear twist has the same thrust coefficient as one of constant θ equal to that of the twisted blade at three-quarters radius.

Equation (3.22) expresses the rotor thrust coefficient as a function of pitch angle and inflow ratio. The sequence from the starting

point of an aerodynamic lift coefficient on the blade section has been:

$$C_T = f_n(C_L) = f_n(\alpha) = f_n(\theta, \phi) = f_n(\theta, \lambda)$$

For a direct relationship between thrust coefficient and pitch setting, we need to invoke also the overall link between thrust and induced velocity given by the momentum theorem. For the rotor in hover, this is Equation (2.5), which on incorporation with Equation (3.22) leads to:

$$C_T = \frac{1}{2}\sigma a \left(\frac{1}{3}\theta - \frac{1}{2} \sqrt{\frac{C_T}{2}} \right) \quad (3.27)$$

$$\text{or } \theta = \frac{6}{\sigma a} C_T + \frac{3}{2} \sqrt{\frac{C_T}{2}} \quad (3.28)$$

in which for a blade with a linear twist, θ is taken at three-quarters radius. It is readily seen that correspondingly the direct relationship between θ and λ is:

$$\lambda = \frac{\sigma a}{16} \left[\sqrt{\left(1 + \frac{64}{3\sigma a} \theta \right)} - 1 \right] \quad (3.29)$$

3.3 Non-uniform inflow

A questionable assumption which has been made so far is that the induced velocity is uniform across the blade span. The effect of non-uniformity can be allowed for by using differential forms of the appropriate equations in the combination of blade element theory and momentum theory. Equation (3.21) in the blade element theory is replaced by

$$dC_T = \frac{1}{2}\sigma a (\theta r^2 - \lambda r) dr \quad (3.30)$$

which expresses the element of thrust on an annulus of the disc at radius r . The corresponding equation from momentum theory, again using the hover case for simplicity, is the replacement of Equation (2.2), namely

$$dT = 2\rho v_i^2 dA \quad (3.31)$$

or

$$dC_T = 2\lambda^2 \frac{dA}{A} = 4\lambda^2 r dr \quad (3.32)$$

Combining Equations (3.30) and (3.32) yields a quadratic equation in λ , the solution of which is

$$\lambda = \frac{\sigma a}{16} \left[\sqrt{\left(1 + \frac{32}{\sigma a} \theta r \right)} - 1 \right] \quad (3.33)$$

The inflow distribution may now be calculated as a function of r and the thrust evaluated from Equation (3.21).

As a numerical example let us consider the case of a blade having linear twist, from a pitch setting 12° at the root to 6° at the tip (the root cutout can be ignored for this purpose). Assume also that the rotor solidity is $\sigma = 0.08$ and the value of σa , using $a = 5.7$, is 0.456. Applying Equation (3.28) for the three-quarters radius point, at which θ is 7.5° , gives a thrust coefficient $C_T = 0.00453$. Turning now to Equation (3.33), the non-uniform λ varies along the span as shown in Fig. 3.3. Superficially this is greatly different from a constant value $\lambda = \frac{1}{2}C_T$. Nevertheless, on evaluating Equation (3.21) the variation of $(\theta r^2 - \lambda r)$ is as shown in the figure, from which the integrated value of thrust coefficient is $C_T = 0.00461$. Thus the assumption of constant inflow has led to underestimating the thrust by a mere 1.7%. The result agrees well with Bramwell's general conclusion (p. 93) and confirms that uniform inflow may be assumed for many, perhaps most, practical purposes.

3.4 Ideal twist

The relation in Equation (3.33) contains one particular case when λ is indeed constant, namely if θr is constant along the span, that is

$$\theta r = \theta_t \quad (3.34)$$

θ_t being the pitch angle at the tip. This non-linear twist is not physically realizable near the root but the case is of interest because, as momentum theory shows, uniform induced velocity corresponds to minimum induced power. The analogy with elliptic loading for a fixed-wing aircraft is again recalled. The twist in Equation (3.34) is known as *ideal twist*. Inserting in Equation (3.21) gives

$$\begin{aligned} C_T &= \frac{1}{2}\sigma a \int_0^1 (\theta_t - \lambda) r dr \\ &= \frac{1}{4}\sigma a (\theta_t - \lambda) \end{aligned} \quad (3.35)$$

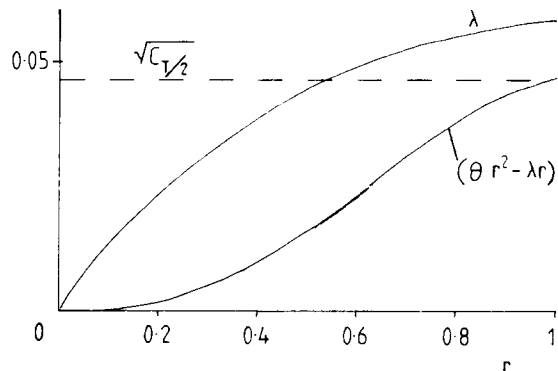


Fig. 3.3 Non-uniform inflow: variation of λ and $(\theta r^2 - \lambda r)$ along blade.

or, since $\lambda = r\phi = \phi_t$,

$$C_T = \frac{1}{4}\sigma a (\theta_t - \phi_t) \quad (3.36)$$

The constant value of λ is

$$\lambda = \frac{\sigma a}{16} \left[\sqrt{\left(1 + \frac{32}{\sigma a} \theta_t \right)} - 1 \right] \quad (3.37)$$

and the direct relationship between θ and C_T is

$$\theta_t = \frac{4}{\sigma a} C_T + \sqrt{\frac{C_T}{2}} \quad (3.38)$$

Some pitch angles for ideal twist and linear twist are compared in Fig. 3.4. The inboard end of the blade is assumed to be at $r = 0$, ignoring for the purposes of comparison the practical necessity of a root cutout. The linear twist is assumed to vary from 12° pitch at the root to 6° at the tip. A straightforward comparison is when the ideal twist has the same pitch at the tip: we see that unrealistically high pitch angles are involved at 40% radius and inboard. A more useful comparison is at equal thrust for the two blades. From Equations (3.28) and (3.38) it follows that for the same thrust coefficient the pitch angle at two-thirds span with the ideal twist is the same as that at three-quarters span with the linear twist, which for the case in point is 7.5° . Thus the ideal twist is given by

$$\theta r = \theta_t = 7.5 \times \frac{2}{3} = 5.0^\circ$$

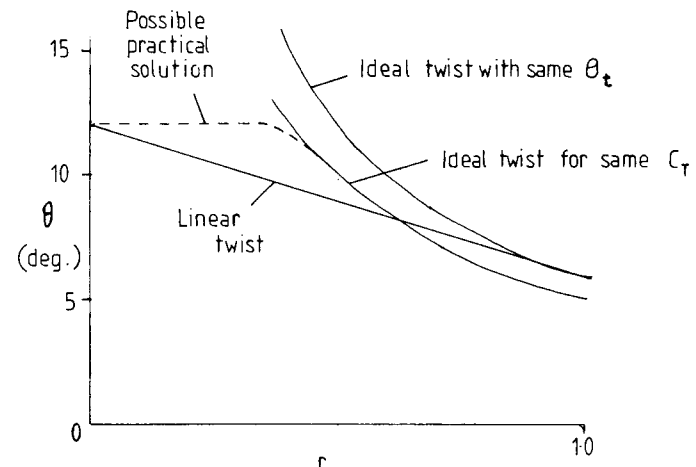


Fig. 3.4 Ideal twist and linear twist compared.

This case is also shown in Fig. 3.4. The two twist distributions give the same pitch angle when $r = (1 - \sqrt{1/6}) \approx 0.59$. Again the ideal twist leads to high pitch angles further inboard but a practical solution, losing little in induced power, might be to transfer to constant pitch from about $0.4r$ inwards.

3.5 Blade mean lift coefficient

Characteristics of a rotor obviously depend on the lift coefficient at which the blades are operating and it is useful to have a simple approximate indication of this. The *blade mean lift coefficient* provides such an indication. As the name implies the mean lift is that which, applied uniformly along the blade span, would give the same total thrust as the actual blade. Writing the mean lift coefficient as \bar{C}_L we have, from Equation (3.12),

$$\begin{aligned} C_T &= \int_0^1 \frac{1}{2}\sigma \bar{C}_L r^2 dr \\ &= \frac{1}{2}\sigma \bar{C}_L \int_0^1 r^2 dr \\ &= \frac{1}{6}\sigma \bar{C}_L \end{aligned}$$

from which

$$\bar{C}_L = 6 C_T / \sigma \quad (3.39)$$

The parameter C_T/σ is thus of fundamental importance and this explains the preference some workers have for using it as the definition of thrust coefficient (see Equation (3.18)) instead of C_T . Expanding the definition gives

$$\frac{C_T}{\sigma} = \frac{T}{\rho A (\Omega R)^2} \frac{A}{A_b} = \frac{T}{\rho A_b (\Omega R)^2} \quad (3.40)$$

where A_b is the total blade area. Thus C_T/σ is the non-dimensional blade loading corresponding to the non-dimensional disc loading C_T .

Blades usually operate in the C_L range 0.3 to 0.6, so typical values of C_T/σ are between 0.05 and 0.1. Typical values of C_T are an order of 10 smaller.

3.6 Power approximations

From Equation (3.13) the differential power coefficient dC_p ($= dC_Q$) may be written as

$$\begin{aligned} dC_p = dC_Q &= \frac{1}{2} \sigma C_L \phi r^3 dr + \frac{1}{2} \sigma C_D r^3 dr \\ &= \frac{1}{2} \sigma C_L \lambda r^2 dr + \frac{1}{2} \sigma C_D r^3 dr \\ &= dC_{p_i} + dC_{p_o} \end{aligned} \quad (3.41)$$

where dC_{p_i} is the differential power coefficient associated with induced flow and dC_{p_o} is that associated with blade section profile drag. The first term, using Equation (3.11), is simply

$$dC_{p_i} = \lambda dC_T \quad (3.42)$$

Thus

$$dC_p = \lambda dC_T + \frac{1}{2} \sigma C_D r^3 dr \quad (3.43)$$

whence

$$C_p = \int_{r=0}^{r=1} \lambda dC_T + \int_0^1 \frac{1}{2} \sigma C_D r^3 dr \quad (3.44)$$

Assuming uniform inflow and a constant profile drag coefficient C_{D_o} , we have the approximation

$$C_p = \lambda C_T + \frac{1}{8} \sigma C_{D_o} \quad (3.45)$$

In the hover, where $\lambda = \sqrt{C_T}/2$, this becomes

$$C_p = \frac{(C_T)^{3/2}}{\sqrt{2}} + \frac{1}{8} \sigma C_{D_o} \quad (3.46)$$

The first term of Equations (3.45) or (3.46) agrees with the result from simple momentum theory (Equation (2.6)). The present λ , defined by Equation (3.9), includes the inflow from climbing speed V_c (if any), so the power coefficient term includes the climb power $P_c = V_c T$.

The total induced power in hover or climbing flight is generally two or three times as large as the profile power. The chief deficiency of the formula at Equation (3.45) in practice arises from the assumption of uniform inflow. Bramwell (p. 94 *et seq.*) shows that for a linear variation of inflow the induced power is increased by approximately 13%. This and other smaller correction factors such as tip loss (Section 3.7) are commonly allowed for by applying an empirical factor κ to the first term of Equation (3.45), so that as a practical formula,

$$C_p = \kappa \lambda C_T + \frac{1}{8} \sigma C_{D_o} \quad (3.47)$$

is used, in which a suggested value of κ is 1.15. The combination of Equations (3.47) and (3.22) provides adequate accuracy for many performance problems.

For the hover, we have

$$C_p = \frac{\kappa}{\sqrt{2}} C_T^{3/2} + \frac{1}{8} \sigma C_{D_o} \quad (3.48)$$

The figure of merit M may be written

$$M = \frac{(C_p)_{\text{ideal}}}{(C_p)_{\text{actual}}} = \frac{C_T^{3/2}}{\kappa C_T^{3/2} + \sigma C_{D_o}/4\sqrt{2}} \quad (3.49)$$

which demonstrates that for a given thrust coefficient a high figure of merit requires a low value of σC_{D_o} . Using a low solidity seems an obvious way to this end but it must be tempered because the lower the solidity the higher are the blade angles-of-incidence required to produce the thrust and the profile drag may then increased significantly from either Mach number effects or the approach of stall. A low solidity subject to retaining a good margin of incidence below the stall would appear to be the formula for producing an efficient design.

For accurate performance work the basic relationships at

Equations (3.12) and (3.14) are integrated numerically along the span. Appropriate aerofoil section data can then be used, including both compressibility effects and stalling characteristics. Further reference to numerical methods is made in Chapter 6.

3.7 Tip loss

A characteristic of the actuator disc concept is that the linear theory of lift is maintained right out to the edge of the disc. Physically, recalling Fig. 2.1, we suppose the induced velocity, in which the pressure is above that of the surrounding air, to be contained entirely below the disc in a well-defined streamtube surrounded by air at rest relative to it. In reality, because the rotor consists of a finite number of separate blades, some air is able to escape outwards between the tips, drawn out by the tip vortices. Thus the total induced flow is less than the actuator disc theory would prescribe, so that for a given pitch setting of the blades the thrust is somewhat lower than that given by Equation (3.22). The deficiency is known as *tip loss* and is shown by a rapid falling off of lift over the last few per cent of span near the tip, in a blade loading distribution such as that of Fig. 2.13.

Although several workers have suggested approximations [Bramwell (p. 111) quotes Prandtl, Johnson (p. 60) quotes in addition Sissingh and Wheatley] no exact theory of tip loss is available. A common method of arriving at a formula is to assume that outboard of a station $r = BR$ the blade sections produce drag but no lift. Then the thrust integral in Equation (3.21) is replaced by

$$C_T = \frac{1}{2}\sigma a \int_0^B (\theta r^2 - \lambda r) dr \quad (3.50)$$

whence is obtained, for uniform inflow and zero twist,

$$C_T = \frac{1}{2}\sigma a \left(\frac{1}{3}B^3\theta - \frac{1}{2}B^2\lambda \right) \quad (3.51)$$

With a typical value $B = 0.97$ or 0.98 Equation (3.51) yields between 5% and 10% lower thrust than Equation (3.22) for a given θ .

To obtain the effect on rotor power at a given thrust coefficient, we need to express the increase in induced velocity corresponding

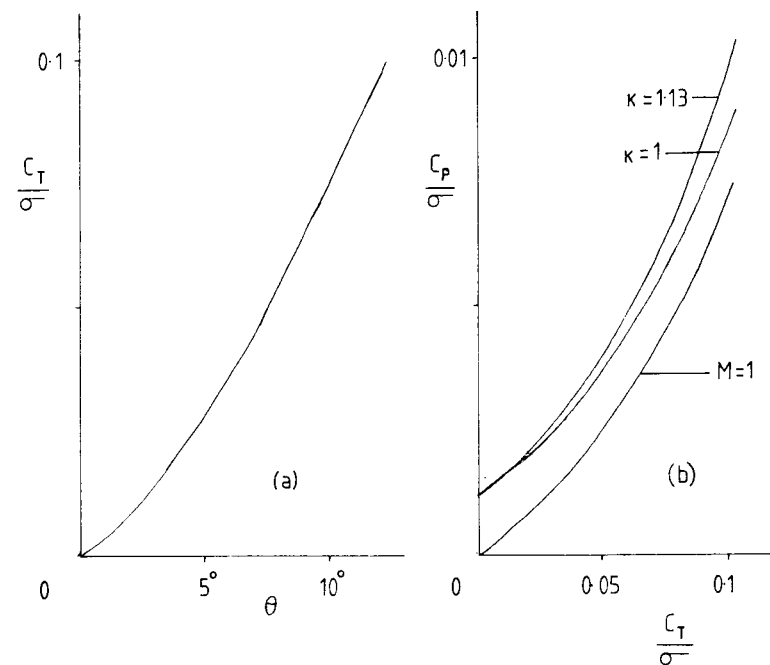


Fig. 3.5 Hover characteristics from sample calculations.

to the effective reduction of disc area. Since the latter is by a factor B^2 and the induced velocity is proportional to the square root of disc loading (Equation (2.3)), the increase in induced velocity is by a factor $1/B$. The rotor induced power in hover thus becomes

$$C_{p_i} = \frac{1}{B} \frac{(C_T)^{3/2}}{\sqrt{2}} \quad (3.52)$$

Typically this amounts to 2–3% increase in induced power. The factor can be incorporated in the overall value assumed for the empirical constant κ in Equation (3.47).

3.8 Example of hover characteristics

Corresponding to C_L/α and C_D/C_L characteristics for fixed wings, we have C_T/θ and C_p/C_T for the helicopter in hover. An example has been evaluated using the following data:

blade radius, $R = 6\text{ m}$

blade chord (constant), $c = 0.5\text{ m}$

blade twist, linear from 12° at root to 6° at tip

number of blades, $N = 4$

empirical constant, $\kappa = 1.13$

blade profile drag coefficient (constant), $C_{D_0} = 0.010$

The variation of C_T/σ with θ is shown in Fig. 3.5(a). The non-linearity results from the $\sqrt{C_T}$ term in Equation (3.28). The variation of C_P/σ with C_T/σ , known as the *hover polar*, is calculated for three cases:

$\kappa = 1.13$, Equation (3.48),

$\kappa = 1.0$, Equation (3.46), the simple momentum theory result, figure of merit $M = 1.0$, which assumes $\kappa = 1$ and $C_{D_0} = 0$.

Over the range shown (Fig. 3.5 (b)), using the factor $\kappa = 1.13$ results in a power coefficient 0–9% higher than that obtained using simple momentum theory. The curve for $M = 1$ is of course unrealistic but gives an indication of the division of power between induced and profile components.

4 Rotor Mechanisms for Forward Flight

4.1 The edgewise rotor

In level forward flight the rotor is edgewise on to the airstream, a basically unnatural state for propeller functioning. Practical complications which arise from this have been resolved by the introduction of mechanical devices, the functioning of which in turn adds to the complexity of the aerodynamics.

Figure 4.1 pictures the rotor disc as seen from above. Blade rotation is in a counter-clockwise sense (the standard adopted for all helicopters of the Western countries) with rotational speed Ω . Forward flight velocity is V and the ratio $V/\Omega R$, R being the blade radius, is known as the *advance ratio* symbol μ , and has a value normally within the range zero to 0.5. Azimuth angle ψ is measured from the downstream blade position: the range $\psi = 0^\circ$ – 180° defines the *advancing side* and that from 180° – 360° (or 0°) the *retreating side*.

A blade is shown in Fig. 4.1 at 90° and again at 270° . These are the positions of maximum and minimum relative air velocity normal to the blade, the velocities at the tip being $(\Omega R + V)$ and $(\Omega R - V)$, respectively. If the blade were to rotate at fixed incidence, then owing to this velocity differential, much more lift would be generated on the advancing side than on the retreating side. Calculated pressure contours for a fixed-incidence rotation with $\mu = 0.3$ are shown in Fig. 4.2. About four-fifths of the total lift is produced on the advancing side. The consequences of this imbalance would be large oscillatory bending stresses at the blade roots and a large rolling moment on the vehicle. Both structurally and dynamically the helicopter would be unflyable.

Clearly a cyclical variation in blade incidence is needed to balance lift on the two sides. The widely adopted method of achieving this

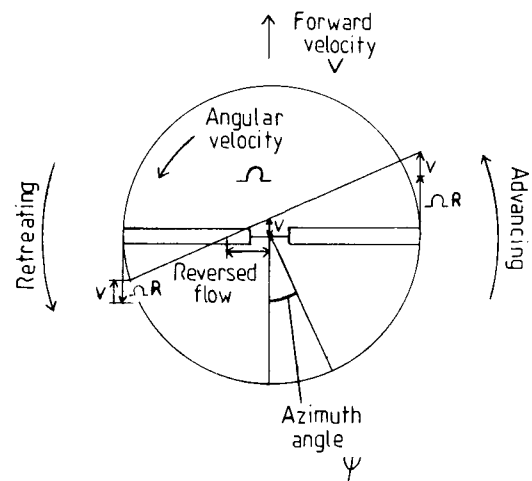


Fig. 4.1 Rotor disc from above showing velocities in forward flight.

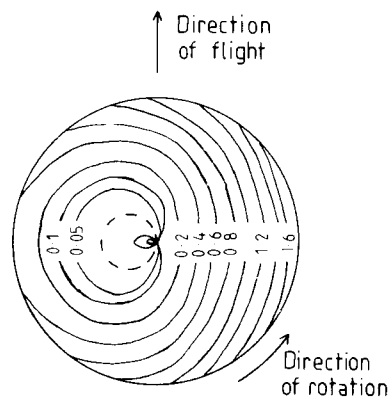


Fig. 4.2 Calculated pressure contours for unbalanced rotation (after J.P. Jones).

is by use of flapping hinges, first introduced by Juan de la Cierva around 1923. The blade is freely hinged as close as possible to the root, allowing it to flap up and down during rotation. Thus as a blade moves on to the advancing side, the rise in relative velocity increases the lift, causing the blade to flap upwards. This motion reduces the effective blade incidence (Fig. 4.3) thereby reducing the lift and ultimately allowing the blade to flap down again. On the retreating side the reverse process occurs. The presence of free

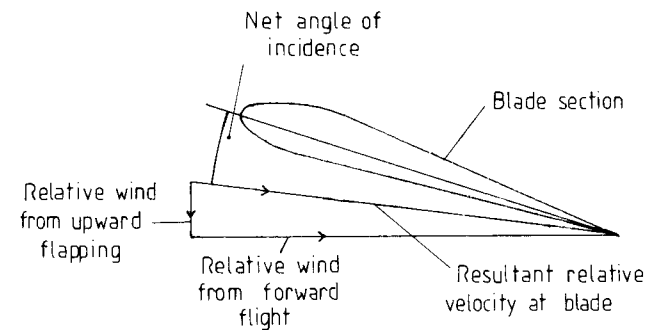


Fig. 4.3 Essence of blade flapping action.

hinges means that blade root stresses are avoided and no rolling moment is communicated to the airframe.

Contours of pressure level for a roll-balanced lift distribution are of the type shown in Fig. 4.4. The mean pressure level is now lower, the lift on the advancing side being greatly reduced, with only small compensation on the retreating side. The fore and aft sectors now carry the main lift load. The total lift can be restored in some degree by applying a general increase in blade incidence level through the pilot's control system (Section 4.3) but as this is done, the retreating blade, producing lift at relatively low airspeed, must ultimately stall. Also, compressibility effects such as shock-induced flow separation enter the picture, both on the advancing side where the Mach number is highest and on the retreating side where lower Mach number is combined with high blade incidence. Since the degree of load asymmetry across the disc increases with forward speed, the retreating-blade stall and its associated effects determine the maximum possible flight speed of the vehicle. For the conventional helicopter a speed of about 400 km/h (250 m/h) is usually regarded as the upper limit.

An additional feature of the asymmetry in velocity across the disc is that there exists a region on the retreating side where the flow over the blade is actually reversed. At 270° azimuth the resultant velocity at a point y of span is

$$U = \Omega y - V$$

or non-dimensionally,

$$u = \frac{U}{\Omega R} = r - \mu \quad (4.1)$$

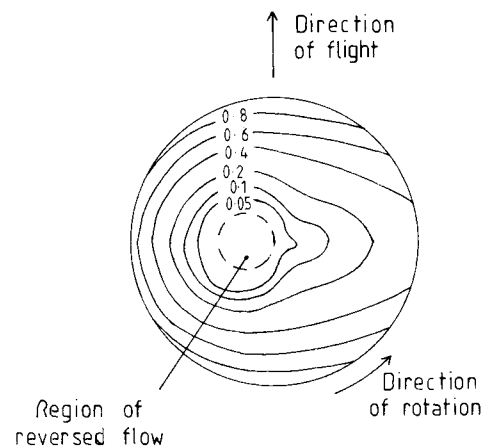


Fig. 4.4 Calculated pressure contours for roll-balanced rotation (after J.P. Jones).

Thus the flow over the blade is reversed inboard of the point $r = \mu$. It will be apparent that the reversed flow boundary is a circle of diameter μ centred at $r = \mu/2$ on the 270° azimuth. Dynamic pressure in this region is low, so the effect of the reversed flow on the blade lift is small, usually negligible from a performance aspect for advance ratios up to 0.4. Very precise calculations may require the reversed flow region to be taken into account and it may be important also in studies of blade vibration.

A flapping blade in rotation sets up Coriolis moments in the plane of the disc, and to relieve this it is usual to provide a second hinge, the *lead-lag hinge*, normal to the disc plane, allowing free in-plane motion. This may need to be fitted with a mechanical damper to ensure dynamic stability. The lead-lag motion of a blade contributes in only a minor way to rotor performance and we shall not study it further in the present book.

Blade rotation about a third axis, approximately normal to the flapping and lead-lag axes, is required for control of the blade incidence or pitch angle. This movement is provided by a *pitch bearing*, known alternatively as the *feathering hinge*, linked to a control system operated by the pilot (Section 4.3). The standard *articulated blade* thus possesses this triple movement system of flapping hinge, lead-lag hinge and pitch bearing in a suitable mechanical arrangement, located inboard of the lifting blade itself. The principles are illustrated in Fig. 4.5.

Strictly the blade root bending stress and helicopter rolling

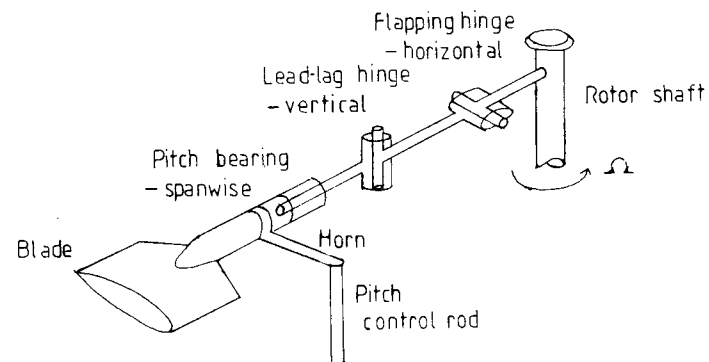


Fig. 4.5 Principles of articulated rotor hinge system.

moment are eliminated by flapping only if the hinge is located on the axis of rotation. This is impracticable for a rotor with more than two blades, so residual moments do exist. These are not important, however, if the offset of the hinge from the axis is only a few per cent of blade radius. The flapping hinge is therefore normally made the innermost, with an offset 3–4%. The lag hinge and pitch bearing can be more freely disposed: sometimes the former is the farther out of the two.

The total mechanical complexity of an articulated rotor is substantial. Hinge bearings operate under high centrifugal loads, so service and maintenance requirements are severe. Hinges, dampers and control rods make up a bulky rotorhead, which is likely to have a high parasitic drag – perhaps as much as the rest of the helicopter.

In modern rotors the flapping and lag hinges are often replaced by flexible elements which allow the flapping and lead-lag motions of the blades to take place, albeit with a degree of stiffness not present with free hinges. With such *hingeless rotors*, bending stresses and rolling moments reappear, in moderation only but sufficient to modify the stability and control characteristics of the helicopter (Chapter 8). The effect of a flexible flapping element can usually be calculated by equating it to a hinged blade with larger offset (10–15%). The use of a hingeless rotor is one way of reducing the parasitic drag of the rotorhead. A pitch bearing mechanism is of course needed for rotor control, as with the articulated rotor. The hingeless rotor of the Westland Lynx helicopter is pictured in Fig. 4.6.

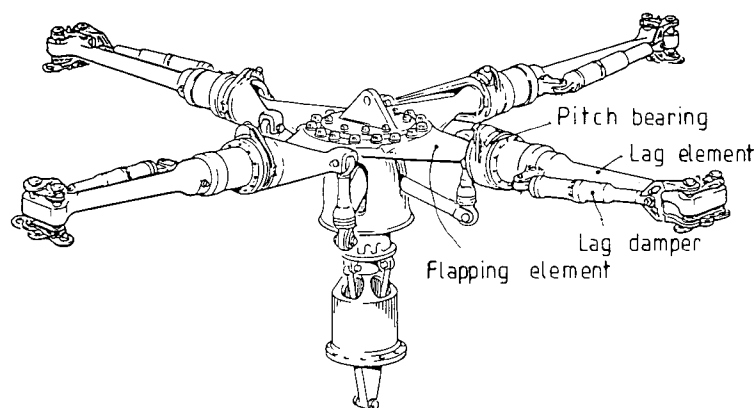


Fig. 4.6 Rotor hub of Lynx helicopter.

4.2 Flapping motion

To examine the flapping motion more fully we assume, unless otherwise stated, that the flapping hinge is on the axis of rotation. This simplifies the considerations without hiding anything of significance.

Referring to Fig. 4.7, the flapping takes place under conditions of dynamic equilibrium, about the hinge, between the aerodynamic lift (the exciting function), the centrifugal force (the 'spring' or restraining force) and the blade inertia (the damping). In other words, the once-per-cycle oscillatory motion is that of a dynamic system in resonance. The flapping moment equation is seen to be

$$\int_0^R y \, dT - \int_0^R m y^2 \ddot{\beta} \, dy - \int_0^R m \beta y^2 \Omega^2 \, dy = 0 \quad (4.2)$$

We shall return to this equation later.

The centrifugal force is by far the largest force acting on the blade and provides an essential stability to the flapping motion. The degree of stability is highest in the hover condition (where the flapping angle is constant) and decreases as the advance ratio increases. Bramwell's consideration of the flapping equation (p. 153 *et seq.*) leads in effect to the conclusion that the motion is dynamically stable for all realistic values of μ .

Maximum flapping velocities occur where the resultant air velocity is at its highest and lowest, that is at 90° and 270° azimuth. Maximum displacements occur 90° later, that is at 180° (upward) and 0°

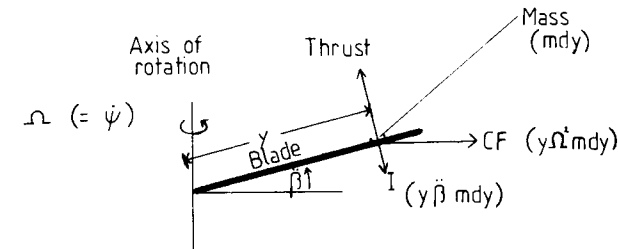


Fig. 4.7 Blade forces in flapping.

(downward). These displacements mean that the plane of rotation of the blade tips, the *tip-path plane* (TPP), is tilted backwards relative to the plane normal to the rotor shaft, the *shaft normal plane* (SNP).

In hover the blades cone upwards at a constant angle a_0 , say, to the shaft normal plane. The coning angle is that at which the blade weight is supported by the aerodynamic lift. Its existence has an additional effect on the orientation of the TPP during rotation in forward flight. Figure 4.8 shows that because of the coning angle, the flight velocity V has a lift-increasing effect on a blade at 180° (the forward blade) and a lift-decreasing effect on a blade at 0° (the rearward blade). This asymmetry in lift is, we see, at 90° to the side-to-side asymmetry discussed earlier: its effect is to tilt the TPP laterally and since the point of lowest tilt follows 90° behind the point of lowest lift, the TPP is tilted downwards to the right, that is on the advancing side. The coning and disc tilt angles are normally no more than a few degrees.

Since in any steady state of the rotor the flapping motion is periodic, the flapping angle can be expressed in the form of a Fourier series:

$$\beta = a_0 - a_1 \cos \psi - b_1 \sin \psi - a_2 \cos 2\psi - b_2 \sin 2\psi - \text{etc.} \quad (4.3)$$

Textbooks vary both in the symbols used and in the sign convention adopted. The advantage of using negative signs for the harmonic terms is that for normal forward flight the coefficients a_1 and b_1 have positive values. For most purposes the series can be limited to the constant and first harmonic terms, thus:

$$\beta = a_0 - a_1 \cos \psi - b_1 \sin \psi \quad (4.4)$$

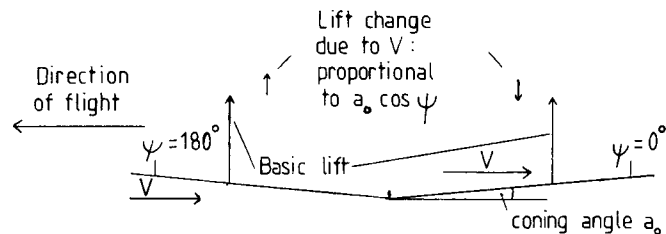


Fig. 4.8 Longitudinal lift asymmetry which leads to lateral tilt.

This form will be used in the aerodynamic analysis of the next chapter. For the moment we note that α_0 is the coning angle, α_1 the angle of backward tilt and b_1 the angle of sideways tilt. The inclusion of second or higher harmonic terms would represent waviness on the tip-path plane but any such is of secondary importance only.

Differentials of β will be needed in the later analysis: using the fact that the rotational speed Ω is $d\psi/dt$, these are:

$$\dot{\beta} = d\beta/dt = (\alpha_1 \sin \psi - b_1 \cos \psi) \quad \Omega = \Omega \frac{d\beta}{d\psi} \quad (4.5)$$

$$\ddot{\beta} = d^2\beta/dt^2 = \Omega^2 (\alpha_1 \cos \psi + b_1 \sin \psi) \quad (4.6)$$

4.3 Rotor control

Control of the helicopter in flight involves changing the magnitude of rotor thrust or its line of action or both. Almost the whole of the control task falls to the lot of the main rotor and it is on this that we concentrate. A change in line of action of the thrust would in principle be obtained by tilting the rotor shaft, or at least the hub, relative to the fuselage. Since the rotor is engine-driven (unlike that of an autogyro) tilting the shaft is impracticable. Tilting the hub is possible with some designs but the large mechanical forces required restrict this method to very small helicopters. Use of the feathering mechanism, however, by which the pitch angle of the blades is varied, either collectively or cyclically, effectively transfers to the aerodynamic forces the work involved in changing the magnitude and direction of the rotor thrust.

Blade feathering, or pitch change, could be achieved in various ways. Thus Saunders (1975)¹ lists the use of aerodynamic servo

tabs, auxiliary rotors, fluidically controlled jet flaps, or pitch links from a control gyro as possible methods. The widely adopted method, however, is through a swashplate system, illustrated in Fig. 4.9. Carried on the rotor shaft, this embodies two parallel plates, the lower of which does not rotate with the shaft but can be tilted in any direction by operation of the pilot's cyclic control column and raised or lowered by means of his collective lever. The upper plate is connected by control rods to the feathering hinge mechanisms of the blades and rotates with the shaft, while being constrained to remain parallel to the lower plate. Raising the collective lever thus increases the pitch angle of the blades by the same amount all round, while tilting the cyclic column applies a tilt to the plates and thence a cyclic pitch change to the blades, these

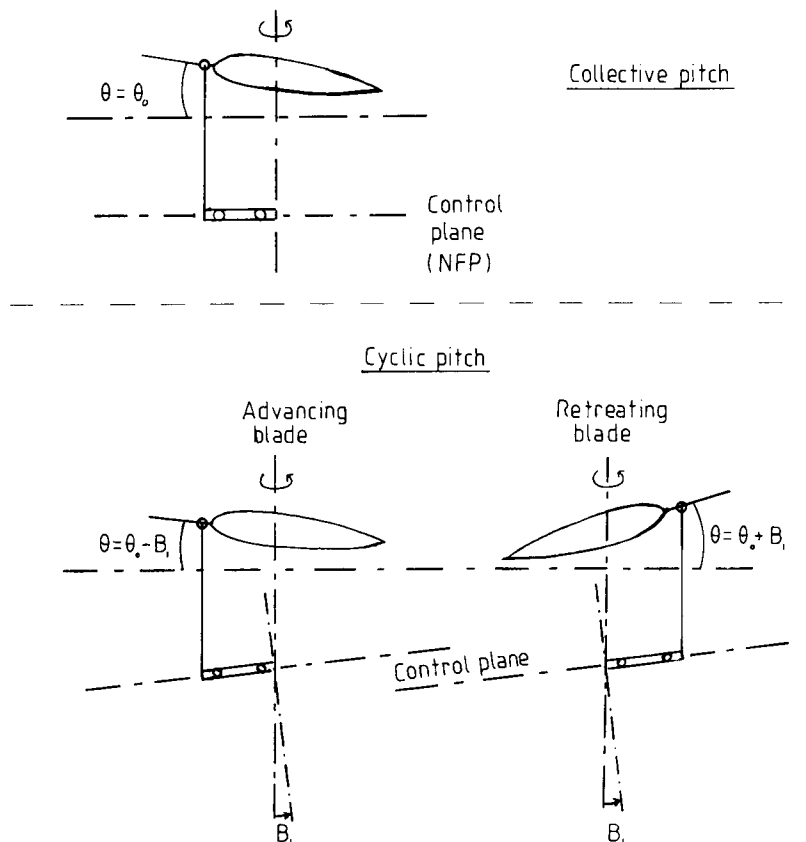


Fig. 4.9 Principles of swashplate system.

being constrained to remain at constant pitch relative to the upper plate. An increase of collective pitch at constant engine speed increases the rotor thrust (short of stalling the blades), as for take-off and vertical control generally. A cyclic pitch change alters the line of action of the thrust, since the tip-path plane of the blades, to which the thrust is effectively perpendicular, tilts in the direction of the swashplate angle.

Rotorhead designs vary considerably in detail but one such is pictured in Fig. 4.10. The rotor is of the hingeless type. Items discernible in the photograph include the flexible flapping elements, the feathering housing, the pitch control rods and, at the base of the arrangement, the swashplate mechanism. A good impression is gained of the mechanical complexity, strength and general bulkiness of this type of rotorhead installation.

Figure 4.11 is an interior view of a pilot's cockpit. The collective pitch lever is down at seat level on the pilot's left (right-hand seat); the cyclic control stick directly in front of him. The foot pedals control the collective pitch of the tail rotor (normally its only control), the purpose of which is to balance the torque of the main rotor, or when required to change the heading of the aircraft.

Cyclic pitch on the main rotor implies a blade angle changing with azimuth, relative to the shaft normal plane. The once-per-cycle periodicity means that the pitch angle can be described mathematically by a Fourier series, in like manner to that used for the flapping angle.

We write

$$\theta = \theta_0 - A_1 \cos \psi - B_1 \sin \psi - A_2 \cos 2\psi - B_2 \sin 2\psi \dots \quad (4.7)$$

in which, as before, only the constant and first harmonic terms are normally required:

$$\theta = \theta_0 - A_1 \cos \psi - B_1 \sin \psi \quad (4.8)$$

θ_0 represents the collective pitch, the terms in ψ the cyclic pitch. The factor A_1 , which applies maximum pitch when the blades are at 0° and 180° , is referred to as the *lateral cyclic coefficient* because the rotor response, phased 90° , produces a control effect in the lateral sense. Correspondingly, the factor B_1 is the *longitudinal cyclic coefficient*.

The value of pitch angle would be different if a different reference plane were used. In any flight condition, there is always one plane

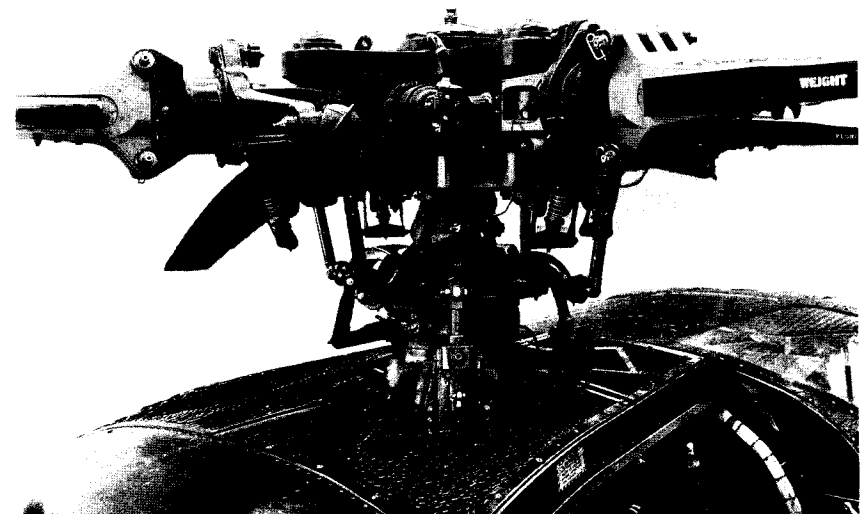


Fig. 4.10 Modern rotorhead showing flexible elements and swashplate system. (Reproduced courtesy of Westland Helicopters Ltd.)

relative to which the blade pitch remains constant with azimuth. This by definition is the plane of the swashplate, which is therefore known as the *control plane* or, referring to the elimination of cyclic pitch variation, the *no-feathering plane* (NFP). The no-feathering plane, though not fixed in the aircraft, is a useful adjustable datum for the measurement of aerodynamic characteristics considered in the next chapter.

In some contexts it is useful to refer to the axes TPA and NFA, perpendicular to the TPP and NFP, rather than to the planes themselves. Generally in forward flight these two axes and also the shaft axis will be away from the vertical (i.e. the normal to the flight path). Fig. 4.12 shows a common arrangement. The thrust line being inclined in the direction of flight, the TPP normal to it is tilted down at the nose relative to the horizontal (the flight direction). The TPA, being also the thrust line, is away from the vertical as shown. The shaft axis is tilted further from the vertical, the angle with the TPA being the tilt-back angle of the flapping motion. The



Fig. 4.11 Example of flight cabin interior. (Reproduced courtesy of Westland Helicopters Ltd.)

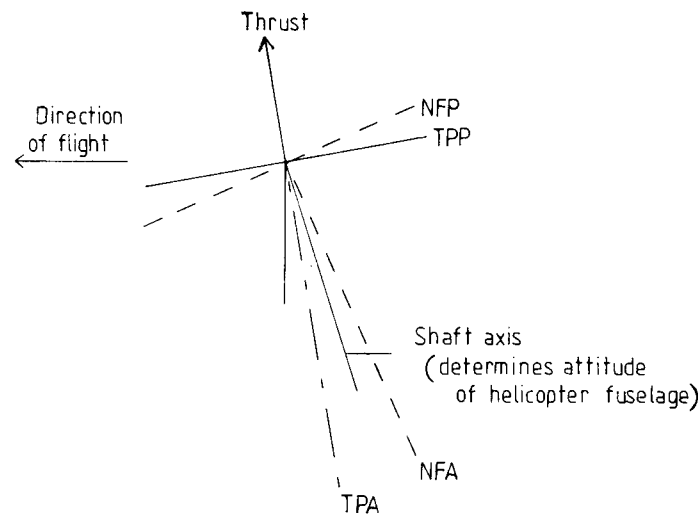


Fig. 4.12 A possible juxtaposition of axes in forward flight.

inclination of the shaft axis to the NFA depends upon the degree of feathering in the helicopter motion.

4.4 Equivalence of flapping and feathering

The performance of the rotor blade depends upon its angle of incidence to the tip-path plane. A given blade incidence can be obtained with different combinations of flapping and feathering. Consider the two situations illustrated in Fig. 4.13: these are views from the left side with the helicopter in forward flight in the direction shown. In situation 1 the shaft axis coincides with the TPA; there is therefore no flapping but the necessary blade incidences are obtained from feathering according to Equation 4.8.

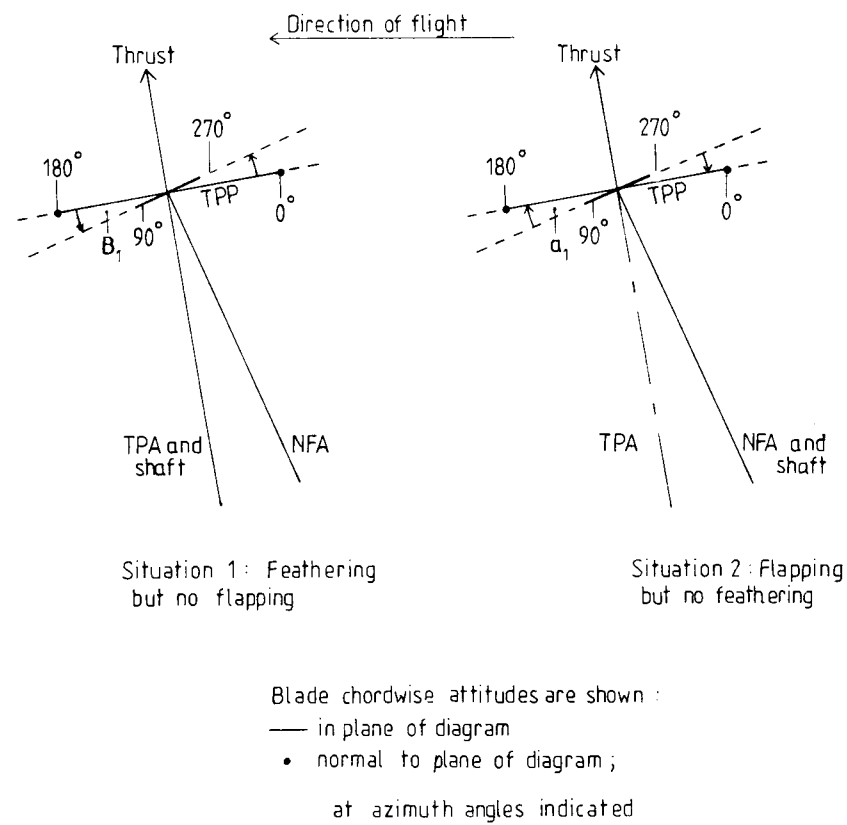


Fig. 4.13 Equivalence of flapping and feathering.

Blade attitudes at the four quarter points of a rotation are as indicated in the diagram. In situation 2 the shaft axis coincides with the NFA. By definition this means that feathering is zero: the blade angles however are obtained from flapping according to Equation (4.4). It is seen that if the feathering and flapping coefficients B_1 and a_1 are equal, the blade attitudes to the tip-path plane are identical around the azimuth in the two situations. The blade perceives a change in nose-down feathering, via the swash-plate, as being equivalent to the same angle change in nose-up flapping.

A pilot uses this equivalence in flying the helicopter, for example to trim the vehicle for different positions of the centre of gravity (CG). The rotor thrust, in direction and magnitude, depends upon the inclination of the tip-path plane in space and the incidence of the blades relative to it. The same blade incidence can be achieved, as we have seen, either with nose-up flapping or with the same degree of nose-down feathering, or of course with a combination of the two. By adjusting the relationship, using his cyclic control stick, the pilot is able to compensate for different nose-up or nose-down moments in the helicopter, arising from different CG positions. The angle of the shaft axis to the vertical, hence the attitude of the helicopter in space, varies with the CG position but the tip-path plane remains at a constant inclination to the direction of flight.

Reference

- ¹ Saunders, George H. (1975) *Dynamics of helicopter flight*. John Wiley and Sons Inc.

5 Rotor Aerodynamics in Forward Flight

The aerodynamic situation in forward flight is complex. Numerical methods have largely taken over the task of evaluation but an analytical treatment, using simplifying assumptions, is valuable for providing a basic understanding of rotor behaviour. Such a treatment is the subject of this present chapter. The mechanisms of the previous chapter affect essentially the details of blade element theory. Before turning to that, however, it is useful to examine briefly what can be made of momentum theory, which as has been said is principally a theory for hover and axial flight: also it may be asked to what situations is one led in considering a more detailed wake analysis under forward flight conditions.

5.1 Momentum theory

A modified actuator disc approach can be used. The basic proposal is due to Glauert¹ who, drawing an analogy between the rotor and an elliptically loaded circular wing, suggested that a mean induced velocity v_i could be expressed by the formula:

$$v_i = T/2\rho A V' \quad (5.1)$$

where

$$V' = \sqrt(V^2 + v_i^2) \quad (5.2)$$

V being the forward flight speed. The formula can be illustrated in flow terms as shown in Fig. 5.1: a circular jet of air at velocity V , of the same area as the rotor, or actuator disc, impinges upon the latter and is deflected downwards at velocity v_i at the disc and ultimately in the downstream flow at velocity $2v_i$. The similarity with the basic momentum flow discussed in Chapter 2 is obvious.

No proof exists, however, that the flow depicted in Fig. 5.1 is other than fictitious: the merit of the proposal is that the formula in Equation (5.1) reduces to that for hover – Equation (2.2) – when V is zero and, at the other extreme, if V is so large that V and V' are virtually identical, the formula converts to that for the induced velocity of an elliptically-loaded fixed wing. And both experiment and more detailed analysis (see for example Bramwell, Chapter 4) confirm that the Glauert proposal works well.

If v_h is written for the induced velocity in hover at the same thrust, we have

$$v_h^2 = T/2\rho A \quad (5.3)$$

and Equation (5.1) may be written:

$$\begin{aligned} v_i^2 &= \left(\frac{T}{2\rho A}\right)^2 \left(\frac{1}{V^2 + v_i^2}\right) \\ &= v_h^2/(V^2 + v_i^2) \end{aligned} \quad (5.4)$$

whence the equation for v_i in forward flight is:

$$\left(\frac{v_i}{v_h}\right)^4 + \left(\frac{V}{v_h}\right)^2 \left(\frac{v_i}{v_h}\right)^2 - 1 = 0 \quad (5.5)$$

The variation of induced velocity with forward speed is therefore as shown in Fig. 5.2. It is seen that v_i decreases rapidly as V increases and for all V/v_h greater than about 2 the fixed-wing analogy applies, that is to say:

$$\frac{v_i}{v_h} \approx \frac{v_h}{V} \quad (5.6)$$

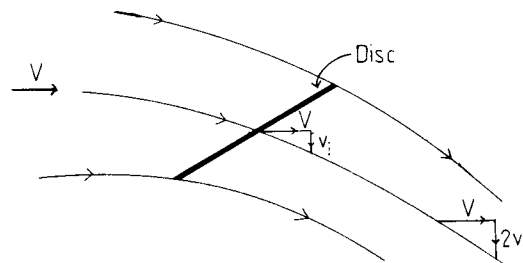


Fig. 5.1 Interpretation of Glauert formula for momentum theory in forward flight (after Bramwell).

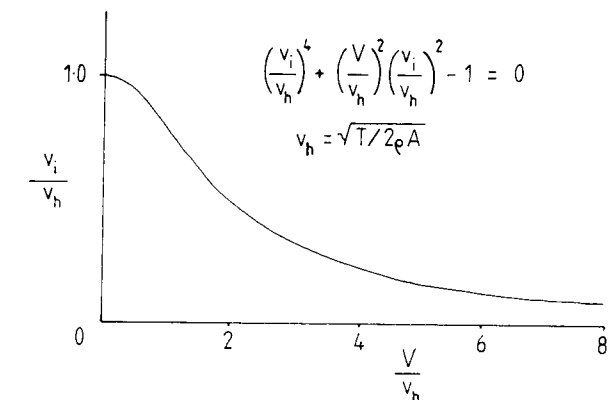


Fig. 5.2 Variation of induced velocity with forward speed.

In practice the induced velocity cannot be expected to be constant over the area of the disc. Standard aerofoil theory would suggest an upwash at the leading edge and a greater-than-mean downwash at the trailing edge. To allow for a variation of this kind, Glauert proposed a second formula:

$$v_i = (v_i)_o (1 + K r \cos \psi) \quad (5.7)$$

where $(v_i)_o$ is the value at the centre, taken to be that given by Equation (5.1), r is the proportionate radius from the centre and ψ is the azimuth angle. If the constant K is chosen to be greater than 1.0 (typically 1.2), the formula gives a negative value, that is an upwash, at the leading edge ($\psi = 180^\circ$). Equation (5.7) is often used as an input to numerical methods.

More elaborate treatments of the non-uniform induced velocity in forward flight have been devised, among which one of the foremost is the method of Mangler and Squire². Described at length by Bramwell (p. 127 *et seq.*), this method has shown satisfactory agreement with controlled experiments and is stated to be very useful in rotor calculations.

Reverting to the Glauert formula for uniform induced velocity, the induced power is:

$$P_i = T v_i = T^2/2\rho A (V^2 + v_i^2)^{1/2} \quad (5.8)$$

which at normal forward flight speeds becomes approximately

$$P_i = T^2/2\rho A V = T w/2\rho V, \quad (5.9)$$

that is directly proportional to the disc loading w .

In non-dimensional terms the first equality of Equation (5.8) is simply

$$C_{p_i} = \lambda_i C_T \quad (5.10)$$

where λ_i is $v_i/\Omega R$. It will be useful for the forward flight case to adopt a suffix i for that part of the total induced flow which is due to the thrust-dependent induced velocity v_i , as distinct from a part due to the forward velocity V .

As with hover, a practical approximation to allow for the effect of non-uniformity in v_i and other smaller correction factors is obtained by applying an empirical factor κ such that

$$C_{p_i} = \kappa \lambda_i C_T \quad (5.11)$$

The value of κ in forward flight is somewhat higher than that in hover, say 1.20 compared with the formerly suggested 1.15 (Section 3.6). Countering this however the induced velocity is seen in Fig. 5.2 to become quite small even at moderate forward speeds: it will duly emerge that C_{p_i} is then much smaller than other components of the total power requirement.

5.2 Wake analysis

As concerns a detailed analysis of the rotor wake, corresponding to that outlined in Chapter 2 for the hover, the complication introduced by forward flight comes down to the fact that at a given radial position, the blade incidence, and hence the circulation, varies widely around the azimuth. Each change of circulation results in a counter vortex being shed into the wake and since the change is a circumferential one, the vortex line in this case lies in the spanwise direction. This system of 'shed' vortices is now additional to the 'trailing' vortex system arising, as in hover, from the spanwise variations in circulation.

Undeterred by such multiplicity of complication, the modern computer, guided by skilled workers among whom may be mentioned Miller, Piziali and Landgrebe, is still capable of providing solutions. An example from Landgrebe's calculations shows in Fig. 5.3 a theoretical wake boundary at low advance ratio, compared with experiment by smoke visualization and also with the Glauert

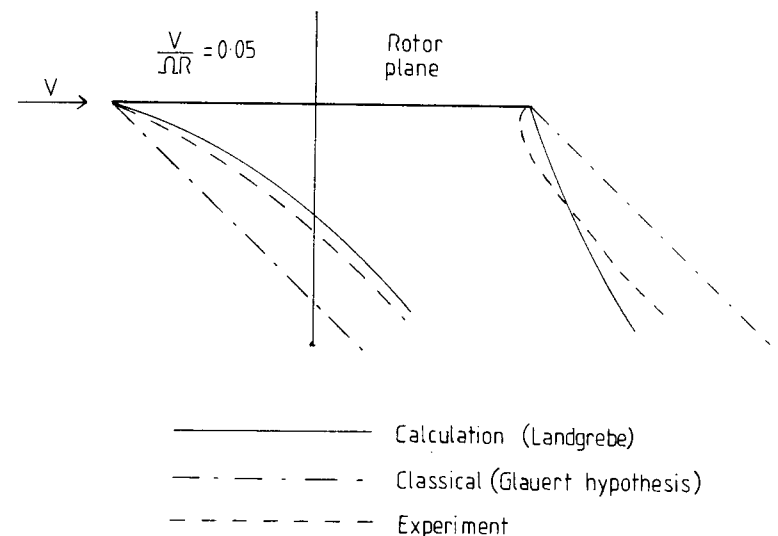


Fig. 5.3 Wake boundaries at low advance ratio (after Landgrebe).

momentum theory solution. The numerical solution and the experimental evidence agree well: momentum theory gives a much less accurate picture. A feature to note is that the boundary at the front of the disc lies close to the disc. At a higher advance ratio, more representative of forward flight, this feature and the general sweeping back of the wake would be much more marked.

This brief reference to what is a large subject in itself will suffice for the purposes of the present book. Extended descriptions can be found in the standard textbooks.

5.3 Blade element theory

5.3.1 Factors involved

An exposition of blade element theory follows the same broad lines as used for hover (Chapter 3), taking into account, however, the extra complexities involved in forward flight. We begin by introducing the additional factors which enter into a forward flight condition. Figure 5.4 shows a side view of the rotor disc – strictly a shallow cone as we have seen. Motion is to the left and is assumed horizontal, that is to say without a climb component. The

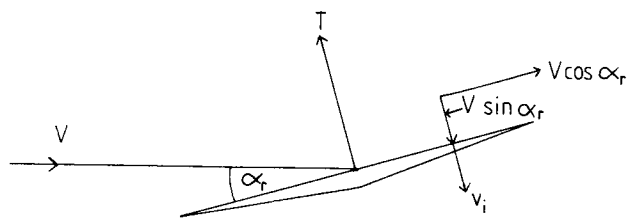


Fig. 5.4 Disc incidence and component velocities in forward flight.

plane enclosing the edge of the disc – the tip-path plane (TPP) – makes an angle α_r with the oncoming stream direction. α_r is reckoned positively downwards since that is the natural direction of tilt needed to obtain a forward component of the thrust. We shall use small-angle approximations as required. The flight velocity V has components $V \cos \alpha_r$ and $V \sin \alpha_r$ along and normal to the TPP. The advance ratio is:

$$\mu = \frac{V \cos \alpha_r}{\Omega R} \simeq \frac{V}{\Omega R} \quad (5.12)$$

as used previously. The total inflow through the rotor is the sum of $V \sin \alpha_r$ and v_i , the thrust related induced velocity.

Referring to Fig. 5.5, the resultant velocity U at a blade section is now a function of rotor rotation, helicopter forward speed, induced velocity and blade flapping motion. Components of U in the plane of the blade section are U_T and U_P ; additionally because of the forward speed factor there is a spanwise component U_R , shown in Fig. 5.6. Components U_T and U_R are readily defined; to first order these are:

$$U_T = \Omega_y + V \sin \psi \quad (5.13)$$

$$U_R = V \cos \psi \quad (5.14)$$

or, in non-dimensional form,

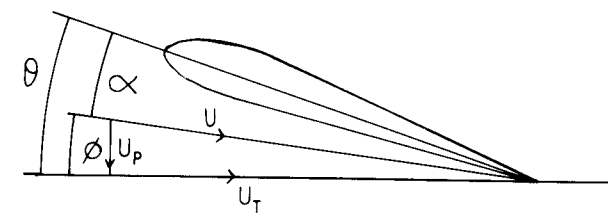
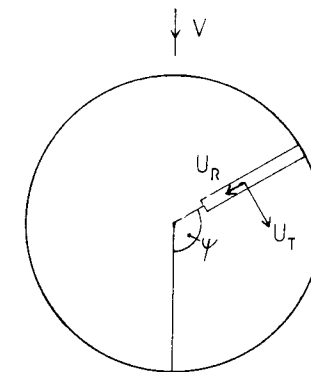
$$u_T = r + \mu \sin \psi \quad (5.15)$$

$$u_R = \mu \cos \psi \quad (5.16)$$

The component U_P has three terms, non-dimensionally as follows:

(1) inflow factor:

$$\lambda = \frac{V \sin \alpha_r + v_i}{\Omega R} = \mu \alpha_r + \lambda_i \quad (5.17)$$

Fig. 5.5 Component velocities U_T and U_P .Fig. 5.6 Component velocities U_T and U_R .

- (2) a component of u_R normal to the blade, which for a flapping angle β relative to the reference plane is seen (Fig. 5.7) to be βu_R or $\beta \mu \cos \psi$;
- (3) a component resulting from the angular motion about the flapping hinge; at station y along the span, this is:

$$y \frac{d\beta}{dt} \text{ or } y \frac{d\beta}{d\psi} \cdot \frac{d\psi}{dt} \text{ or } y \Omega \frac{d\beta}{d\psi} \text{ or } r \frac{d\beta}{d\psi}$$

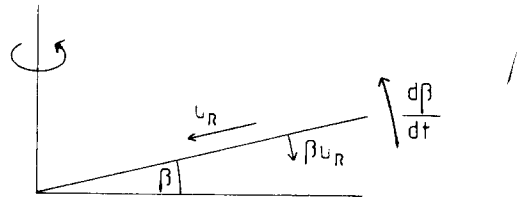
when non-dimensionalized.

Thus adding together,

$$u_p = \lambda + \beta \mu \cos \psi + r \frac{d\beta}{d\psi} \quad (5.18)$$

For small angles the resultant velocity U may be approximated by U_T . Blade angle of incidence may be written:

$$\alpha = \theta - \phi = \theta - U_p/U_T = \theta - u_p/u_T \quad (5.19)$$

Fig. 5.7 Flapping term in U_P .

Note that whereas the values of θ and ϕ depend upon the choice of reference plane, the actual blade incidence α does not, so the expression $(\theta - u_P/u_T)$ is independent of the reference plane used.

5.3.2 Thrust

Following the lines of the hover analysis in Chapter 3 we write an elementary thrust coefficient of a single blade at station y as

$$dC_T = \frac{\frac{1}{2}\rho U^2 c}{\rho \pi R^2 (\Omega R)^2} dy C_L = \frac{1}{2} \frac{c}{\pi R} \frac{U_T^2}{(\Omega R)^2} C_L \frac{dy}{R}$$

and for N blades, introducing the solidity factor σ and non-dimensionalizing,

$$dC_T = \frac{1}{2}\sigma u_T^2 C_L dr \quad (5.20)$$

On expressing C_L in the linear form

$$C_L = a\alpha = a(\theta - u_P/u_T), \quad (5.21)$$

Equation (5.20) becomes

$$dC_T = \frac{1}{2}\sigma a (\theta u_T^2 - u_T u_P) dr \quad (5.22)$$

For the hover we were able to write $u_T = r$, $u_P = \lambda$: in forward flight, however, u_T and u_P , and in general θ also, are functions of azimuth angle ψ . The elementary thrust must therefore be averaged around the azimuth and integrated along the blade. It is convenient to perform the azimuth averaging first and we therefore write the thrust coefficient of the rotor as:

$$C_T = \int_0^1 \frac{1}{2}\sigma a \left[\frac{1}{2\pi} \int_0^{2\pi} (\theta u_T^2 - u_P u_T) d\psi \right] dr \quad (5.23)$$

To expand the terms within the inside brackets, we recall from

Chapter 4 that the flapping angle β may be expressed in the form

$$\beta = a_0 - a_1 \cos \psi - b_1 \sin \psi, \quad (4.4)$$

from which also we have

$$\frac{d\beta}{d\psi} = a_1 \sin \psi - b_1 \cos \psi \quad (5.24)$$

For the feathering angle θ a similar Fourier expansion (Equation (4.8)) can be used: however, there is always one plane, the plane of the swashplate or no-feathering plane (NFP), relative to which there is no cyclic change in θ ; for our analytical solution therefore this will be used as the reference plane. Thus we have $\theta = \theta_0$, constant in azimuth, and following the same procedure as for hover we shall assume an untwisted blade, giving θ_0 constant also along the span. Averaging round the azimuth involves recognition that the operators

$$\int_0^{2\pi} \sin \psi d\psi, \int_0^{2\pi} \cos \psi d\psi \text{ and } \int_0^{2\pi} \sin \psi \cos \psi d\psi$$

are each equal to zero, whilst

$$\int_0^{2\pi} \sin^2 \psi d\psi \text{ and } \int_0^{2\pi} \cos^2 \psi d\psi$$

are each equal to π . Breaking down Equation (5.23) then, we obtain

$$\begin{aligned} \frac{1}{2\pi} \int_0^{2\pi} \theta u_T^2 d\psi &= \frac{1}{2\pi} \int_0^{2\pi} \theta_0 (r + \mu \sin \psi)^2 d\psi \\ &= \theta_0 (r^2 + \frac{1}{2}\mu^2) \end{aligned} \quad (5.25)$$

while

$$\begin{aligned} \frac{1}{2\pi} \int_0^{2\pi} u_P u_T d\psi &= \frac{1}{2\pi} \int_0^{2\pi} \left(\lambda + \beta \mu \cos \psi + r \frac{d\beta}{d\psi} \right) (r + \mu \sin \psi) d\psi \\ &= \lambda r \end{aligned} \quad (5.26)$$

all other terms cancelling out after substituting for β and $(d\beta/d\psi)$ and integrating. Hence finally,

$$\begin{aligned} C_T &= \int_0^1 \frac{1}{2}\sigma a \left[\theta_0 (r^2 + \frac{1}{2}\mu^2) - \lambda r \right] dr \\ &= \frac{1}{2}\sigma a [\frac{1}{3}\theta_0 (1 + 3\mu^2/2) - \frac{1}{2}\lambda] \end{aligned} \quad (5.27)$$

This is the simplest expression for the lift coefficient of a rotor in forward level flight. The assumptions on which it is based are the ones assumed for hover in Chapter 3, namely uniform induced velocity across the disc, constant solidity σ along the span and zero blade twist. As before it may be assumed that for a linearly twisted blade, Equation (5.27) can be used if the value of θ is taken to be that at three quarters radius. Also in Equation (5.27) the values of θ and λ are taken relative to the non-feathering plane as reference. Bramwell (p. 157) derives a significantly more complex expression for thrust when referred to disc axes (the tip-path plane) but since the transformation involves the assumption that actual thrust, to the accuracy required, is not altered as between the two reference planes, the change is a purely formal one and Equation (5.27) stands as a working formula.

5.3.3 In-plane H force

In hover the in-plane H force, representing principally the blade profile drag, contributed only to the torque (Fig. 3.2). Here, however, since the resultant velocity at the blade is $\Omega y + V \sin \psi$ (Equation (5.13)), the drag force on the advancing side exceeds the reverse drag force on the retreating side, leaving a net drag force on the blade, positive in the rearward direction.

Seen in azimuth (Fig. 5.8) the elementary H force, reckoned normal to the blade span and resolved in the rearward direction, is

$$dH = (dD \cos \phi + dL \sin \phi) \sin \psi \quad (5.28)$$

which may be written as dH_o plus dH_i where the suffices relate to the drag and lift-dependent terms, respectively. Treating the drag

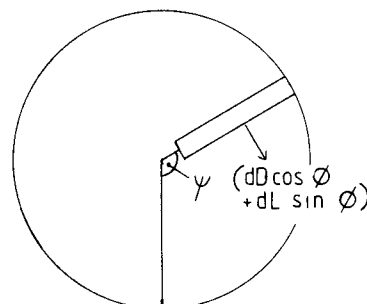


Fig. 5.8 Elementary H force.

term separately and making the usual approximations, we have

$$dH_o = dD \sin \psi = \frac{1}{2} \rho U_T^2 c dy C_{D_o} \sin \psi \quad (5.29)$$

In coefficient form, for N blades, this gives

$$\begin{aligned} dC_{H_o} &= \frac{\frac{1}{2} N_p U_T^2 c C_{D_o} \sin \psi dy}{\rho \pi R^2 (\Omega R)^2} \\ &= \frac{1}{2} \sigma C_{D_o} u_T^2 \sin \psi dr \\ &= \frac{1}{2} \sigma C_{D_o} (r + \mu \sin \psi)^2 \sin \psi dr \end{aligned} \quad (5.30)$$

Hence

$$\begin{aligned} C_{H_o} &= \frac{1}{2} \sigma C_{D_o} \int_0^1 \left[\frac{1}{2\pi} \int_0^{2\pi} (r + \mu \sin \psi)^2 \sin \psi d\psi \right] dr \\ &= \frac{1}{2} \sigma C_{D_o} \int_0^1 \mu r dr \\ &= \frac{1}{4} \sigma C_{D_o} \cdot \mu \end{aligned} \quad (5.31)$$

Overall then for the in-plane H force

$$C_H = \frac{1}{4} \sigma C_{D_o} \cdot \mu + C_{H_i} \quad (5.32)$$

Expressions can be obtained for the induced component C_{H_i} in terms of θ , λ , μ and the flapping coefficients a_0 , a_1 and b_1 : these are derived in varying forms in the standard textbooks, for example Bramwell p. 148 and Johnson p. 177. The relations are somewhat complex and since we shall not require to make further use of them in the present treatment and moreover in the usual case C_{H_i} is small compared with C_{H_o} , we can be satisfied with the reduction at Equation (5.32).

5.3.4 Torque and power

The elementary torque is

$$dQ = dH \cdot y = y(dD \cos \phi + dL \sin \phi) \quad (5.33)$$

Again there is a profile drag term, dQ_o say, and an induced term dQ_i . The former is readily manipulated thus (in coefficient form):

$$\begin{aligned} C_{Q_o} &= \frac{1}{2} \sigma C_{D_o} \int_0^1 \left[\frac{1}{2\pi} \int_0^{2\pi} (r + \mu \sin \psi)^2 r d\psi \right] dr \\ &= \frac{1}{2} \sigma C_{D_o} \int_0^1 (r^3 + \frac{1}{2} \mu^2 r) dr \end{aligned}$$

$$= \frac{1}{8}\sigma C_{D_o} (1 + \mu^2) \quad (5.34)$$

The induced term, after a lengthier manipulation, is shown (Bramwell p. 151) to be

$$C_{Q_i} = \lambda C_T - \mu C_H \quad (5.35)$$

giving for the total torque

$$C_Q = \frac{1}{8}\sigma C_{D_o} (1 + \mu^2) + \lambda C_T - \mu C_H \quad (5.36)$$

Using Equation (5.32) this becomes

$$\begin{aligned} C_Q &= \frac{1}{8}\sigma C_{D_o} (1 + \mu^2) + \lambda C_T - \mu C_H + \frac{1}{4}\sigma C_{D_o} \cdot \mu^2 \\ &= \frac{1}{8}\sigma C_{D_o} (1 + 3\mu^2) + \lambda C_T - \mu C_H \end{aligned} \quad (5.37)$$

Now by Equation (5.17) the inflow factor λ is a function of the inclination α_r of the tip-path plane, which clearly depends upon the drag not only of the rotor but of the helicopter as a whole. Examining the relationships for trimmed level flight, illustrated in Fig. 5.9, we have approximately

$$T = W \quad (5.38)$$

$$T\alpha_r = H + D_p \quad (5.39)$$

D_p being the parasite drag of the fuselage, including tail rotor, tail plane and any other attachments. Thus

$$\begin{aligned} \alpha_r &= \frac{H}{T} + \frac{D_p}{T} \\ &= \frac{C_H}{C_T} + \frac{D_p}{W} \end{aligned} \quad (5.40)$$

whence

$$\begin{aligned} \lambda &= \lambda_i + \mu\alpha_r \\ &= \lambda_i + \mu \frac{C_H}{C_T} + \mu \frac{D_p}{W} \end{aligned} \quad (5.41)$$

Using this in Equation (5.37) the power coefficient is expressed in the form

$$C_P = C_Q = \lambda_i C_T + \frac{1}{8}\sigma C_{D_o} (1 + 3\mu^2) + \mu \frac{D_p}{W} C_T \quad (5.42)$$

which is seen to be the sum of terms representing the induced or

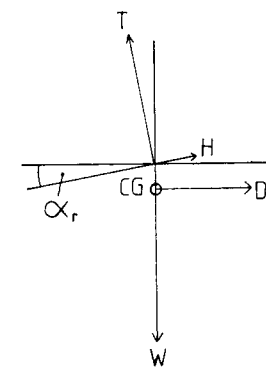


Fig. 5.9 Forces in trimmed level flight.

lift-dependent drag, the rotor profile drag and the fuselage parasite drag. The first of these had already been derived (Equation (5.10)) when considering the adaptation of momentum theory to forward flight.

In practice both the induced and profile-drag power requirements are somewhat higher than are shown in Equation (5.42). An empirical correction factor κ for the induced power was suggested in Equation (5.11). For the profile-drag power the deficiency of the analytical formula arises from neglect of:

- (1) a spanwise component of drag (Fig. 5.8);
- (2) a yawed-wing effect on the profile drag coefficient at azimuth angles significantly away from 90° and 270°;
- (3) the reversed flow region on the retreating side.

The first of these factors is probably the most important. They are conventionally allowed for by substituting for the factor 3 in Equation (5.42) an empirical, larger factor, k say. Studies by Bennett³ and Stepniewski⁴ suggest that an appropriate value is between 4.5 and 4.7. Industrial practice tends to be based on a firm's own experience: thus a value commonly used by Westland Helicopters is 4.65.

With the empirical corrections embodied, the power equation takes the form:

$$C_P = \kappa \lambda_i C_T + \frac{1}{8}\sigma C_{D_o} (1 + k \mu^2) + \mu \frac{D_p}{W} C_T \quad (5.43)$$

This will be followed up in the chapter on helicopter performance

(Chapter 7). In the present chapter we take our analytical study of the rotor aerodynamics two stages further; firstly examining the nature of the flapping coefficients a_0 , a_1 and b_1 in terms of θ , λ and μ ; and secondly looking at some typical values of collective pitch θ , inflow factor λ and the flapping coefficients in relation to the forward speed parameter μ and the level of thrust coefficient C_T .

5.3.5 Flapping coefficients

The flapping motion is determined by the condition that the net moment of forces acting on the blade about the flapping hinge is zero. Referring back to Fig. 4.7, the forces on an element dy of blade span, of mass $m dy$ where m is the mass per unit span, are:

- (1) the aerodynamic lift, expressed as an element of thrust dT , acting on a moment arm y ;
- (2) a centrifugal force $y\Omega^2 m dy$, acting on a moment arm $y\beta$;
- (3) an inertial force $y \ddot{\beta} m dy$, acting on a moment arm y ;
- (4) a blade weight moment, small in comparison with the rest and therefore to be neglected.

These lead to the flapping moment relationship given in Equation (4.2). Writing the aerodynamic or thrust moment for the time being as M_T , we have

$$\int_0^R \beta y^2 \Omega^2 m dy + \int_0^R \ddot{\beta} y^2 m dy = M_T$$

Assuming the spanwise mass distribution is uniform, m is constant and the equation integrates to

$$\beta \Omega^2 m \frac{1}{3} R^3 + \ddot{\beta} m \frac{1}{3} R^3 = M_T \quad (5.44)$$

Substituting the first order Fourier expressions for β and $\ddot{\beta}$ leads to

$$m \Omega^2 \frac{1}{3} R^3 a_0 = M_T \quad (5.45)$$

Thus the aerodynamic moment M_T is invariant with azimuth angle ψ . If I is written for the moment of inertia of the blade about its hinge, that is to say

$$I = \int_0^R y^2 m dy = \frac{1}{3} m R^3 \quad (5.46)$$

we have

$$a_0 = M_T / I \Omega^2 \quad (5.47)$$

Now M_T may be written:

$$M_T = \int_0^R y \frac{dT}{dy} dy = \frac{1}{2} \rho ac \int_0^R (\theta U_T^2 - U_P U_T) y dy$$

so that, in dimensionless form,

$$a_0 = \frac{1}{2} \gamma \int_0^1 (\theta u_T^2 - u_P u_T) r dr \quad (5.48)$$

where γ is written for the quantity $\rho ac R^4/I$ and is known as the Lock number. Replacing u_T and u_P by their definitions in Equation (5.15) and (5.18), and substituting for β and $d\beta/d\psi$ the right-hand side of Equation (5.48) develops to:

$$\begin{aligned} \frac{1}{2} \gamma \int_0^1 [\theta (r^2 + \frac{1}{2}\mu^2) - \lambda r + \text{terms in } \sin \psi \\ + \text{terms in } \cos \psi] r dr \end{aligned}$$

Since M_T is independent of ψ , its value can be obtained by integrating only the first part of this expression. Hence

$$\begin{aligned} a_0 &= \frac{1}{2} \gamma \int_0^1 [\theta (r^3 + \frac{1}{2}r\mu^2) - \lambda r^2] dr \\ &= \frac{1}{8} \gamma [\theta (1 + \mu^2) - 4\lambda/3] \end{aligned} \quad (5.49)$$

This is for an untwisted blade ($\theta = \text{constant } \theta_0$) or in the usual way for a linearly twisted blade with θ taken at three-quarters radius.

Also because of the independence of M_T the terms in $\sin \psi$ and those in $\cos \psi$ are each separately equatable to zero. These two equations yield expressions for the first harmonic coefficients a_1 and b_1 , namely

$$a_1 = \frac{\mu(\frac{1}{3}8\theta_0 - 2\lambda)}{1 - \frac{1}{2}\mu^2} \quad (5.50)$$

$$b_1 = \frac{4 \mu a_0 / 3}{1 + \frac{1}{2}\mu^2} \quad (5.51)$$

The above three equations represent the classical definitions of flapping coefficients, in which θ and λ have been defined relative to the no-feathering plane. Equivalent though rather more complex definitions relative to the tip-path plane are given by Johnson p. 189 or Bramwell p. 157. Bramwell's equations, whilst not completely general, are probably accurate enough for most purposes

and are quoted here for ease of reference:

$$a_0 = \frac{1}{8}\gamma [\theta (1 + \mu^2) - \frac{1}{3}4 \lambda_T + \mu a_1] \quad (5.52)$$

$$a_1 = \mu [\frac{1}{3}8 \theta - 2 \lambda_T]/(1 + \frac{1}{2}3 \mu^2) \quad (5.53)$$

$$b_1 = \frac{1}{3}4 \mu a_0/(1 + \frac{1}{2}\mu^2) \quad (5.54)$$

The corresponding relationship for thrust coefficient is:

$$C_T = \frac{1}{2}\sigma a [\frac{1}{3}\theta (1 + \frac{1}{2}3 \mu^2) - \frac{1}{2}\lambda_T - \frac{1}{2}\mu a_1] \quad (5.55)$$

5.3.6 Typical numerical values

Calculations have been made to illustrate in broad fashion the ways in which parameters discussed in the foregoing analysis vary with one another and particularly with forward speed. For this purpose the following values have been used:

rotor solidity $\sigma = 0.08$

blade lift slope $a = 5.7$

Lock number $\gamma = 8$

aircraft weight ratio $W/\rho(\Omega R)^2 A = 0.008$

parasite drag factor $f/A = 0.016$

The parasite drag factor is a form of expression in common use, in which f is the 'equivalent flat plate area' defined by

$$D_p = \frac{1}{2}\rho V^2 f \quad (5.56)$$

D_p being the parasite drag and A the rotor disc area.

Figure 5.10 shows the variation of inflow factor λ with advance ratio μ at two levels of thrust coefficient. λ as defined in Equation (5.17) is relative to the tip-path plane, so is denoted by λ_T in the diagram. The variation shows a minimum value at moderate μ , inflow being high at low μ because the induced velocity is large and high again at high μ because of the increased forward tilt of the tip-path plane required to overcome the parasite drag. The lower the thrust coefficient, the more marked is the high μ effect.

The corresponding variation of collective thrust angle θ , for $C_T/\sigma = 0.1$, is shown in the same diagram. The variations of θ and λ are similar in character, as might be expected from Equation (5.55).

Combination of Equations (5.17) and (5.55) leads, on elimination

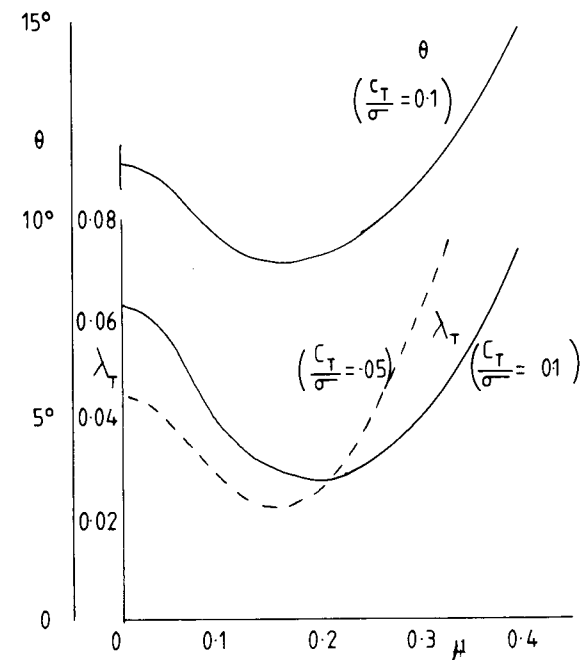


Fig. 5.10 Calculated values of λ_T and θ versus μ

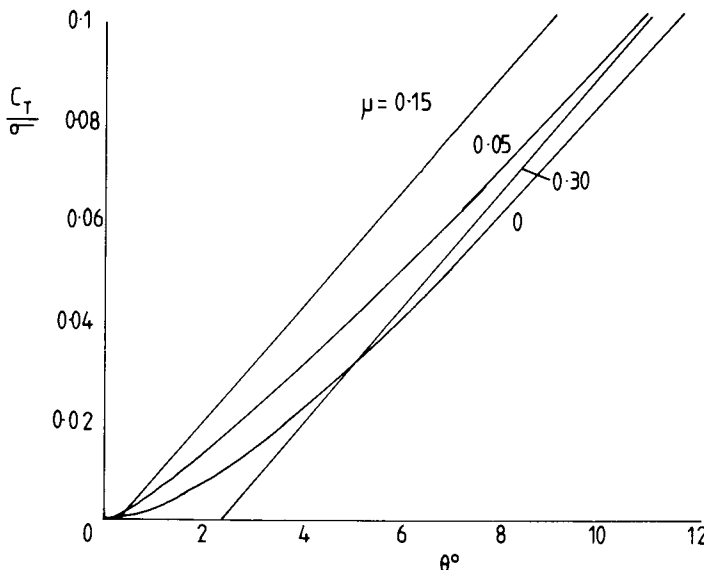
of λ , to a direct relationship between C_T and θ which, using the chosen values of aircraft weight ratio and parasite drag factor in the final term, is:

$$\theta = \frac{2}{\sigma a B} C_T + \frac{3}{2} \frac{v_i}{v_h} \sqrt{\frac{1}{2} C_T} + \frac{3}{2} \mu^3 \quad (5.57)$$

where B is a slowly decreasing function of μ :

$$B = \frac{1}{3} (1 + \frac{1}{2}3 \mu^2) + \mu^2 (\frac{4}{3} - 2\mu^2) \quad (5.58)$$

Note that when μ is zero, $B = \frac{1}{3}$ and $v_i/v_h = 1$, so that we have Equation (3.28) as previously derived for the hover. Figure 5.11 shows variations of θ with C_T for different levels of μ . The characteristics at low and high forward speed are significantly different. When μ is zero or small the variation is non-linear, θ increasing rapidly at low thrust coefficient owing to the induced flow term (the second expression in the equation) and more slowly at higher C_T as the first term becomes dominant. At high μ , however, the

Fig. 5.11 Calculated values of C_T/σ versus θ

induced velocity factor v_i/v_h is so small that the second term becomes negligible for all C_T , so the θ/C_T relationship is effectively linear. The intercept on the θ axis reflects the particular value of μ while, more interestingly, with μ and σ known the slope is a function only of the lift slope 'a'. This provides an experimental method for determining 'a' in a practical case.

A final illustration of (Fig. 5.12) shows the flapping coefficients a_0 , a_1 and b_1 as functions of μ . These have been calculated using Equations (5.52) to (5.54). The coning angle a_0 varies only slightly with μ , being essentially determined by the thrust coefficient. It may readily be shown in fact that a_0 is approximately equal to $(6 C_T \gamma)/(8 \sigma a)$ which with our chosen numbers has the value 0.105° or 6.0°. The longitudinal coefficient a_1 is approximately linear with forward speed, showing however an effect of the increase of λ at high speed. The lateral coefficient b_1 is also approximately linear, at about one third the value of a_1 . In practice b_1 at low speeds depends very much on the longitudinal distribution of induced velocity (assumed uniform throughout the calculations) and tends to rise to an early peak as indicated by a broken line in the diagram.

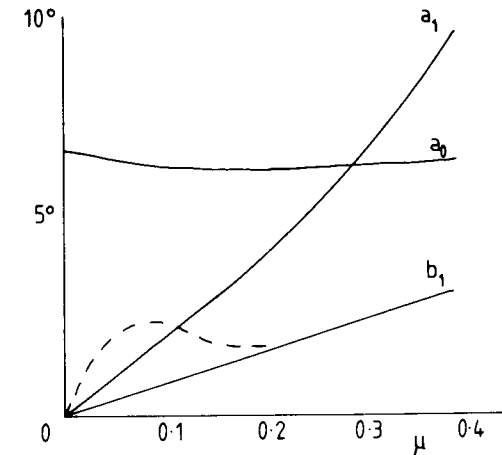


Fig. 5.12 Calculated values of flapping coefficients.

References

- 1 Glauert, H. (1926) 'A general theory of the autogiro'. *R & M 1111*.
- 2 Mangler, K.W. and Squire, H.B. (1950) 'The induced velocity field of a rotor'. *R & M 2642*.
- 3 Bennett, J.A.J. (1940) 'Rotary wing aircraft'. *Aircraft Engineering*, March 1940.
- 4 Stepniewski, W.Z. (1973) 'Basic aerodynamics and performance of the helicopter'. *AGARD Lecture Series 63*.

6 Aerodynamic Design

6.1 Introductory

In this chapter are described some of the trends in aerodynamic design which in the latter part of the twentieth century are making the helicopter a considerably more efficient flying vehicle than it formerly was. In earlier years the low power-to-weight ratio of piston engines necessitated the use of large rotors to provide the all-important vertical lift capability: both profile drag and parasite drag were unavoidably high in consequence and forward speeds were therefore so low as to consign the problems of refining either the lift or drag performance to a low, even zero, priority. With the adoption of gas-turbine engines, and an ever increasing list of useful and important applications for helicopters, in both military and civil fields of exploitation, forward-flight performance has become a more lively issue, even to the point of encouraging comparisons with fixed-wing aircraft in certain specialized contexts (an example is given in Chapter 7). Some improvements in aerodynamics stem essentially and naturally from fixed-wing practice. A stage has now been reached at which these appear to be approaching, or even to have arrived at, optimum levels in the helicopter application and therefore a substantial description here is appropriate. Further enhancements, concerned with the fundamental nature of the rotor system, may yet emerge to full development: one such is the use of higher harmonic control, which is described briefly. In the concluding section an account is given of a step-by-step method of defining the aerodynamic design parameters of a new rotor system.

6.2 Blade section design

In the design of rotor blade sections there is an *a priori* case for following the lead given by fixed-wing aircraft. It could be said, for instance, that the use of supercritical aerofoil sections for postponing the drag-rise Mach number is as valid an objective for the advancing blade of a rotor as for the wing of a high-subsonic transport aircraft. Or again, the use of blade camber to enhance maximum lift may be as valuable for the retreating blade as for a fixed wing approaching stall. Having accepted, say, this latter principle, there remains a problem of adapting it to the helicopter environment: this calls for particularized research, a great deal of which has been done in recent years.

The widely ranging conditions of incidence and Mach number experienced by a rotor blade in forward flight are conveniently illustrated by a ‘figure-of-eight’ diagram (Fig. 6.1(a)) which plots these conditions for a particular station on the blade near the tip ($r = 0.91$ in the case shown) at a specified value of μ . The hover would be represented by a single point: as μ is increased the figure-of-eight expands, extending into regions of higher α (or C_L) and higher M .

Plotting on such a diagram the α - M loci of $C_{L_{\max}}$ and M_D (the drag-rise Mach number) for a particular blade section, these being obtained independently, as for example by two-dimensional section tests in a wind tunnel, gives an indication of whether either blade stall or drag divergence will be encountered in the rotor at the particular level of μ . The example in Fig. 6.1(b) relates to a symmetrical, 12% thick, NACA 0012 section. It is seen that the retreating-blade loop passes well into the stalled region and the advancing-blade loop likewise into the drag-rise region.

NACA 0012 was the standard choice for helicopter blade sections over many years. Modern sections embodying camber to increase maximum lift have been developed in various series, of which the ‘VR’ Series in the USA and the ‘96’ Series in the UK are examples. Results for a 9615 section are shown in Fig. 6.1(c). The figure-of-eight now lies wholly within the $C_{L_{\max}}$ locus, confirming an improvement in lift performance. Additionally the high Mach number drag rise now affects a much reduced portion of the retreating-blade loop, and the advancing-blade loop not at all, so a reduction in power requirement can be expected.

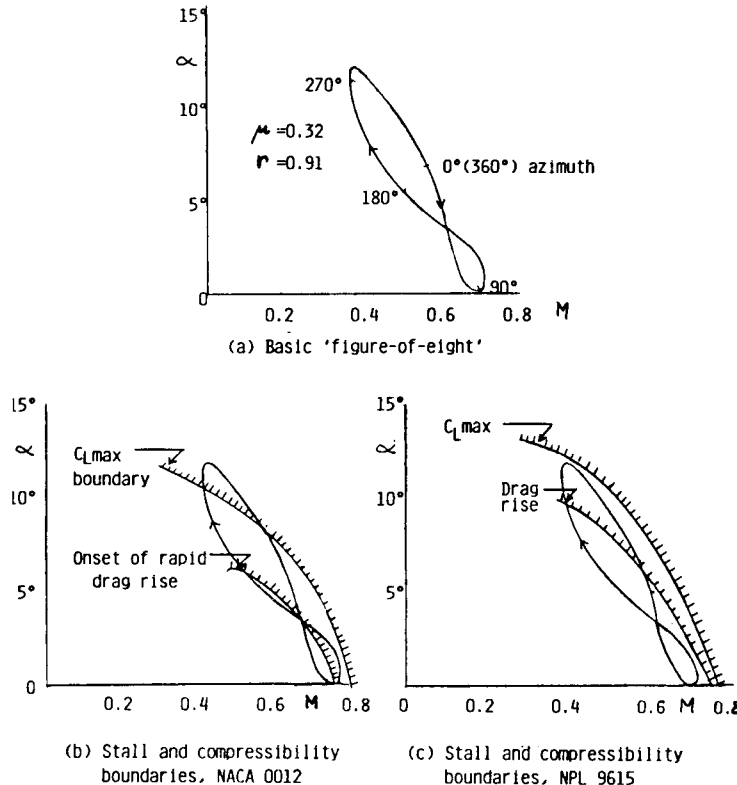


Fig. 6.1 Figure-of-eight diagrams for a typical blade.

The evidence, though necessary, is not of itself sufficient, however. To ensure acceptability of the cambered section for the helicopter environment, additional aspects of a major character need to be considered. One is the question of section pitching moments. The use of camber introduces a nose-down C_{M_0} (pitching moment at zero lift), which has an adverse effect on loads in the control system. A gain in $C_{L_{max}}$ must therefore be considered in conjunction with the amount of C_{M_0} produced. One way of controlling the latter is by the use of reflex camber over the rear of a profile. Wilby¹ gives comparative results for a number of section shapes of the '96' Series, tested in a wind tunnel under two-dimensional steady-flow conditions. A selection of his results is reproduced in Fig. 6.2, from which we can see that the more spectacular gains in $C_{L_{max}}$, (30% to 40%) tend to be associated with more adverse

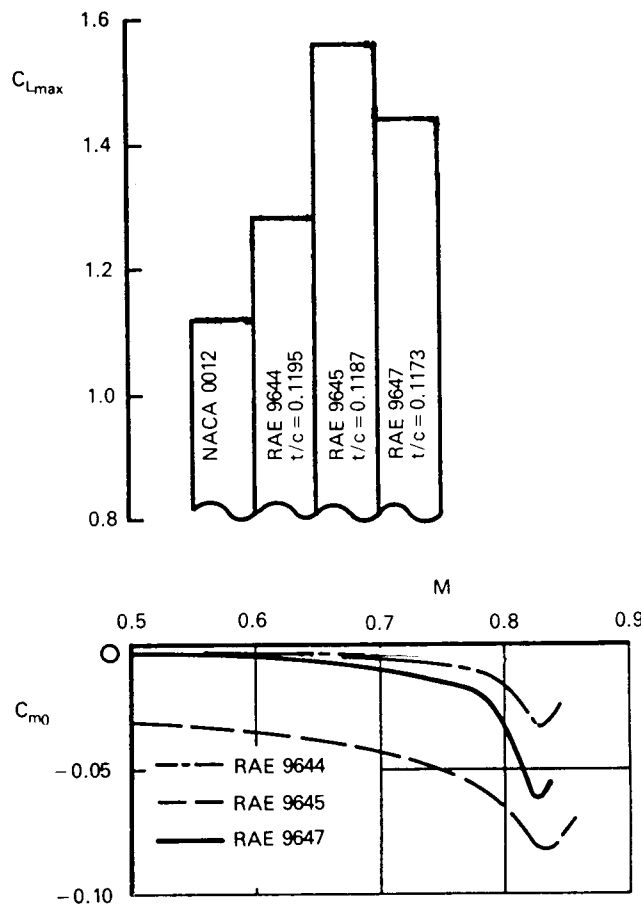


Fig. 6.2 Comparison of $C_{L_{max}}$ and C_{M_0} for various blade section shapes (after Wilby).

pitching moments, especially above about 0.75 Mach number which would apply on the advancing side of a rotor. Generally, therefore, compromises must be sought through much careful section shaping and testing. Moreover, whilst aiming to improve blade lift performance for the retreating sector, care must be taken to see that the profile drag is not increased, either at low C_L and high Mach number for the advancing sector, or at moderate C_L and moderate Mach number for the fore and aft sectors which in a balanced forward flight condition will carry the main thrust load.

Whilst static testing of this nature is very useful in a comparative sense, it cannot be relied upon to give an accurate final value of

$C_{L_{\max}}$, because the stall of a rotor blade in action is known to be dynamic in character, owing to the changes in incidence occurring as the blade passes through the retreating sector. Farren² recorded as long ago as 1935 that when an aerofoil is changing incidence, the stalling angle and $C_{L_{\max}}$ may be different from those occurring under static conditions. Carta³ in 1960 reported oscillation tests on a wing with 0012 section suggesting that this dynamic situation would apply in a helicopter context. Figure 6.3 shows a typical result of Carta's tests. When the aerofoil was oscillated through 6° on either side of 12° incidence (just above the static stalling angle), with a representative rotor frequency, a hysteresis loop in lift coefficient was obtained, in which the maximum C_L reached during incidence increase was about 30% higher than the static level.

Many subsequent researchers, among them Ham⁴, McCroskey⁵, Johnson and Ham⁶ and Beddoes⁷, have contributed to the provision of data and the evolution of theoretical treatments on dynamic stall and in the process have revealed the physical nature of the flow, which is of intrinsic interest. As blade incidence increases beyond the static stall point, flow reversals are observed in the upper-surface boundary layer but for a time these are not transmitted to the outside potential flow. Consequently the lift goes on increasing with incidence. Eventually, flow separation develops at the leading edge (or it may be behind a recompression shock close to the leading edge), creating a transverse vortex which begins to travel downstream. As the vortex rolls back along the upper surface into the mid-chord region, lift continues to be generated but a large nose-down pitching moment develops owing to the redistribution of upper surface pressure. Passage of the vortex beyond the trailing edge results in a major breakdown of flow. Finally, when the incidence falls below the static stall angle as the blade approaches the rear of the disc, the flow reattaches at the leading edge and normal linear lift characteristics are re-established.

Some further results for the RAE 9647 aerofoil section are shown in Fig. 6.4, in this case from blade oscillation tests over four different incidence ranges. As the range is moved up the incidence scale, the hysteresis loop develops in normal-force coefficient (representing C_L) and the pitching moment 'break' comes into play. In practice it is the latter which limits the rotor thrust, by reason of the large fluctuations in pitch-control loads and in blade torsional vibrations which are set up. It is of interest to note that in

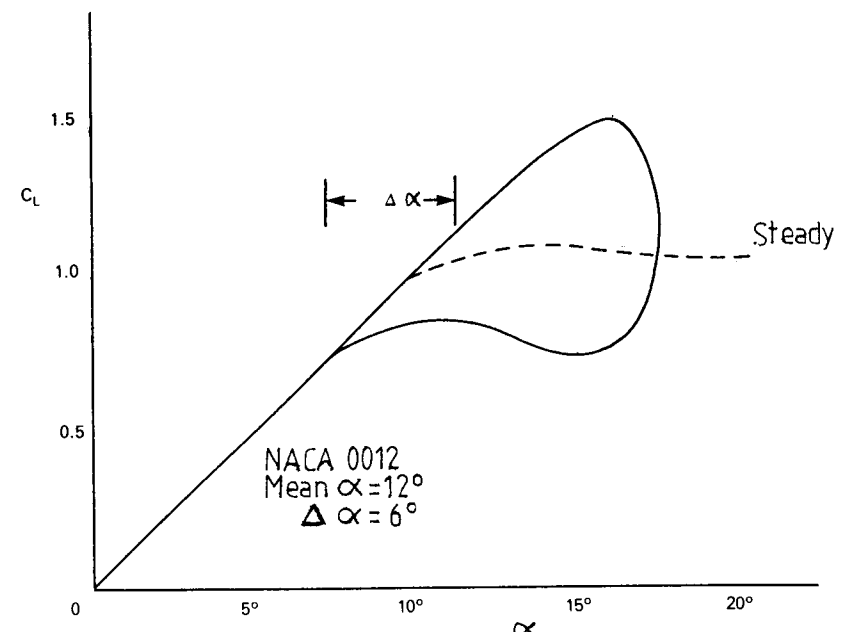


Fig. 6.3 Lift hysteresis for oscillating blade (after Carta).

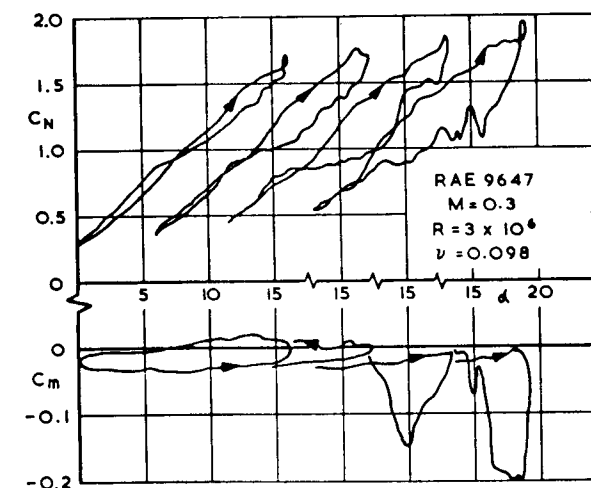


Fig. 6.4 Development of lift hysteresis and pitching moment break as incidence range is raised (after Wilby).

the results shown the normal coefficient reached at the point of pitching-moment break is about 1.8. Considerably higher values may in fact be attained; however it is to be noted that this value on the retreating blade is not particularly important in itself, since what matters more is the amount of lift produced by the other blades in the fore and aft sectors, where in a balanced rotor the major contributions to thrust are made.

Writing in 1989, one sees a situation on blade section design still capable of further development. So far the emphasis has been placed on improving the lift capability of the retreating blade. As the aspect of fuel economy in helicopter flight gains in importance, the incentive grows to reduce blade profile drag, particularly for the advancing sector. In this area there are probably improvements to be had by following the lead given by fixed-wing aircraft in the use of so-called supercritical wing sections. A further comment putting the incentive into context is made in Chapter 7.

6.3 Blade tip shapes

The loading on a helicopter blade is highly concentrated in the region of the tip, as has been seen (Fig. 2.12). It is unlikely that a plain rectangular planform is the optimum shape for the task of carrying this load and consequently investigations into tip design are a feature of modern aerodynamic research. Since resultant velocities in the tip region on the advancing blade are close to Mach 1.0, it is natural to enquire whether sweepback can be incorporated to delay the compressibility drag rise and thereby reduce the power requirement at a given flight speed or alternatively raise the maximum speed attainable. The answer is not so immediately obvious as in the case of a fixed wing, because a rotor blade tip which at one moment is swept back relative to the resultant airflow, in the next moment lies across the stream. In fact, however, the gain from sweepback outweighs the loss, as is indicated in a typical case by Wilby and Philippe⁸ (Fig. 6.5): a large reduction in Mach number normal to the leading edge is obtained over the rear half of the disc, including a reduction in maximum Mach number of the cycle (near $\psi = 90^\circ$), at the expense of a small increase in the forward sector ($\psi = 130^\circ$ to 240°). Reductions in power required were confirmed in the case shown.

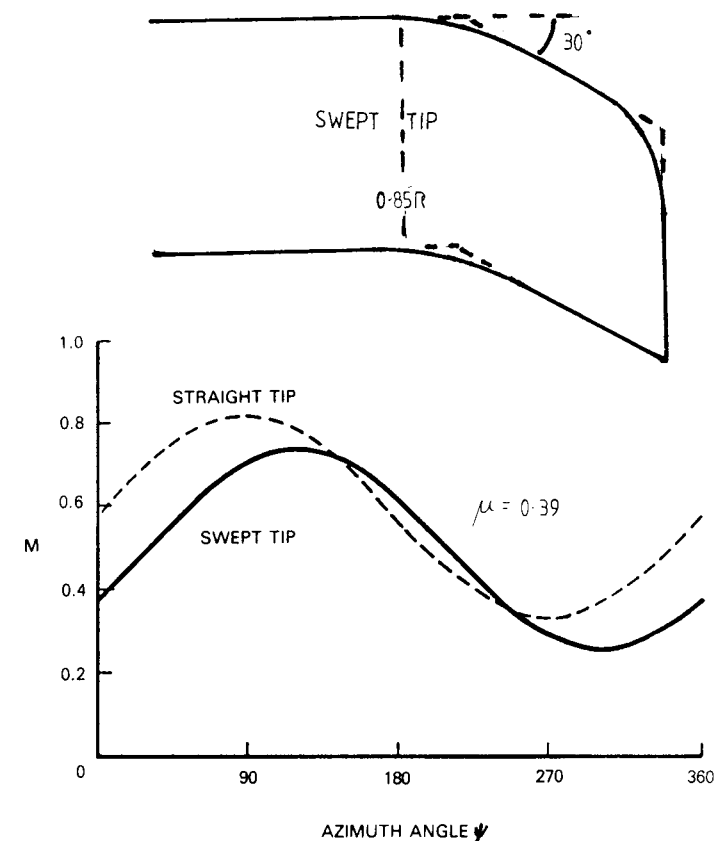


Fig. 6.5 Variation of Mach number normal to leading edge for straight and swept tips (after Wilby and Philippe).

Shaping the blade tip can also be used to improve the stalling characteristics of the retreating blade. A particular all-round solution devised by Westland Helicopters is pictured in Fig. 6.6. The principal features are:

- (1) approximately 20° sweepback of the outboard 15% of blade span;
- (2) a forward extension of the leading edge in this region, to safeguard dynamic stability;
- (3) a sharply swept outer edge to promote controlled vortex separation and thereby delay the tip stall.

Wind tunnel tests (static conditions) showed this last effect to have

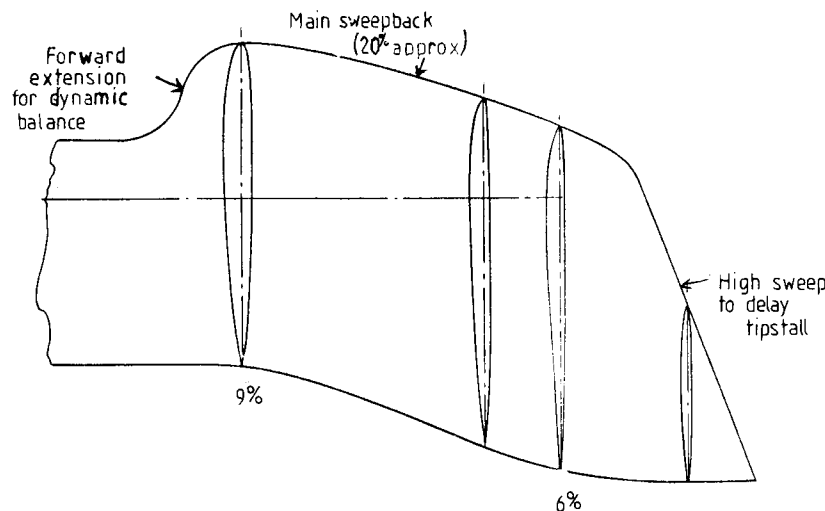


Fig. 6.6 Westland development blade tip.

been achieved in remarkable degree (Fig. 6.7). Subsequently the tip proved highly successful in flight and was used on a version of the Lynx helicopter which captured the world speed record (see Chapter 7).

6.4 Parasite drag

Parasite drag – drag of the many parts of a helicopter, such as the fuselage, rotorhead, landing gear, tail rotor and tail surfaces, which make no direct contribution to main rotor lift – becomes a dominant factor in aircraft performance at the upper end of the forward speed range. Clearly the incentive to reduce parasite drag grows as emphasis is placed on speed achievement or on fuel economy. Equally clearly, since the contributing items all have individual functions of a practical nature, their design tends to be governed by practical considerations rather than by aerodynamic desiderata. Recommendations for streamlining, taken on their own, tend to have a somewhat hollow ring. What the research aerodynamicist can and must do, however, is provide an adequate background of reliable information which allows a designer to calculate and understand the items of parasite drag as they relate to his particular requirement and so review his options.

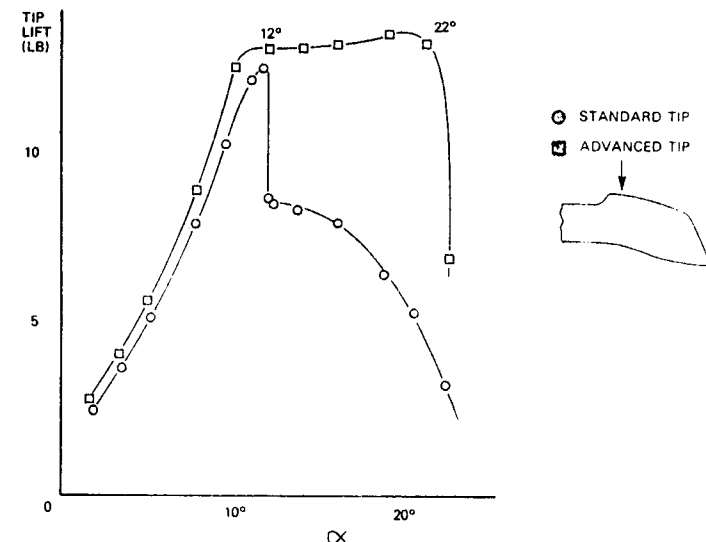


Fig. 6.7 Wind tunnel results (non-oscillating) showing large advantage in stalling angle for Westland tip.

Such a background has been accumulated through the years and much of what is required can be obtained from review papers, of which an excellent example is that of Keys and Wiesner⁹. These authors have provided, by means of experimental data presented non-dimensionally, values of fuselage shape parameters that serve as targets for good aerodynamic design. These include such items as corner radii of the fuselage nose-section, fuselage cross-section shape, afterbody taper and fuselage camber. Guidelines are given for calculating the drag of engine nacelles and protuberances such as aerials, lights and handholds. Particular attention is paid to the trends of landing-gear drag for wheels or skids, exposed or faired. Obviously the best solution for reducing the drag of landing gear is full retraction, which however adds significantly to aircraft weight. Keys and Wiesner have put this problem into perspective by means of a specimen calculation, which for a given mission estimates the minimum flight speed above which retraction shows a net benefit. The longer the mission, the lower is the break-even speed.

The largest single item in parasite drag is normally the rotorhead drag, known also briefly as hub drag. This relates to the driving mechanism between rotor shaft and blades, illustrated in Fig. 4.5, and includes as drag components the hub itself, the shanks linking

hub to blades, the hinge and feathering mechanisms and the control rods. Conventionally all these components are non-streamlined parts creating large regions of separated flow and giving a total drag greater than that of the basic fuselage, despite their much smaller dimensions. The drag of an articulated head may amount to 40% or 50% of total parasite drag, that of a hingeless head to about 30%. The application of aerodynamic fairings is possible to a degree, the more so with hingeless than with articulated heads, but is limited by the relative motions required between parts.

Sheehy¹⁰ conducted a review of drag data on rotorheads from American sources and showed that projected frontal area was the determining factor for unfaired heads. Additionally, allowance had to be made for the effects of local dynamic pressure and head-fuselage interference, both of which factors increased the drag. Fairings needed to be aerodynamically sealed, especially at the head-fuselage junction. The effect of head rotation on drag was negligible for unfaired heads and variable for faired heads.

Picking up the lines of Sheehy's review, a systematic series of wind tunnel model tests was made at Bristol University, UK¹¹, in which a simulated rotorhead was built up in stages. Figure 6.8 shows the model in the University low-speed tunnel and in Fig. 6.9

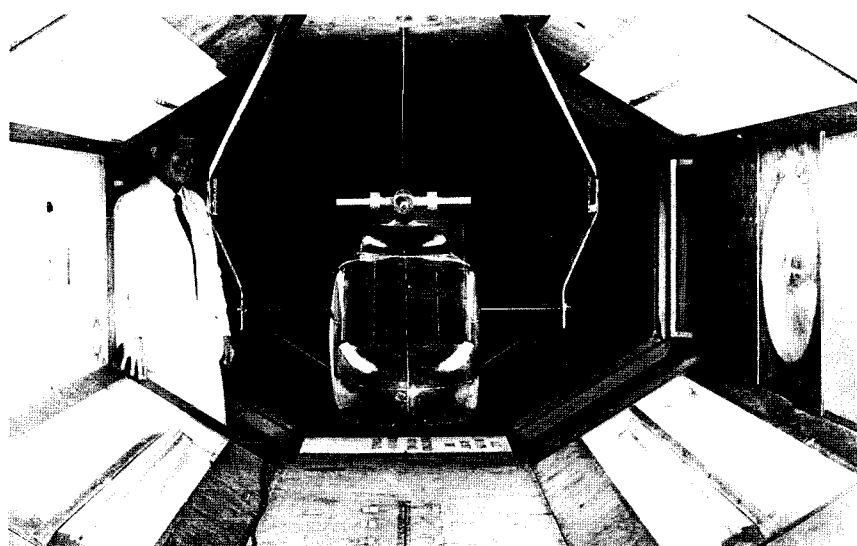


Fig. 6.8 Analysis of rotorhead drag: model in wind tunnel.

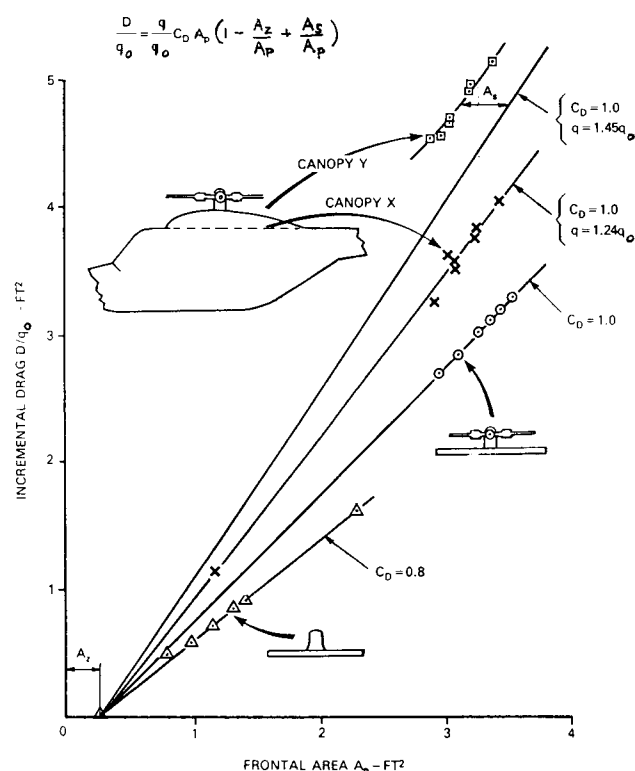


Fig. 6.9 Rotorhead drag results.

the drag results are summarized. An expression for rotorhead drag D emerges in the form

$$\frac{D}{q_0} = \frac{q}{q_0} C_D A_P \left(1 - \frac{A_z}{A_p} + \frac{A_s}{A_p} \right) \quad (6.1)$$

with the following definitions.

q_0 is the free stream dynamic pressure $\frac{1}{2}\rho V_0^2$. q is the local dynamic pressure at the hub position, measured in absence of the rotorhead. In a general case, the local supervelocity and hence q can be calculated from a knowledge of the fuselage shape.

C_D is the effective drag coefficient of the bluff shapes making up the head. This may be assumed to be the same as for a circular cylinder at the same mean Reynolds number. For the results of Fig. 6.9 it is seen that a value $C_D = 1.0$ fits the experimental data

well, apart from an analytically interesting but unreal case of the hub without shanks, where the higher Reynolds number of the large diameter unit is reflected in a lower C_D value. In default of more precise information it is suggested that the value $C_D = 1.0$ should be used for general estimation purposes. One might expect the larger Reynolds number of a full scale head to give a lower drag coefficient but the suggestion rests to a degree on Sheehy's comment that small scale model tests tend to undervalue the full scale drag, probably because of difficulties of accurately modelling the head details.

A_p is the projected frontal area of the head, as used by Sheehy. A_z represents a relieving factor on the drag, illustrated in Fig. 6.9 and resulting from the fact that the head is partly immersed in the fuselage boundary layer. In magnitude A_z turns out to be equal to the projected area contained in a single thickness of the boundary layer as estimated in absence of the head. The last quantity A_s represents in equivalent area terms the flow spoiling effect of the head on the canopy. This is a function jointly of the separation distance of the blade shanks above the canopy (the smaller the separation, the greater the spoiling) and the taper ratio of the canopy afterbody (the sharper the taper, the greater the spoiling). The ratio A_s/A_p may be estimated from a chart given in Fig. 6.10 constructed by interpolation from the results for different canopies tested.

In light of the evidence quoted, the situation on rotorhead drag may be summed up in the following points.

- (1) The high drag of unfaired rotorheads is explained in terms of exposed frontal area and interference effects and can be calculated approximately for a given case.
- (2) Hingeless systems have significantly lower rotorhead drag than articulated systems.
- (3) The scope for aerodynamic fairings is limited by the mechanical nature of the systems but some fairings are practical, more especially with hingeless rotors, and can give useful drag reductions.
- (4) The development of head design concepts having smaller exposed frontal areas carries considerable aerodynamic benefit.

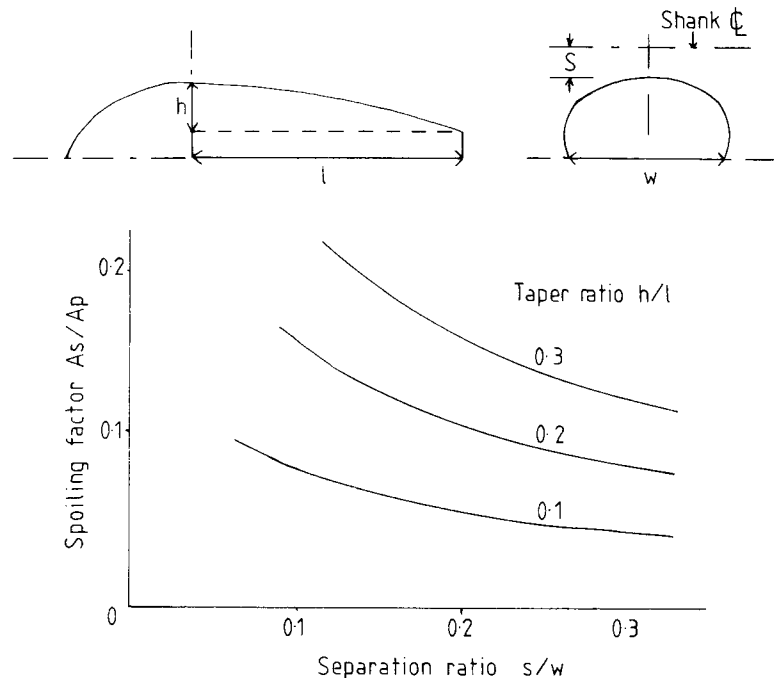


Fig. 6.10 Chart for estimating spoiling factor A_s .

6.5 Rear fuselage upsweep

A special drag problem relates to the design of the rear fuselage upsweep for a helicopter with rear loading doors, where the width across the back of the fuselage needs to be more or less constant from bottom to top. In the 1960s, experience on fixed-wing aircraft¹² revealed that where a rear fuselage was particularly bluff, drag was difficult to predict and could be considerably greater than would have been expected on a basis of classical bluff-body flow separation. Light was thrown on this problem in the 1970s by T. Morel^{13,14}: studying the drag of hatchback automobiles he found that the flow over a slanted base could take either of two forms (1) the classical bluff-body flow consisting of cross-stream eddies or (2) a flow characterized by streamwise vortices. Subsequently the problem was put into a helicopter context by Seddon¹⁵, using wind tunnel model tests of which the results are summarized in Figs 6.11 to 6.14. The combination of upsweep angle of the rear fuselage and

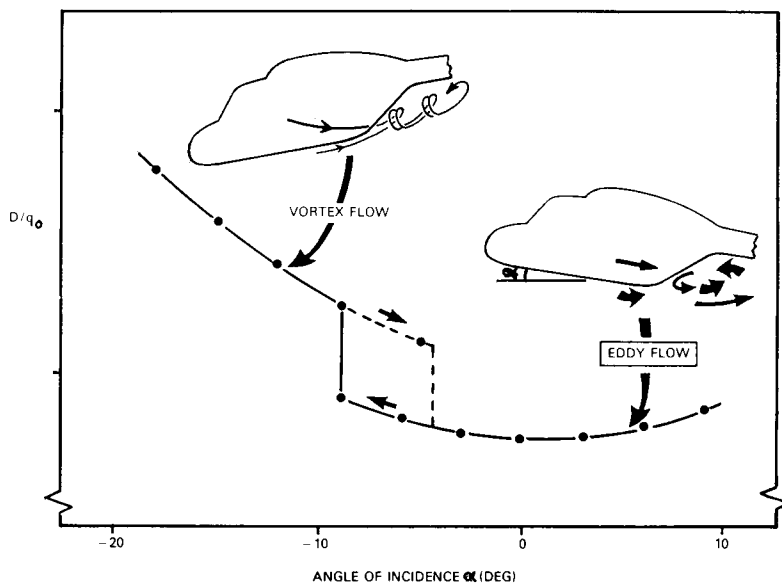


Fig. 6.11 Types of flow from rear fuselage upsweep with associated critical drag change.

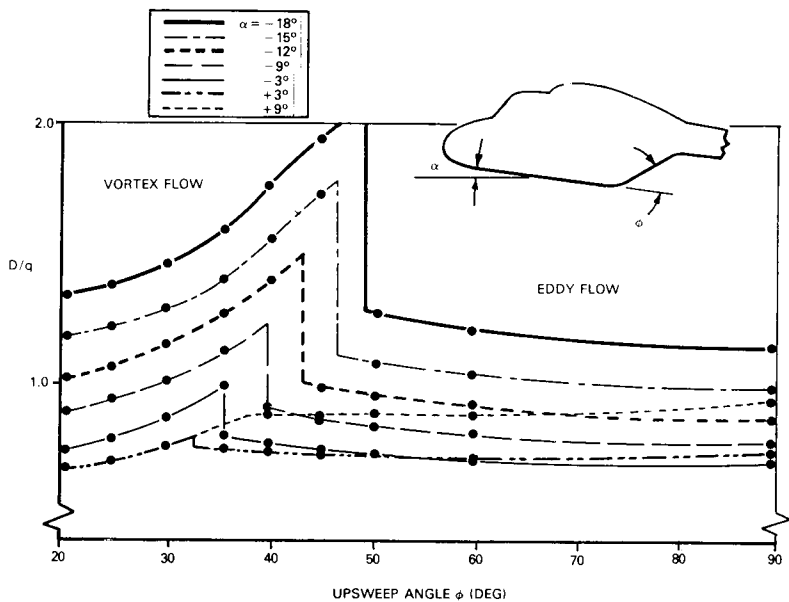


Fig. 6.12 Variation of drag with upsweep angle at constant incidence.

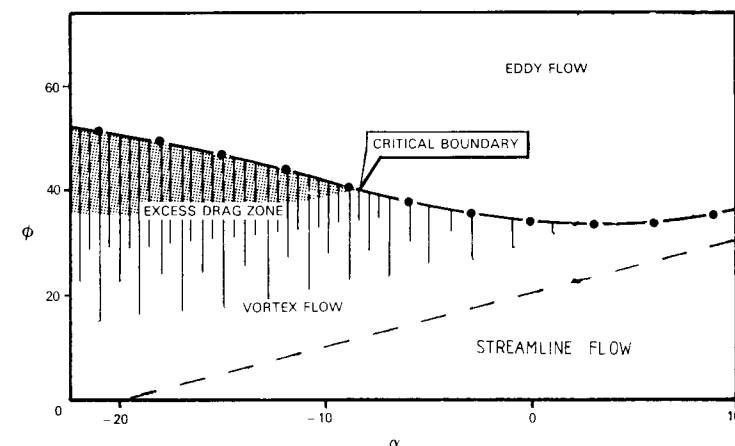


Fig. 6.13 $\alpha-\phi$ diagram showing all types of flow and indicating excess drag region.

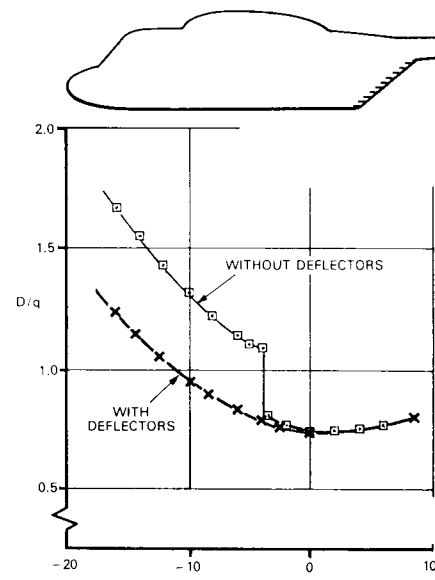


Fig. 6.14 Vortex flow development prevented by deflectors.

incidence of the helicopter to the airstream determines the type of flow obtained. At positive incidence eddy flow persists. As incidence is decreased (nose going down as in forward flight) a critical angle is reached at which the flow changes suddenly to the vortex type

and the drag jumps to a much higher level (Fig. 6.11), which is maintained for further incidence decrease. If incidence is now increased the reverse change takes place, though at a less negative incidence than before. The high drag corresponds to a high level of suction on the inclined surface, which is characteristic of the vortex flow. The suction force also has a downward lift component which is additionally detrimental to the helicopter. The type of flow is similar to that found on aerodynamically slender wings (as for example on the supersonic Concorde aircraft) but there the results are favourable because the lift component is upwards and the drag component is small except at high angle of attack.

The effect of changing upsweep angle is shown in Fig. 6.12. Here each curve is for a constant fuselage incidence. With upsweep angles near 90° , eddy flow exists as would be expected. At a point in the mid-angle range of upsweep, depending on incidence, the flow change occurs, accompanied by the drag increase. As upsweep angle is further reduced the drag falls progressively but there is a significant range of angle over which the drag is higher than in eddy flow.

As an aid to design, the situation can be presented in the form of an $\alpha - \phi$ diagram, ϕ being here the upsweep angle. The full line in Fig. 6.13 is the locus of the drag jump when incidence is decreasing. If required, a locus can be drawn alongside to represent the situation with incidence increasing. Below the critical boundary is the zone of excess drag. From such a diagram a designer can decide what range of upsweep angles is to be avoided for his aircraft. Of associated interest is the broken line shown: this marks an estimated boundary between vortex flow and streamlined flow, that is when no separation occurs at the upsweep. General considerations of aerodynamic streamlining suggest that the flow will remain attached if the upswept surface is inclined at not more than 20° to the direction of flight, in other words when

$$\phi - \alpha \leq 20^\circ$$

The final diagram Fig. 6.14 shows that if vortex flow occurs naturally, it can be prevented by an application of short, closely-spaced deflectors on the fuselage side immediately ahead of the upswept face. The action is one of preventing the vortex from building up by cutting it off at multiple points along the edge.

6.6 Higher harmonic control

In forward flight with a rotor operating under first-order cyclic control, a considerable proportion of the lifting capacity of the blades has been sacrificed, as we have seen in Chapter 4, in order to balance out the roll tendency. The lift carried in the advancing sector is reduced to very low level, while the main load is taken in the fore and aft sectors but at blade incidences (and hence lift coefficients) well below the stall. This can be seen explicitly in a typical figure-of-eight diagram, for example that at Fig. 6.1(c). Little can be done to change the situation in the advancing sector but in the fore and aft sectors, where the loading has only a minor effect on the roll problem, the prospect exists of producing more lift without exceeding stalling limits in the retreating sector. In principle the result can be achieved by introducing second and possibly other harmonics into the cyclic control law. The concept is not new: Stewart in 1953 proposed the use of second harmonic pitch control, predicting an increase of at least 0.1 in available advance ratio. Up to the present time (1980s), however, the potential of higher harmonic control has not received general development. Overall the problem is not a simple one, as it involves the fields of control systems and rotor dynamics at least as extensively as that of aerodynamics. Moreover the benefits could until now be obtained by less complicated means, such as increasing tip speed or blade area. As these other methods reach a stage of diminishing returns, the attraction of higher harmonic control is enhanced by comparison. Also, modern numerical methods allow the rotor performance to be related to details of the flow and realistic blade aerodynamic limitations, so that the prediction of performance benefits is much more secure than it was.

A calculation provided by Westland Helicopters illustrates the aerodynamic situation. The investigation consisted in comparing thrust performances of two rotors with and without second harmonic control, of quite small amplitude – about 1.5° of blade incidence. Local lift conditions near the tip were monitored round the azimuth and related to the $C_L - M$ boundary of the blade section. The results shown in Fig. 6.15 indicate that second harmonic control gave an advantage of at least 0.2 in lift coefficient in the middle Mach number region appropriate to the disc fore and aft sectors.

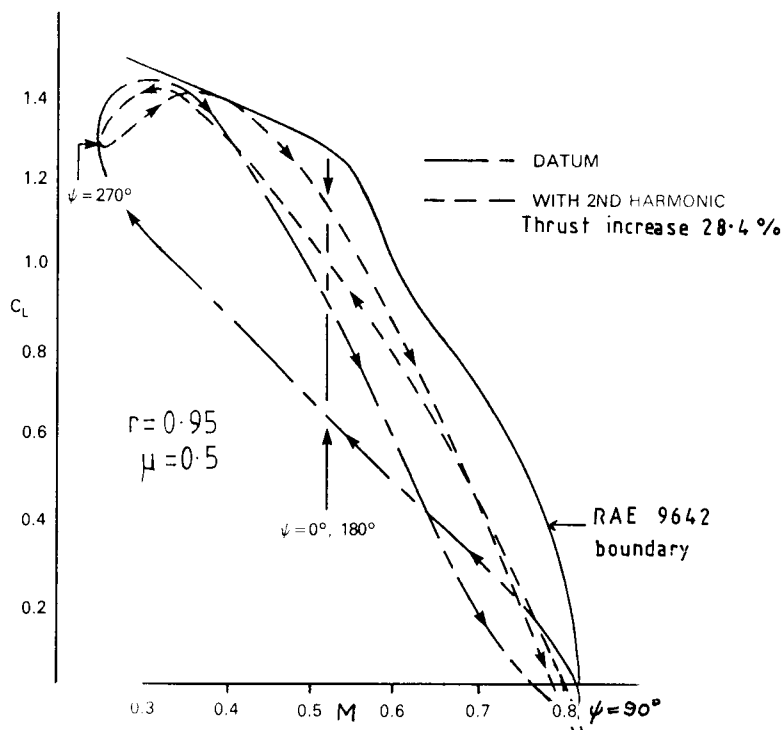


Fig. 6.15 Use of second harmonic control: calculated example.

This translated into a 28.4% increase in thrust available for the same retreating-blade boundary. A further advantage was that the rotor with second harmonic control required a 22% smaller blade area than the datum rotor, which, whether exploited as a reduction say from six blades to five or as a weight saving at equal blade numbers, would represent a considerable benefit in terms of component size and mission effectiveness.

6.7 Aerodynamic design process

To end this chapter we turn from research topics to the practical problem of determining the aerodynamic design of a rotor for a new helicopter project. A step-by-step process enables the designer to take into account the many and varied factors that influence his choice – aircraft specification, limitations in hover and at high

forward speed, engine characteristics at various ratings, vibratory loads, flyover noise and so on. The following exposition comes from an unpublished instructional document kindly supplied by Westland Helicopters.

The basic requirement is assumed to be for a helicopter of moderate size, payload and range, with good manoeuvrability, robust and reliable. Maximum flight speed is to be at least 80 m/s and a good high-temperature altitude performance is required, stipulated as 1200 metres at ISA + 28 K. Prior to determining the rotor configuration, a general study of payload and range diagrams, in relation to the intended roles, leads to a choice of all-up weight, namely 4100 kG. Empty weight is set at 55% of this, leaving 45% disposable weight, of which it is assumed one half can be devoted to fuel and crew. Consideration of various engine options follows and a choice is made of a pair of engines having a continuous power rating at sea level ISA of 560 kW each, with take-off and contingency ratings to match. Experience naturally plays a large part in the making of these choices, as indeed it does throughout the design process.

First choice for the rotor is the *tip speed*: this is influenced by the factors shown in Fig. 6.16. The tip Mach number in hover is one possible limitation. Allowing a margin for the fact that in high speed forward flight a blade at the front or rear of the disc will be at the same Mach number as in hover but at a higher lift coefficient, corresponding to the greater power required, the hover tip speed limit is set at Mach 0.69 (235 m/s). On the advancing tip in forward flight the lift coefficient is low and the Mach number limit can be between 0.8 and 0.9: recognizing that an advanced blade section will be used, the limit is set at 0.88. Flyover noise is largely a function of advancing tip Mach number and may come into this consideration. High advance ratio brings on rotor vibratory loads and hence fuselage vibration, so a limiting μ for normal maximum speed is set at 0.4. Lastly the maximum speed called for is at least 80 m/s. It is seen that to satisfy these requirements constrains the rotor tip speed to about 215 m/s, the targeted maximum flight speed being 160 knots (82 m/s).

Next to be decided is the *blade area*. The area required increases as design speed increases, because the retreating blade operates at decreasing relative speed while its lift coefficient is stall-limited. The non-dimensional thrust coefficient C_T/σ is limited as shown in

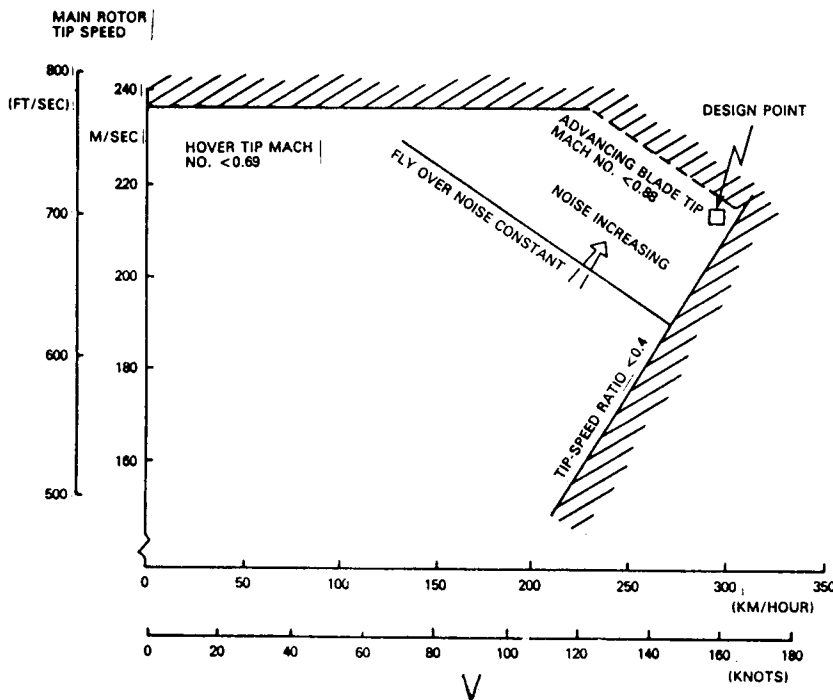


Fig. 6.16 Determination of tip speed for new rotor design.

Fig. 6.17(a) – see Equation (3.39). Writing

$$\frac{C_T}{\sigma} = \frac{W}{\rho A (\Omega R)^2} \cdot \frac{\pi R}{Nc}$$

$$= \frac{W}{\rho Nc R (\Omega R)^2} \quad (6.2)$$

we have for the total blade area NcR ,

$$NcR = \frac{W}{\rho (\Omega R)^2} / \frac{C_T}{\sigma} \quad (6.3)$$

From a knowledge of tip speed (ΩR) and aircraft weight the blade area diagram, Fig. 6.17(b), is constructed. The design maximum speed then corresponds to a total blade area of 10 m^2 . Note that use of the advanced blade section results in about 10% saving in blade area, which translates directly into rotor overall weight.

Choice of the *rotor radius* requires a study of engine performance. For the vertical axis in Fig. 6.18 specific power loading (kW/kg)

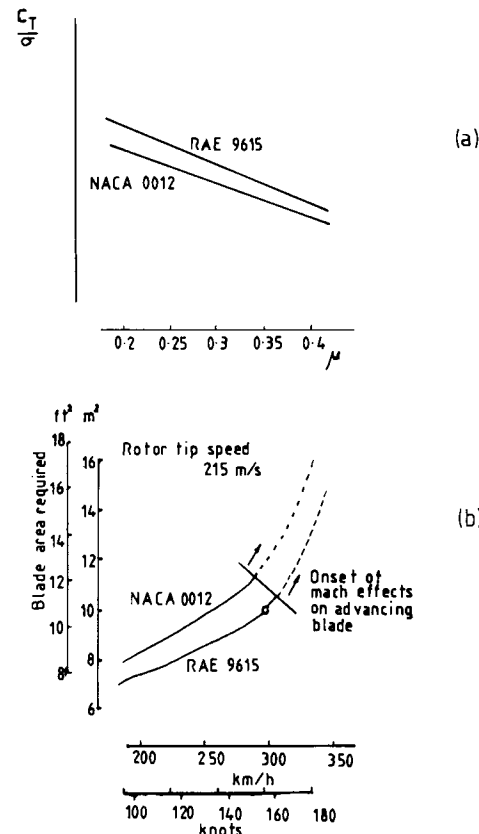


Fig. 6.17 Determination of blade area for new rotor design.

from the engine data is translated into actual power in W for the 4100 kG helicopter. Both twin-engine and single-engine values are shown, in each case for take-off, continuous and contingency ratings. Curves of power required for various hover conditions are plotted in terms of disc loading (kG/m^2) on the established basis (Chapter 2) that induced power is proportional to the square root of disc loading. The four curves shown, reading from the lowest upwards, are:

- (1) ideal induced power at sea level ISA, given by

$$P_i = W \sqrt{\frac{\omega}{2\rho}} \quad (6.4)$$

ω being the disc loading;

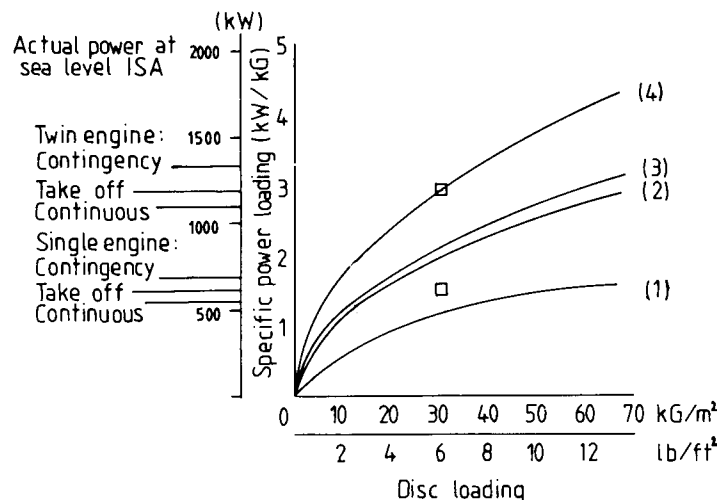


Fig. 6.18 Determination of rotor radius for new design.

- (2) actual total power at sea level ISA, scaled up from induced power to include blade profile power, tail rotor power, transmission loss, power to auxiliaries and an allowance for excess of thrust over weight caused by downwash on the fuselage;
- (3) actual total power calculated for 1200 m altitude at ISA + 28°;
- (4) total power at sea level necessary to meet the requirement at (3), taking into account the decrease of engine power with increasing altitude and temperature.

A design point for disc loading can now be read off corresponding to the twin-engine take-off power rating (or using the contingency rating if preferred). From disc loading the blade radius follows, since

$$\omega = \frac{W}{A} = \frac{W}{\pi r^2} \quad (6.5)$$

hence

$$R = \frac{W}{\pi \omega} \quad (6.6)$$

In the present example the selected disc loading is 32 kG/m^2 and the corresponding blade radius is 6.4 m. The single-engine capability

has also to be considered. It is seen that on contingency rating the helicopter does not have quite enough power from a single engine to hover at sea level ISA and full all-up weight. The deficit is small enough, however, to ensure that a good fly-away manoeuvre would be possible following an engine failure; while at 90% all-up weight, hovering at the single-engine contingency rating is just possible.

Undetermined so far is the *number of blades*. From a knowledge of the blade radius and total blade area, the blade aspect ratio is given by

$$\frac{R}{c} = \frac{R^2 N}{N c R} = 4.1 N \quad (6.7)$$

Using three blades, an aspect ratio 12.3 could be considered low from a standpoint of three-dimensional effects at the tip. Five blades, giving aspect ratio 20.5, could pose problems in structural integrity and in complexity of the rotor hub and controls. Four blades is therefore the natural choice. Consideration of vibration characteristics is also important here: it is concluded that whereas with three blades vibration levels could be high, the advantage of five blades over four would not be very significant, so the choice of four blades is acceptable.

The choice between an articulated and a hingeless rotor is mainly a matter of dynamics and relates to flight handling criteria for the aircraft. A criterion often used is a time constant in pitch or roll when hovering; this is the time required to reach a certain percentage – 60% or over – of the final pitch or roll rate following an application of cyclic control. For the case in point, recalling the requirement for good manoeuvrability, low time constants are targeted. It is then found that, using flapping hinges with about 4% offset, the targets cannot be reached except by mounting the rotor on a very tall shaft, which is incompatible with the stated aims for robustness and compactness. A hingeless rotor produces greater hub moments, equivalent to flapping offsets 10% and more, and is therefore seen as the natural choice.

References

- 1 Wilby, P.G. (1980) 'The aerodynamic characteristics of some new RAE blade sections and their potential influence on rotor performance'. *Vertica*, 4.

- 2 Farren, W.S. (1935) 'Reaction on a wing whose angle of incidence is changing rapidly'. *ARC R & M 1648*.
- 3 Carta, F.O. (1960) 'Experimental investigation of the unsteady aerodynamic characteristics of NACA 0012 airfoil'. *United Aircraft Lab. Rep. M-1283-1*.
- 4 Ham, N.D. (1968) 'Aerodynamic loading on a two-dimensional airfoil during dynamic stall'. *AIAA Journal* 6, no. 10.
- 5 McCroskey, W.J. (1972) 'Dynamic stall of airfoils and helicopter rotors'. *AGARD Rep. 595*.
- 6 Johnson, W. and Ham, N.D. (1972) 'On the mechanism of dynamic stall' *JAHS* 17, no. 4.
- 7 Beddoes, T.S. (1976) 'A synthesis of unsteady aerodynamic effects including stall hysteresis'. *Vertica* 1, no. 2.
- 8 Wilby, P.G. and Philippe, J.J. (1982) 'An investigation of the aerodynamics of an RAE swept tip using a model rotor'. *Eighth European Rotorcraft Forum, Paper 25*.
- 9 Keys, C.R. and Wiesner, R. (1975) 'Guidelines for reducing helicopter parasite drag'. *JAHS*.
- 10 Sheehy, T.W. (1975) 'A general review of helicopter hub drag data'. Paper for Stratford AHS Chapter Meeting.
- 11 Seddon, J. (1979) 'An analysis of helicopter rotorhead drag based on new experiment'. *Fifth European Rotorcraft Forum, Paper 19*, Amsterdam.
- 12 Lowe, B.G. and Trebble, W.J.G. (1968) 'Drag analysis on the Short SC5 Belfast'. Unpublished RAE Report.
- 13 Morel, T. (1976) 'The effect of base slant on the flow pattern and drag of 3-D bodies with blunt ends'. *GM Res. Lab. Symposium*.
- 14 Morel, T. (1978) 'Aerodynamic drag of bluff body shapes characteristic of hatchback cars'. *SAE Congress and Exposition*, Detroit.
- 15 Seddon, J. (1982) 'Aerodynamics of the helicopter rear fuselage upsweep'. *Eighth European Rotorcraft Forum, Paper 2.12*, Aix-en-Provence.

7 Performance

7.1 Introductory

The preceding chapters have been mostly concerned with establishing the aerodynamic characteristics of the helicopter main rotor. We turn now to considerations of the helicopter as a total vehicle. The assessment of helicopter performance, like that of a fixed-wing aircraft, is at bottom a matter of comparing the power required with that available, in order to determine whether a particular flight task is feasible. The number of different performance calculations that can be made for a particular aircraft is of course unlimited, but aircraft specification sets the scene in allowing meaningful limits to be prescribed. A typical specification for a new or updated helicopter might contain the following requirements, exclusive of emergency operations such as personnel rescue and life saving.

- (1) Prescribed missions, such as a hover role, a payload/range task or a patrol/loiter task. More than one are likely to be called for. A mission specification leads to a weight determination for payload plus fuel and thence to an all-up weight, in the standard fashion illustrated in Fig. 7.1.
- (2) Some specific atmosphere-related requirements, for example the ability to perform the mission at standard (ISA) temperature plus, say, 15°; the ability to perform a reduced mission at altitude; the ability to fly at a particular cruise speed.
- (3) Specified safety requirements to allow for an engine failure.
- (4) Specified environmental operating conditions, such as to and from ships or oil rigs.
- (5) Prescribed dimensional constraints for stowage, air portability etc.
- (6) Possibly a prescribed power plant.

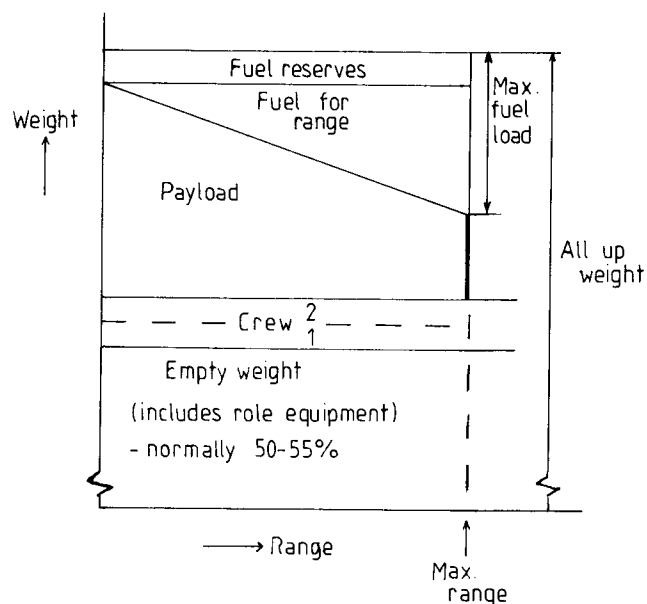


Fig. 7.1 Determination of all-up weight for prescribed mission.

Calculations at the flexible design stage are only a beginning; as a design matures, more will be needed to check estimates against actual performance, find ways out of unexpected difficulties, or enhance achievement in line with fresh objectives.

Generally, in a calculation of achievable or required performance, the principal characteristics to be evaluated are:

- (1) power needed in hover
- (2) power needed in forward flight
- (3) envelope of thrust limitations imposed by retreating-blade stall and advancing-blade compressibility drag rise.

The following sections concentrate on these aspects, using simple analytical formulae, mostly already derived. Factor (3) must always be kept under review because the flight envelope so defined often lies inside the power limits and is thus the determining factor on level flight speed and manoeuvre capability.

A brief descriptive section is included on more accurate performance estimation using numerical methods. The chapter concludes with three numerical examples: the first concerns a practical

achievement from advanced aerodynamics, the others are hypothetical relating to directions in which advanced aerodynamics may lead in the future.

7.2 Hover and vertical flight

The formula relating thrust and power in vertical flight, according to blade element theory, was derived in Equation (3.47). The power required is the sum of induced power, related to blade lift, and profile power, related to blade drag. Converting to dimensional terms the equation is

$$P = k(V_c + v_i)T + \frac{1}{8}C_{D_0} \rho A_b V_T^3 \quad (7.1)$$

where in the induced term, using momentum theory as in Equation (2.10), one may write

$$V_c + v_i = \frac{1}{2}V_c + \sqrt{\left\{ \left(\frac{1}{2}V_c \right)^2 + \frac{T}{2\rho A} \right\}} \quad (7.2)$$

In the profile term, A_b is the total blade area, equal to σA , and V_T is the tip speed, equal to ΩR . This term is independent of the climb speed V_c , that is to say the profile drag power is the same in climb as in hover.

If in Equation (7.1) the thrust is expressed in newtons, velocities in m/s, area in m^2 and air density in kg/m^3 , the power is then in watts or, when divided by 1000, in kW. Using imperial units, thrust in lb, velocities in ft/sec, area in ft^2 and density in slugs/ ft^3 lead to a power in $lb \cdot ft/sec$ or, on dividing by 550, to HP.

To make a performance assessment, Equation (7.1) is used to calculate separately the power requirements of main and tail rotors. For the latter, V_c disappears and the level of thrust needed is such as to balance the main rotor torque in hover: this requires an evaluation of hover trim, based on the simple equation

$$T \cdot \ell = Q \quad (7.3)$$

where Q is the main rotor torque and ℓ is the moment arm from the tail rotor shaft perpendicular to the main rotor shaft. The tail rotor power may be 10–15% of main rotor power. To these two are added allowances for transmission loss and auxiliary drives, perhaps a further 3%. This leads to a total power requirement,

P_{req} say, at the main shaft, for a nominated level of main rotor thrust or vehicle weight. The power available, P_{av} say, is ascertained from engine data, debited for installation loss. Comparing the two powers determines the *weight capability* in hover, out of ground effect (OGE), under given ambient conditions. The corresponding capability in ground effect (IGE) can be deduced using a semi-empirical relationship such as Equation (2.18). The *aircraft ceiling* in vertical flight is obtained by matching P_{req} and P_{av} for nominated weights and atmospheric conditions. The difference in induced power for climbing at V_c and for hover is the incremental power required to climb, which may be written:

$$\Delta P = \kappa T \left[\frac{1}{2} V_c + \frac{1}{2} \sqrt{\left(V_c^2 + \frac{2T}{A} \right)} - \frac{T}{2\rho A} \right] \quad (7.4)$$

Knowing the incremental power available the *climb speed* can be calculated iteratively. For low rates of climb it is seen that, approximately,

$$V_c = \frac{2\Delta P}{\kappa T} \quad (7.5)$$

which, if κ is given a value 1.15 and T is assumed to 1.025 W (to allow for fuselage download), approximates to

$$V_c = 1.7 \frac{\Delta P}{W} \quad (7.6)$$

This result was foreshadowed at Equation (2.12) where, using only the simple momentum theory, the numerical factor was 2. That a factor greater than 1.0 emerges is because for a given thrust the induced velocity v_i is reduced owing to an increase in rotor inflow caused by climbing vertically. As rate of climb increases the power is increasingly determined by the climb work term $T \cdot V_c$, so that at high climb rates Equation (7.5) is replaced by

$$V_c = \frac{\Delta P}{\kappa T} \quad (7.7)$$

which with our chosen empirical values gives

$$V_c = 0.85 \frac{\Delta P}{W} \quad (7.8)$$

The two-to-one variation in factor between zero climb rate and a high climb rate (say 6000 ft/min) is typical. Stepniewski and Keys (Vol. II, p. 55) suggest a linear variation between the two extremes. It should be borne in mind, however, that at low rates of either climb or descent, vertical movements of the tip vortices relative to the disc plane are liable to change the power relationships in ways which cannot be reflected by momentum theory and which are such that the power relative to that in hover is actually *decreased* initially in climb and *increased* initially in descent. These effects, which have been pointed out by Prouty¹, were mentioned in Chapter 2. Obviously in such situations Equation (7.4) and the deductions from it do not apply.

7.3 Forward level flight

The power-thrust relationship for level flight was derived in Chapter 5 and is given in idealized form in Equation (5.42), or with empirical constants incorporated in Equation (5.43). Generally we assume the latter form to be the more suitable for practical use and indeed to be adequate for most preliminary performance calculation. The equation shows the power coefficient to be the linear sum of separate terms representing, respectively, the induced power (rotor-lift dependent), profile power (blade-section drag dependent) and parasite power (fuselage-drag dependent). It is in effect an energy equation, in which each term represents a separately identifiable sink of energy, and might have been calculated directly as such. In dimensional terms we have

$$P = \kappa v_i T + \frac{1}{8} C_{D_0} \rho A_b V_T^3 \left[1 + k \left(\frac{V}{V_T} \right)^2 \right] + \frac{1}{2} \rho V^3 f \quad (7.9)$$

in which V_T is the rotor tip speed, V the forward-flight speed and f the fuselage-equivalent flat-plate area, defined in Equation (5.56). The induced velocity v_i is given according to momentum theory by Equation (5.5) and may be written in the form

$$v_i^2 = -\frac{1}{2} V^2 + \frac{1}{2} \sqrt{V^4 + 4(T/2\rho A)^2} \quad (7.10)$$

Allowances should be added for tail rotor power and power to transmission and accessories: collecting these together in a miscellaneous item, the total is perhaps 15% of P at $V = 0$ (Section 7.2)

and half this, say 8%, at high speed. Otherwise, if the evidence is available, the items may be assessed separately. The thrust T may be assumed equal to the aircraft weight W for all forward speeds above 5 m/s (10 knots).

A typical breakdown of the total power as a function of flight speed is shown in Fig. 7.2. Induced power dominates the hover but makes only a small contribution in the upper half of the speed range. Profile power rises only slowly with speed unless and until the compressibility drag rise begins to be shown at high speed. Parasite power, zero in the hover, increases as V^3 and is the largest component at high speed, contributing about half the total. As a result of these variations the total power has a typical 'bucket' shape, high in the hover falling to a minimum at moderate speed and rising rapidly at high speed to levels above the hover value. Except at high speed, therefore, the helicopter uses less power in forward flight than in hover.

Charts are a useful aid for rapid performance calculation. If power is expressed as P/δ , where δ is the relative air density at altitude, a power carpet can be constructed giving the variation of P/δ with W/δ and V . Figure 7.3 shows an example, in which for convenience the carpet is presented in two parts, covering the low and high speed ranges. When weight, speed and density are known, the power required for level flight is read off directly.

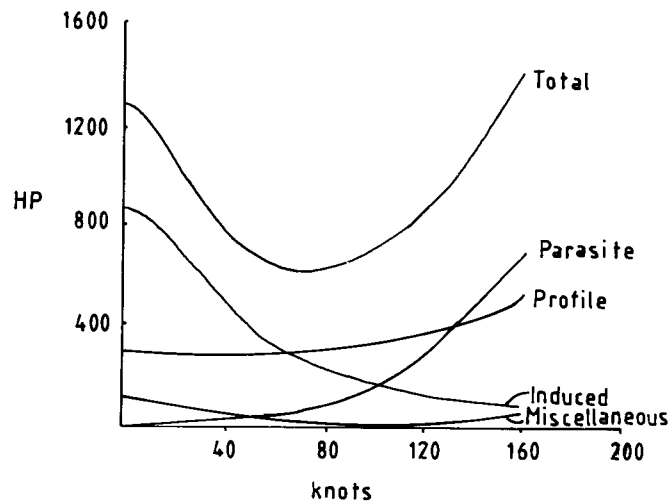


Fig. 7.2 Typical power breakdown for forward level flight.

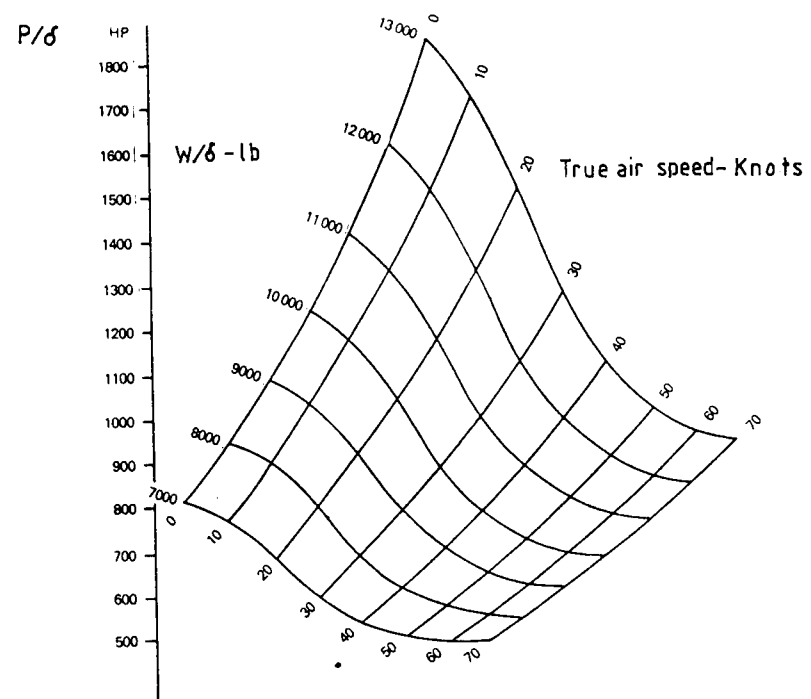
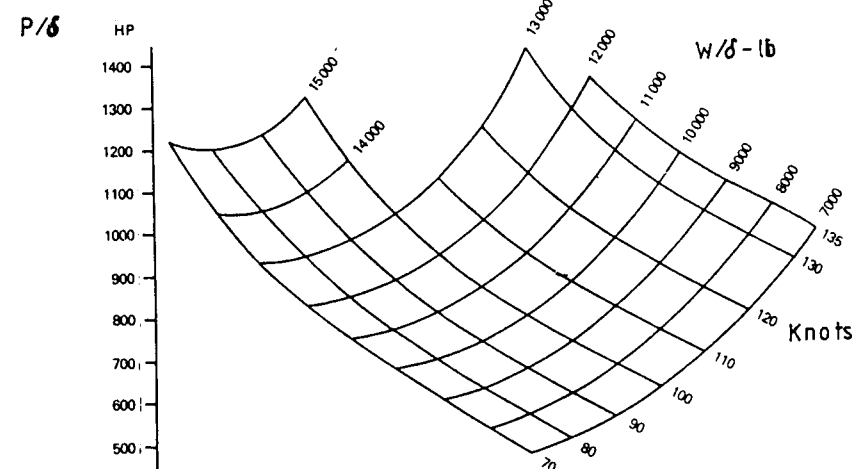


Fig. 7.3 Power carpets for rapid calculation.



7.4 Climb in forward flight

As a first approximation let us assume that for climbing flight the profile power and parasite power remain the same as in level flight and only the induced power has to be reassessed. The forced downflow alleviates the v_i term but the climb work term, $T \cdot V_c$, must be added. In coefficient form the full power equation is now:

$$C_p = \kappa \lambda_i C_T + \frac{1}{8} \sigma C_{D_0} (1 + k \mu^2) + \frac{1}{2} \mu^3 \frac{f}{A} + \lambda_c C_T \quad (7.11)$$

The usual condition for calculating climb performance is that of minimum-power forward speed. Here v_i is small compared with V , its variation from level flight to climb can be neglected and the incremental power ΔP required for climb is simply $T V_c$. Thus the *rate of climb* is

$$V_c = \Delta P / T \quad (7.12)$$

The result is a useful approximation but requires qualification on the grounds that since climbing increases the effective nose-down attitude of the fuselage, the parasite drag may be somewhat higher than in level flight. Also, because the main rotor torque is increased in climb – Equation (7.11) – an increase in tail rotor power is needed to balance it. Some of the incremental power available is absorbed in overcoming these increases and hence the climb rate potential is reduced, perhaps by as much as 30%. A further effect is that the increase in drag moves the best climb speed to a somewhat lower value than the level flight minimum power speed.

For a given aircraft weight the incremental power available for climb decreases with increasing altitude, mainly because of a decrease in the engine power available. When the incremental power runs out at best climb speed the aircraft has reached its *absolute ceiling* at that weight. In practice, as Equation (7.12) shows, the absolute ceiling can only be approached asymptotically and it is normal to define instead a *service ceiling* as the height at which the rate of climb has dropped to a stated low value, usually about 0.5 m/s (100 ft/min). Increasing the weight increases the power required at all forward speeds and thereby lowers the ceiling.

7.5 Optimum speeds

The bucket shape of the level-flight power curve allows the ready definition of speeds for optimum efficiency and safety for a number of flight operations. These are illustrated in Fig. 7.4. The minimum-power speed (A) allows the *minimum rate of descent* in autorotation. It is also, as discussed in the previous section, the speed for *maximum rate of climb*, subject to a correction to lower speed (A') if the parasite drag is increased appreciably by climbing. Subject to a further qualification, point A also defines the speed for *maximum endurance* or loiter time. Strictly the endurance relates directly to the rate of fuel usage, the curve of which, while closely similar to, is not an exact copy of the shaft-power curve, owing to internal fuel consumption within the engine: the approximation is normally close enough to be acceptable.

Maximum glide distance in autorotative descent is achieved at speed B, defined by a tangent to the power curve from the origin. Here the ratio of power to speed is a minimum: the condition corresponds to that of gliding a fixed-wing aircraft at its maximum lift-to-drag ratio. Point B is also the speed for *maximum range*, subject to the fuel-flow qualification stated above. This is for the range in zero wind: in a headwind the best-range speed is at B', obtained by striking the tangent from a point on the speed axis corresponding to the wind strength. Obviously, for a tailwind the tangent is taken from a point on the negative speed axis, leading to a lower best-range speed than B.

7.6 Maximum level speed

The *maximum speed* attainable in level flight is likely to be limited by the envelope of retreating-blade stall and advancing-blade drag rise (Section 7.7). If and when power limited, it is defined by the intersection of the curves of shaft power required and shaft power available, (C) in Fig. 7.4. In the diagram the power available has been assumed to be greater than that required for hover (out of ground effect) and, typically, to be nearly constant with speed, gaining a little at high speed from the effect of ram pressure in the engine intakes.

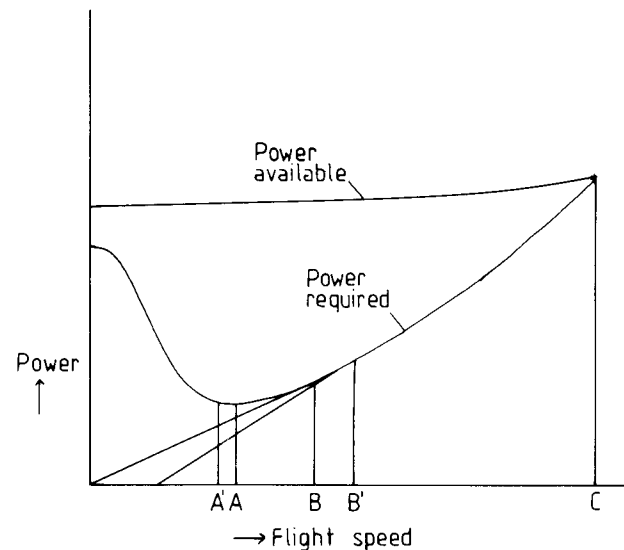


Fig. 7.4 Optimum speeds and maximum speed.

Approaching maximum speed, the power requirement curve is rising rapidly owing to the V^3 variation of parasite drag. For a rough approximation one might suppose the sum of the other components, induced drag, profile drag and miscellaneous additional drag, to be constant and equal to, say, half the total. Then at maximum speed, writing P_p for the parasite power, we have

$$P_{av} = 2 P_p = \rho V_{max}^3 f \quad (7.13)$$

whence

$$V_{max} = (P_{av}/\rho f)^{1/3} \quad (7.14)$$

For a helicopter having 1000 kW available power, with a flat-plate drag area 1 m^2 , the top speed at sea level density would by this formula be 93.4 m/s (181 knots).

Increasing density altitude reduces the power available and may either increase or decrease the power required. Generally the reduction of available power dominates and V_{max} decreases. Increasing weight increases the power required (through the induced power P_i) without changing the power available, so again V_{max} is reduced.

7.7 Rotor limits envelope

The envelope of rotor thrust limits is the outcome of operation on the blades of stall effects at high angle of incidence and compressibility effects at high Mach number. Usually the restrictions occur within the limits of available power. The nature of the envelope is sketched in Fig. 7.5. In hover, conditions are uniform around the azimuth and blade stall sets a limit to the thrust available. As forward speed increases, maximum thrust on the retreating blade falls because of the drop in dynamic pressure (despite some increase in maximum lift coefficient with decreasing resultant Mach number) and this limits the thrust achievable throughout the forward-speed range. By the converse effect, maximum thrust possible on the advancing side increases but is unrealizable because of the retreating-blade restriction. Then at higher speeds, as the advancing-tip Mach number approaches 1.0, its lift becomes restricted by shock-induced flow separation, leading to drag or pitching moment divergence, which eventually limits the maximum speed achievable. Thus the envelope comprises a limit on thrust from retreating-blade stall and a limit on forward speed from advancing-blade Mach effects. Without the advancing-blade problem, the retreating-blade stall would itself eventually set a maximum to the forward speed, as the figure-of-eight diagrams in Fig. 6.1 show.

Calculation of the limits envelope is best done by computer, allowing the inclusion of sophisticated factors, natural choices

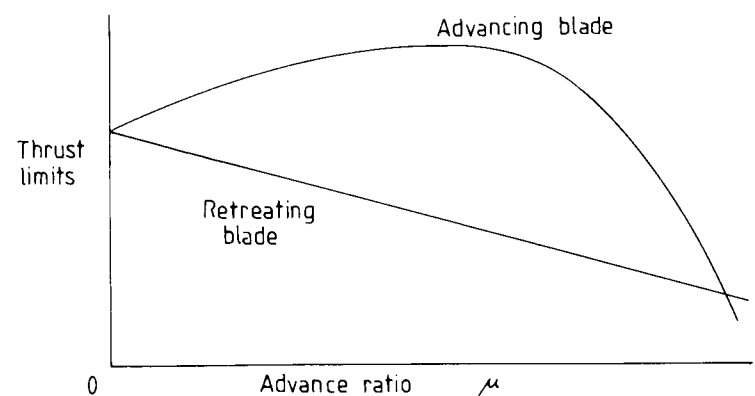


Fig. 7.5 Nature of rotor thrust limits.

among which are a non-uniform induced velocity distribution, a compressibility factor on lift slope (usually $1/\beta$ where $\beta = \sqrt{1 - M^2}$, M being the blade section Mach number) and a representation of blade dynamic stall characteristics.

An example of the way in which the limits envelope can dominate performance issues is given later in Section 7.11.

7.8 Accurate performance prediction

The ability to deploy computer methods in performance calculation has been a major factor in the rapid development of helicopter technology since the Second World War. Results may often not be greatly different from those derived from the simple analytical formulae but the fact that the feasibility of calculation is not dependent upon making a large number of challengeable assumptions is important in pinning down a design, making comparisons with flight tests or meeting guarantees. So it is that commercial organizations and research centres are equipped nowadays with computer programmes for use in all the principal phases of performance calculation – hover characteristics, trim analysis, forward-flight performance, rotor-thrust limits and so on.

It may be noted *en passant* that performance calculation is generally not the primary factor determining the need for numerical methods. The stressing of rotor blades makes a greater demand for complexity in calculation. Another highly important factor is the need for quantification of handling characteristics, as for example to determine the behaviour of a helicopter flying in a bad aerodynamic environment.

Within the realm of performance prediction are contained many sub-items, not individually dominant but requiring detailed assessment if maximum accuracy is to be achieved. One such sub-item is parasite drag, *in toto* an extensive subject, as with fixed-wing aircraft, about which not merely a whole chapter but a whole book could be written. For computation purposes the total drag needs to be broken down into manageable groupings, among which are streamlined and non-streamlined components, fuselage angle of attack, surface roughness, leakage and cooling-air loss. Maximum advantage must be taken of review literature, as compiled by Hoerner², Keys and Wiesner³ and others, and of background information on projects similar to the one in hand.

Once a best estimate of parasite drag has been made, the accuracy problem in power calculation devolves upon the induced and profile items, as Equation (7.11) shows, together with the additional sub-items of tail-rotor power, transmission loss and power to auxiliaries. Improving the estimation of induced and profile power comes down to the ability to use a realistic distribution of induced velocity over the disc area and the most accurate blade section lift and drag characteristics, including dynamic effects. This information has to be provided separately; the problem in the rotor is then to ascertain the angles of attack and Mach numbers of all blade sections, these varying from root to tip and round the azimuth as the blade rotates. That is basically what the focal computer programmes do. Iterative calculations are normally required among the basic equations of thrust, collective and cyclic pitch and the flapping angles. Starting with, say, values of thrust and the flapping coefficients, corresponding values of the pitch angle, collective and cyclic, can be calculated; the information then allows the blade angles and local Mach numbers to be determined, from which the lift forces can be integrated into overall thrust for comparison with the value initially assumed. When the iterations have converged, the required output data – power requirement, thrust limits, etc. – can be ascertained.

These sketchy notes must suffice for the purposes of the present book. Going more deeply into the subject would immerse one immediately into copious detail, for which there is no place here. An excellent and thorough exposition of the total process of performance prediction is available in Stepniewski and Keys, Volume II, to which the reader who wishes to come to grips with the whole computational complex is referred.

7.9 A world speed record

In the context of advanced rotor-blade design as discussed in Chapter 6, and as an example of realized performance, it is of interest to record the capture of the world speed record for helicopters by a Westland Lynx aircraft in August 1986. The incentive to make the attempt was provided by the results of a programme of test flying on the Lynx fitted with an experimental set of blades in which lift-enhancing aerofoil sections of the RAE '96' series (Section 6.2) were used throughout the length of the blade, together

with the Westland tip design (Section 6.3) combining a sweepback benefit on local Mach number with delaying the tip stall. The tests showed the flight envelope to be improved by the equivalent of 35% to 40% increase in blade area and made it clear that level flight speeds beyond the existing record were achievable.

Different aerofoil sections were used for the inboard, mid-span and tip parts of the blade, chosen in relation to the local speed conditions and lift requirements. The section used for the tip was thinner than the other two. The blade was built in glass fibre with a single spar, special construction methods being employed.

The aircraft was a standard Lynx (Utility version) with a skid undercarriage, in which protuberance drag had been reduced to a minimum and an attempt had been made to reduce rotorhead drag by fairings. The engine power was enhanced by water-methanol injection. The purpose of these measures was to ensure that, given a large alleviation in the flight envelope, the aircraft would not then be power limited unnecessarily.

For the record attempt, the course of 15 km was flown at 150 m above ground, this being well within the altitude band officially required. The mean speed of two runs in opposite directions was 400.87 km/hr (216 knots), exceeding the previous record by 33 km/hr. The aircraft also had an extraordinarily good rate of climb near the bucket speed (80–100 knots), this being well over 20 m/sec (4000 ft/min) – exceeding the capacity of the indicator instrument – and generally exhibited excellent flying characteristics. Fig. 7.6 shows a photograph of the aircraft in flight and Fig. 7.7 presents a spectacular view of the rotor blade.

7.10 Speculation on the really-low-drag helicopter

The ideas in this section come mainly from M.V. Lowson⁴. It is of interest to consider, at least in a hypothetical manner, the lowest level of cruising power that might be envisaged for a really-low-drag helicopter of the future, by comparison with levels typically achieved in current design. The demand for fuel-efficient operation is likely to increase with time, as more range-flying movements are undertaken, whether in an industrial or a passenger-carrying context. Any increase in fuel costs will narrow the operating cost differential between helicopters (currently dominated by maintenance costs)

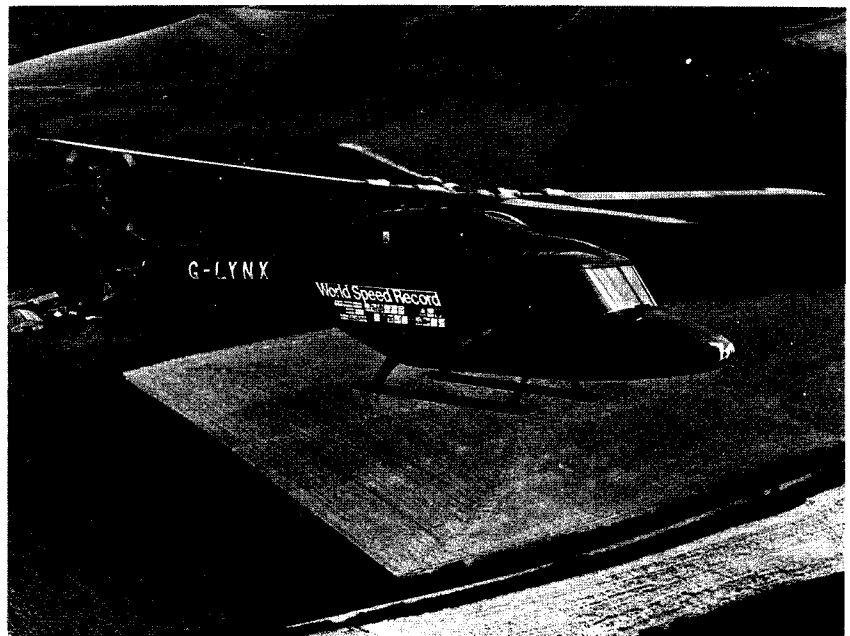


Fig. 7.6 World speed record helicopter in flight. (Reproduced courtesy of Westland Helicopters Ltd.)

and fixed-wing aircraft and the possibility of the helicopter achieving comparability is an intriguing one.

Reference to Fig. 7.2 shows that at high forward speed, whilst all the power components need to be considered, the concept of a really-low-drag (RLD) helicopter stands or falls on the possibility of a major reduction in parasite drag being achieved. This is not *a priori* an impossible task, since current helicopters have from four to six times the parasite drag of an aerodynamically clean fixed-wing aircraft. For the present exercise let us take as the datum case a 4500 kG (10000 lb) helicopter, the parasite drag of which, in terms of equivalent flat plate area, is broken down in Table 7.1. All calculations were made in Imperial units and for simplicity these are used in the presentation. The total, 14.05 ft², is somewhat higher than the best values currently achievable but is closely in line with the value of 19.1 ft² for a 18000 lb helicopter used by Stepniewski and Keys, Vol. II, for their typical case.

In setting target values for the RLD helicopter, as given in Table 7.1, the arguments used are as follows. Minimum fuselage

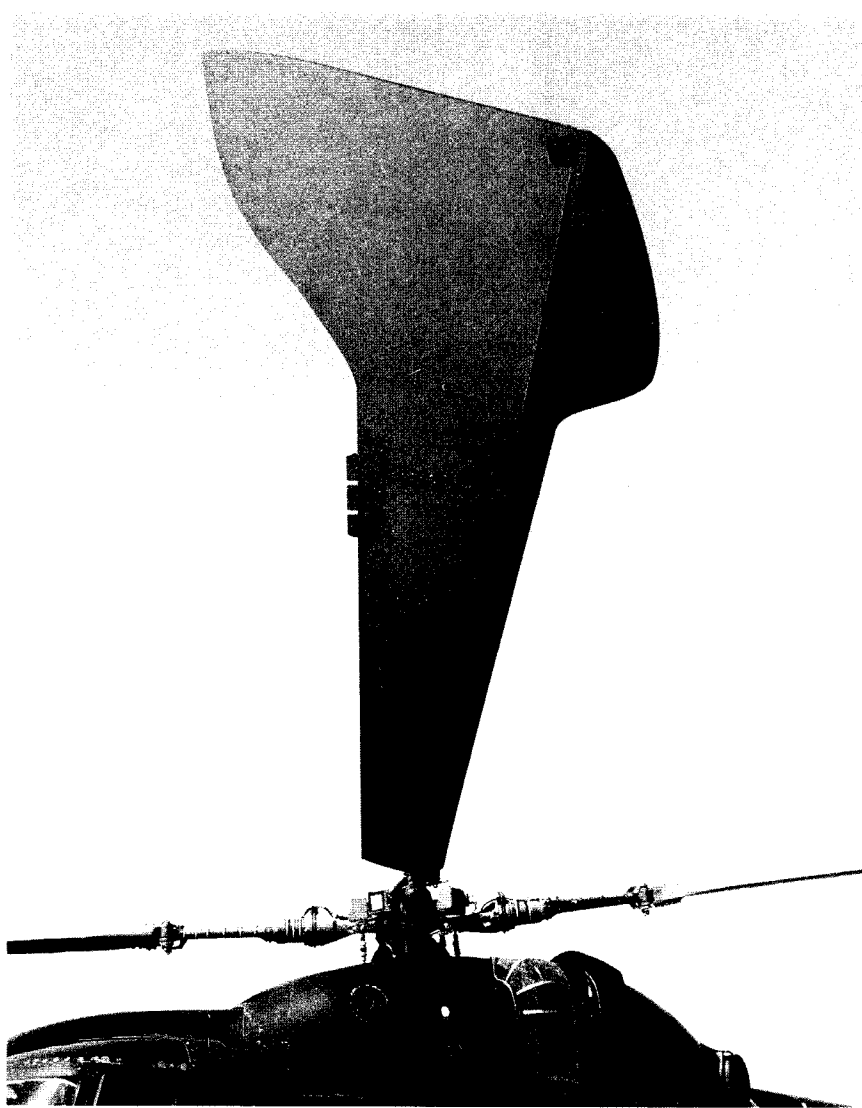


Fig. 7.7 Rotor blade on speed record aircraft. (Reproduced courtesy of Westland Helicopters Ltd.)

drag, inferred from standard texts such as Hoerner (*loc. cit.*) and Goldstein⁵, would be based on a frontal-area drag coefficient of 0.05. This corresponds to 2 ft^2 flat plate area in our case, which is not strictly the lowest possible because helicopters traditionally

Table 7.1

	Datum aircraft, ft^2	Target for RLD aircraft, ft^2
Basic fuselage	2.74	2.3
Nacelles	0.80	0.4
Tail unit	0.45	0.3
Rotorhead	4.29	0.8
Landing gear	1.55	0
Total	14.05	5.0

have spacious cabins with higher frontal areas, weight for weight, than fixed-wing aircraft. A target value of 2.3 ft^2 is therefore entirely reasonable and might be bettered. The reductions in nacelle and tail unit drags may be expected to come in time and with special effort. A large reduction in rotorhead drag is targeted but the figure suggested corresponds to a frontal-area drag coefficient about double that of a smooth ellipsoidal body, so while much work would be involved in reshaping and fairing the head, the target seems not impossible of attainment. Landing-gear drag is assumed to be eliminated by retraction or other means. In the miscellaneous item of the datum helicopter, a substantial portion is engine-cooling loss, on which much research could be done. Tail rotorhead drag can presumably be reduced in much the same proportion as that of the main rotorhead. Roughness and protuberance losses will of course have to be minimized.

In total the improvement envisaged is a 64% reduction in parasite drag. Achievement of this target would leave the helicopter still somewhat inferior to an equivalent clean fixed-wing aircraft.

Such a major reduction in parasite drag will leave the profile power as the largest component of RLD power at cruise. The best prospect for reducing blade profile drag below current levels probably lies in following the lead given by fixed-wing technology in the development of supercritical aerofoil sections. Using such sections in the tip region postpones the compressibility drag rise to higher Mach number: thus a higher tip speed can be used which, by Equation (6.3), reduces the blade area required and thereby the

profile drag. Advances have already been made in this direction but whereas in the rotor design discussed in Chapter 6 a tip Mach number 0.88 was assumed, in fixed-wing research drag-rise Mach numbers as high as 0.95 were described by Haines⁶ more than a decade ago. Making up this kind of deficiency would reduce blade profile drag by about 15%. If it is supposed that in addition advances will be made in the use of thinner sections, a target of 20% lower profile power for the RLD helicopter seems reasonable.

Reduction in induced power will involve the use of rotors of larger diameter and lower disc loading than in current practice. Developments in blade materials and construction techniques will be needed for the higher aspect ratios involved. These can be expected, as can also the relaxation of some operational requirements framed in a military context, for example that of take-off in a high wind from a ship. A 10% reduction of induced power at cruise is therefore anticipated. The same proportion is assumed for the small residual power requirement of the miscellaneous items.

Table 7.2 shows the make-up of cruise power at 160 knots from Fig. 7.2, representing the datum aircraft, and compares this with the values for the RLD helicopter according to the foregoing analysis.

The overall reduction for the RLD helicopter is 41% of the power requirement of the datum aircraft. An improvement of this magnitude would put the RLD helicopter into a competitive position with certain types of small, fixed-wing, propeller-driven business aircraft for low-altitude operation. Qualitatively it may be said that the RLD helicopter has a slightly higher parasite drag than the

Table 7.2

	Datum aircraft, HP	RLD aircraft, HP
Parasite	680	245
Profile	410	328
Induced	130	117
Miscellaneous	80	72
Total	1300	762

fixed-wing aircraft, about the same profile drag or slightly less (since the fixed-wing aircraft normally carries a greater wing area than is needed for cruise, while the helicopter blade area can be made to suit, provided that adverse Mach effects are avoided) and a lower induced drag if the rotor diameter is greater than the fixed-wing span. The helicopter, however, has no ready answer to the ability of the fixed-wing aircraft to reduce drag by flying at high altitude. Equally of course, the fixed-wing aircraft cannot match the low-speed and hover capability of the helicopter.

7.11 An exercise in high-altitude operation

Fixed-wing aircraft operate more economically at high altitude than at low. Aircraft drag is reduced and engine (gas turbine) efficiency is improved, leading to increases in cruising speed and specific range (distance per unit of fuel consumed). With gas-turbine powered helicopters, the incentive to realize similar improvements is strong: there are, however, basic differences to be taken into account. On a fixed-wing aircraft, the wing area is determined principally by the stalling condition at ground level; increasing the cruise altitude improves the match between area requirements at stall and cruise. On a helicopter, the blade area is fixed by a cruise speed requirement, while low speed flight determines the installed power needed. The helicopter rotor is unable to sustain the specified cruising speed at altitudes above the density design altitude, the limitation being that of retreating blade stall. The calculations now to be described are of a purely hypothetical nature, intended to illustrate the kind of changes that could in principle convey a high-altitude flight potential. The altitude chosen for the exercise is 3000 m (10 000 ft), this being near the limit for zero pressurization. I am indebted to R.V. Smith for the work involved.

Imperial units are used as in the previous section. The datum case is that of a typical light helicopter, of all-up weight 10 000 lb and having good clean aerodynamic design, though traditional in the sense of featuring neither especially low drag nor advanced blade design. Power requirements are calculated by the simple methods outlined earlier in the present chapter. Engine fuel flow is related to power output in a manner typical of modern gas turbine

engines. Specific range (nautical miles per pound fuel) is calculated thus:

$$\text{specific range (nm/lb)} = \text{forward speed (knots)}/\text{fuel flow (lb/hr)}$$

A flight envelope of the kind described in Section 7.7 is assumed: this is primarily a retreating-blade limitation in which the value of W/δ (δ being the relative density at altitude) decreases from 14 000 lb at 80 knots to 8000 lb at 180 knots.

The results are presented graphically in Fig. 7.8. Specific range is plotted as a function of flight speed for sea level, 5000 ft and 10 000 ft altitude. Intersecting these curves are (a) the flight envelope limit, (b) the locus of best-range speeds and (c) the power limitation curve. We see that in case A, which is for the datum helicopter, the flight envelope restricts the maximum specific range to 0.219 nm/lb, this occurring at 5000 ft and low speed (only 114 knots). So far as available power is concerned it would be possible to realize the best-range speeds up to 10 000 ft and beyond.

Case B examines the effect of a substantial reduction in parasite drag. Using a less ambitious target than that envisaged in Section 7.10, a parasite drag two thirds that of the datum aircraft is assumed. At best-range speed a large increase in specific range at all altitudes is possible but, as before, the restriction imposed by the flight envelope is severe, allowing an increase to only 0.231 nm/lb, again at approximately 5000 ft and low speed (120 knots). It is clear that the full benefit of drag reduction cannot be realized without a considerable increase in rotor thrust capability. A comparison of cruising speeds emphasises the deficiency: without the flight-envelope limitation the best-range speeds would be usable, namely at all heights a little above 150 knots for the datum aircraft and 20 knots higher for the low-drag version.

The increase in thrust capability required by the low-drag aircraft to raise the flight envelope limit to the level of best-range speed at 10 000 ft is approximately 70%. Case C shows the performance of the low-drag aircraft supposing the increase to be obtained from the same percentage increase in blade area. Penalties of weight increase and profile power increase are allowed for, assumed to be in proportion to the area change. The best-range speed is now attainable up to over 9000 ft, while at 10 000 ft the specific range is virtually the same as at best-range speed, namely 0.267 nm/lb at 170 knots: this represents a 22% increase in specific range over the datum aircraft, attained at 60 knots higher cruising speed.

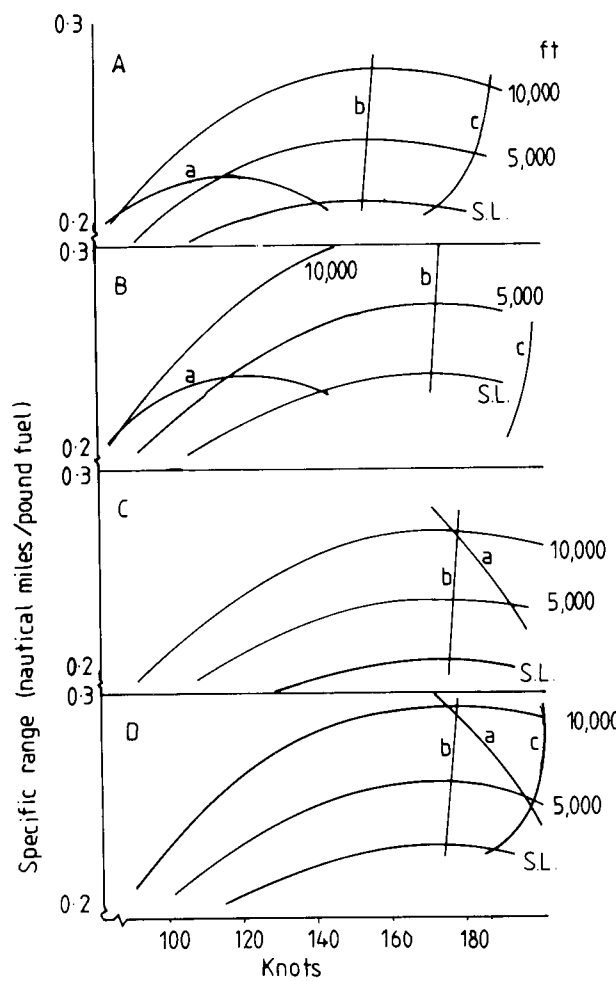


Fig. 7.8 Specific range calculations for high-altitude operation.

For a final comparison, case D shows the effect of obtaining the required thrust increase by combination of a much smaller increase in blade area (24.5%) with conversion to an advanced rotor design, using an optimum distribution of cambered blade sections and the Westland advanced tip. The penalties in weight and profile power are thereby reduced considerably. The result is a further increase in specific range, to 0.293 nm/lb or 34% above that of the datum aircraft, attained at the same cruising speed as in case C.

The changes are seen to further advantage by calculating also the maximum range achievable. This has been done in alternative

Table 7.3

Datum	Best-range speed, kt	Altitude, ft	Specific range, nm/lb	Weight penalty, lb	Max. range, nm (1)	nm (2)
A	114	5000	0.219		357	357
B	120	4200	0.231	0		
C	174	10 000	0.267	652	274	458
D	174	10 000	0.293	225	433	503

ways, assuming that the weight penalty reduces (1) the fuel load or (2) the payload. On the first supposition, the weight penalty of case C results in a range reduction but with case D the gain more than compensates for the smaller weight penalty.

The characteristics of the various configurations are summarized in Table 7.3.

References

- 1 Prouty, R.W. (1985) *Helicopter aerodynamics*. PJS Publications Inc, Peoria Illinois.
- 2 Hoerner, S.F. (1975) *Fluid dynamic drag*. Published by author.
- 3 Keys, C.R. and Wiesner, R. (1975) 'Guidelines for reducing helicopter parasite drag'. *Jour. Amer. Hel. Soc.*
- 4 Lowson, M.V. (1980) *Thoughts on an efficient helicopter*. WHL Res. Memo. (unpublished).
- 5 Goldstein, S. (1938) *Modern developments in fluid dynamics*. Oxford U.P.
- 6 Haines, A.B. (1976) 'Aerodynamics'. *Aero. Jour.*, July 1976.

8 Trim, Stability and Control*

8.1 Trim

The general principle of flight with any aircraft is that the aerodynamic, inertial and gravitational forces and moments about three mutually perpendicular axes are in balance at all times. In helicopter steady flight (non-rotating), the balance of *forces* determines the orientation of the main rotor *in space*. The balance of *moments* about the aircraft centre of gravity (CG) determines the attitude adopted by the airframe and when this balance is achieved, the helicopter is said to be trimmed. To a pilot the trim may be 'hands on' or 'hands off': in the latter case in addition to zero net forces and moments on the helicopter the control forces are also zero: these are a function of the internal control mechanism and will not concern us further, apart from a brief reference at the end of this section.

In deriving the performance equation for forward flight in Chapter 5 (Equation (5.42)), the longitudinal trim equations were used in their simplest approximate form (Equations (5.38) and (5.39)). They involve the assumption that the helicopter parasite drag is independent of fuselage attitude, or alternatively that Equation (5.42) is used with a particular value of D_p for a particular attitude, which is determined by solving a moment equation (see Fig. 8.2 and the accompanying description below). This procedure is adequate for many performance calculations, which explains why the subject of trim was not introduced at that earlier stage. For the most accurate performance calculations, however, a trim analysis programme is needed in which the six equations of force and

* This chapter makes liberal use of unpublished papers by B. Pitkin, Flight Mechanics Specialist, Westland Helicopters.

moment are solved simultaneously, or at least in longitudinal and lateral groups, by iterative procedures such as Stepniewski and Keys (Vol. II) have described.

Consideration of helicopter moments has not been necessary up to this point in the book. To go further we need to define the functions of the *horizontal tailplane* and *vertical fin* and the nature of *direct head moment*.

In steady cruise the function of a tailplane is to provide a pitching moment to offset that produced by the fuselage and thereby reduce the net balancing moment which has to be generated by the rotor. The smaller this balancing moment can be, the less is the potential fatigue damage on the rotor. In transient conditions the tailplane pitching moment is stabilizing, as on a fixed-wing aircraft, and offsets the inherent static instability of the fuselage and to some extent that of the main rotor. A fixed tailplane setting is often used, although this is only optimum for one combination of flight condition and CG location.

A central vertical fin is multi-functional: it generates a stabilizing yawing moment and also provides a structural mounting for the tail rotor. The central fin operates in a poor aerodynamic environment, as a consequence of turbulent wakes from the main and tail rotors and blanking by the fuselage, but fin effectiveness can be improved by providing additional fin area near the tips of the horizontal tailplane.

When the flapping hinge axis is offset from the shaft axis (the normal condition for a rotor with three or more blades), the centrifugal force on a blade produces (Fig. 8.1) a pitching or rolling moment proportional to disc tilt. Known as direct rotor moment, the effect is large because although the moment arm is small the centrifugal force is large compared with the aerodynamic and inertial forces. A hingeless rotor produces a direct moment perhaps four times that of an articulated rotor for the same disc tilt. Analytically this would be expressed by according to the flexible element an *effective offset* four times the typical 3% to 4% span offset of the articulated hinge.

Looking now at a number of trim situations, in hover with zero wind speed the rotor thrust is vertical in the longitudinal plane, with magnitude equal to the helicopter weight corrected for fuselage downwash. For accelerating away from hover the rotor disc must be inclined forward and the thrust magnitude adjusted so that it is

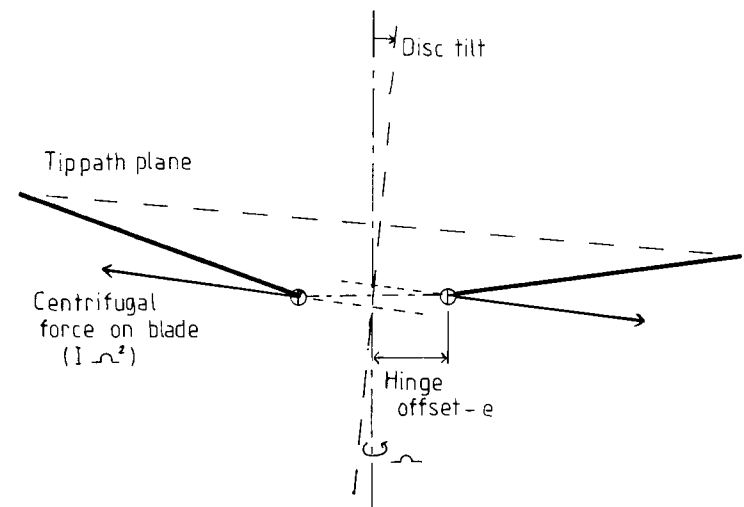


Fig. 8.1 Direct rotor moment.

equal to, and directly opposed to, the vector sum of the weight and the inertial force due to acceleration. In steady forward flight the disc is inclined forward and the thrust magnitude is adjusted so that it is equal to, and directly opposed to, the vector sum of the weight and aerodynamic drag.

The pitch attitude adopted by the airframe in a given flight condition depends upon a balance of pitching moments about the CG. Illustrating firstly without direct rotor moment or tailplane-and-airframe moment, the vector sum of aircraft drag (acting through the CG) and weight must lie in the same straight line as the rotor force. This direction being fixed in space, the attitude of the fuselage depends entirely upon the CG position. A forward location results in a more nose-down attitude than an aft location. The effect of a direct rotor moment is illustrated in Fig. 8.2 for a forward CG location. Now the rotor thrust and resultant force of drag and weight, again equal in magnitude, are not in direct line but must be parallel, creating a couple which balances the other moments. A similar situation exists in the case of a net moment from the tailplane and airframe. For a given forward CG position, the direct moment makes the fuselage attitude less nose-down than it would otherwise be. Reverse results apply for an aft CG position. At high forward speeds, achieving a balanced state may involve

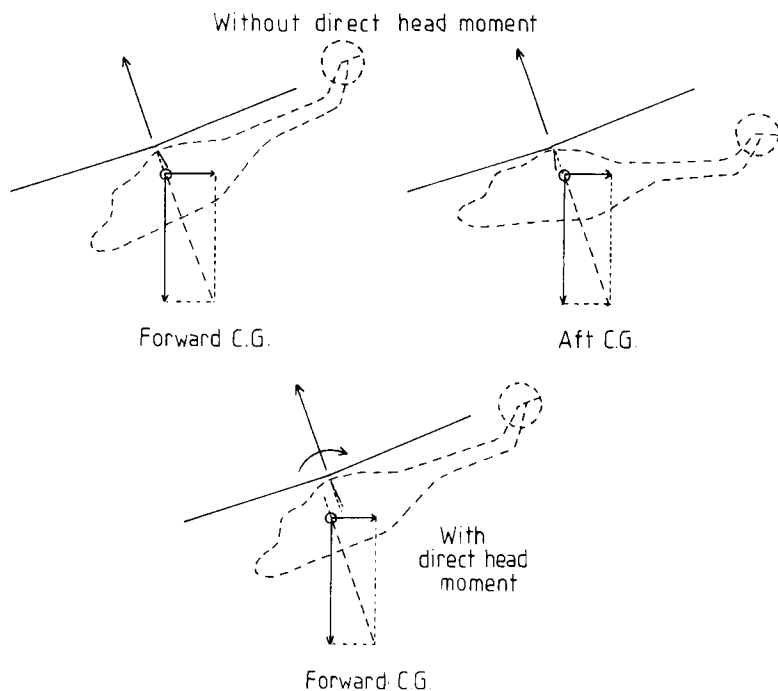


Fig. 8.2 Fuselage attitudes in forward flight.

excessive nose-down attitudes unless the tailplane can be made to supply a sufficient restoring moment.

Turning to the balance of lateral forces, in hover the main rotor thrust vector must be inclined slightly sideways to produce a force component balancing the tail rotor thrust. This results in a hovering attitude tilted two or three degrees to port (Fig. 8.3). In sideways flight the tilt is modified to balance sideways drag on the helicopter: the same applies to hovering in a crosswind. In forward flight the option exists, by sideslipping to starboard, to generate a sideforce on the airframe which, at speeds above about 50 knots, will balance the tail rotor thrust and allow a zero-roll attitude to be held.

With the lateral forces balanced in hover, the projection of the resultant of helicopter weight and tail-rotor thrust will not generally pass through the main-rotor centre, so a rolling couple is exerted which has to be balanced out by a direct rotor moment. This moment depends upon the angle between disc axis and shaft axis and since the first of these has been determined by the force balance, the airframe has to adopt a roll attitude to suit. For the

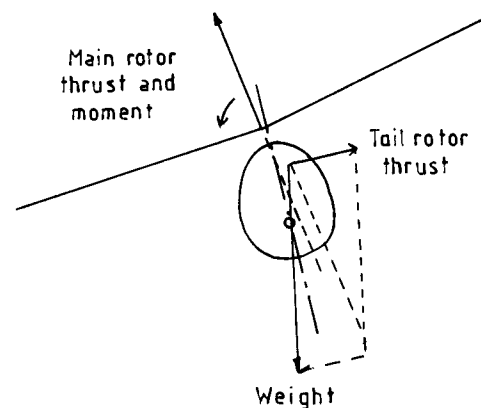


Fig. 8.3 Lateral tilt in hover.

usual situation, in which the line of action of the sideways thrust component is above that of the tail-rotor thrust, the correction involves the shaft axis moving closer to the disc axis, that is to say the helicopter hovers with the fuselage in a small left roll attitude. Positioning the tail rotor high (close to hub height) minimizes the amount of left roll angle needed.

Yawing moment balance is provided at all times by selection of the tail-rotor thrust, which balances the combined effects of main-rotor torque reaction, airframe aerodynamic yawing moment due to sideslip and inertial moments present in manoeuvring.

The achievement of balanced forces and moments for a given flight condition is closely linked with stability. An unstable aircraft theoretically cannot be trimmed, because the slightest disturbance, atmospheric or mechanical, will cause it to diverge from the original condition. A stable aircraft may be difficult to trim, because although the combination of control positions for trim exists, oversensitivity may make it difficult to introduce any necessary fine adjustments to the aerodynamic control surfaces.

8.2 Treatment of stability and control

As with a fixed-wing aircraft, both static stability and dynamic stability contribute to the flying qualities of a helicopter. Static stability refers to the initial tendency of the aircraft to return to its trimmed condition following a displacement. Dynamic stability

considers the subsequent motion in time, which may consist of a dead-beat return, an oscillatory return, a no-change motion, an oscillatory divergence or a non-return divergence; the first two signifying positive stability, the third neutral stability and the last two negative stability (instability). A statically unstable motion is also dynamically unstable but a statically stable motion may be either stable or unstable dynamically.

The subject of stability and control in totality is a formidable one. The part played by the rotor is highly complicated, because strictly each blade possesses its own degrees of freedom and makes an individual contribution to any disturbed motion. Fortunately, however, analysis can almost always be made satisfactorily by considering the behaviour of the rotor as a whole. Even so it is useful to make additional simplifying assumptions: those which pave the way for a classical analysis, similar to that made for a fixed-wing aircraft, come essentially from the work of Hohenemser¹ and Sissingh² and are the following:

- (1) in disturbed flight the accelerations are small enough not to affect the rotor response, in other words the rotor reacts in effect instantaneously to speed and angular rate changes;
- (2) rotor speed remains constant, governed by the engine;
- (3) longitudinal and lateral motions are uncoupled so can be treated independently.

Given these important simplifications, the mathematics of helicopter stability and control are nevertheless heavy (Bramwell, Chapter 7), edifying academically but hardly so otherwise, and in practice strongly dependent upon the computer for results. In this chapter we shall be content with descriptive accounts, which bring out the physical characteristics of the motions involved.

No absolute measure of stability, static or dynamic, can be stipulated for helicopters in general, because flying qualities depend on the particular blend of natural stability, control and autostabilization. Also, stability must be assessed in relation to the type of mission to be performed.

8.3 Static stability

We consider the nature of the initial reaction to various forms of disturbance from equilibrium. Longitudinal and lateral motions are

treated independently. The contributions of the rotor to forces and moments arise from two sources, variations in magnitude of the rotor force vector and variations in the inclination of this vector associated with disc tilt, that is with blade flapping motion.

8.3.1 Incidence disturbance

An upward imposed velocity (for example a gust) increases the incidence of all blades, giving an overall increase in thrust magnitude. Away from hover, the dissimilarity in relative airspeed on the advancing and retreating sides leads to an incremental flapping motion, which results in a nose-up tilt of the disc. Since the rotor centre lies above the aircraft CG, the pitching moment caused by the change of inclination is in a nose-up sense, that is destabilizing and increasingly so with increase of forward speed. In addition, the change in thrust magnitude itself generates a moment contribution, the effect of which depends upon the fore-and-aft location of the CG relative to the rotor centre. In a practical case, the thrust vector normally passes ahead of an aft CG location and behind a forward one, so the increase in thrust magnitude aggravates the destabilizing moment for an aft CG position and alleviates it for a forward one. The important characteristic therefore is a degradation of longitudinal static stability with respect to incidence, at high forward speed in combination with an aft CG position. This is also reflected in a degradation of dynamic stability under the same flight conditions.

It should be noted that these fundamental arguments relate to rigid blades. With the advent of modern composite materials for blade construction, judicious exploitation of the distribution of inertial, elastic and aerodynamic loadings allows the possibility of tailoring the blade aeroelastic characteristics to alleviate the inherently destabilizing features just described.

Of the other factors contributing to static stability, the fuselage is normally destabilizing in incidence, a characteristic of all streamlined three-dimensional bodies. Hinge offset, imparting an effective stiffness, likewise aggravates the incidence instability. The one stabilizing contribution comes from the horizontal tailplane. Figure 8.4 represents the total situation diagrammatically. The tailplane compensates for the inherent instability of the fuselage, leaving the rotor contributions as the determining factors. Of these, the stiffness effect for an articulated rotor is generally of similar magnitude to

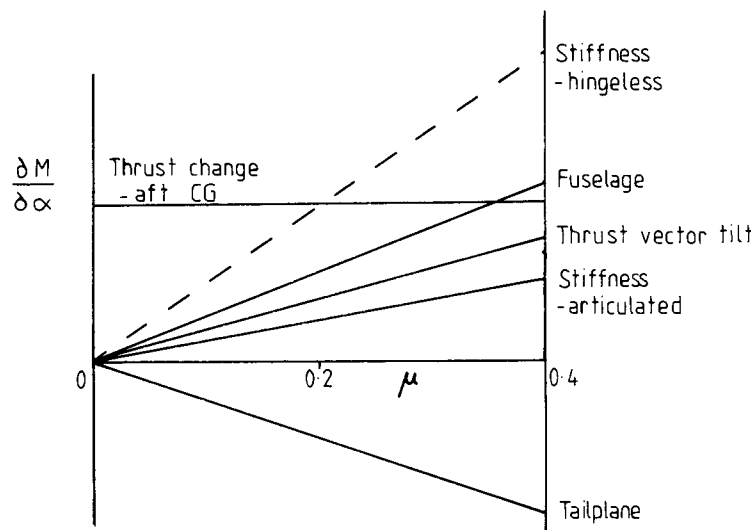


Fig. 8.4 Contributions to static stability in incidence.

the thrust vector tilt moment. With a hingeless rotor (Section 8.5) the stiffness effect is much greater.

8.3.2 Forward speed disturbance

An increase in forward speed leads to incremental flapping, resulting in a change in nose-up disc tilt. The amount of change is reckoned to be about one degree per 10 m/s speed increase, independently of the flight speed. The thrust vector is effectively inclined rearwards, supported by the nose-up pitching moment produced, providing a retarding force component and therefore *static stability* with respect to forward speed. This characteristic is present in the hover but nevertheless contributes to a *dynamic instability* there (Section 8.4.2).

Speed increase increases the airframe drag and this contributes, increasingly with initial forward speed, to a positive speed-stability characteristic for the helicopter, except in the hover.

8.3.3 Angular velocity (pitch or roll rate) disturbance

The effect of a disturbance in angular velocity (pitch or roll) is complex. In brief, a gyroscopic moment about the flapping hinge produces a phased flapping response and the disc tilt resulting from

this generates a moment opposing the particular angular motion. Thus the rotor exhibits damping in both pitch and roll. Moments arising from non-uniform incidence over the disc lead to cross-coupling, that is rolling moment due to rate of pitch and vice versa.

8.3.4 Sideslip disturbance

In a sideslip disturbance, the rotor 'sees' a wind unchanged in velocity but coming from a different direction. As a result the direction of maximum flapping is rotated through the angle of sideslip change and this causes a sideways tilt of the rotor away from the wind. There is therefore a rolling moment opposing the sideslip, corresponding effectively to the dihedral action of a fixed-wing aircraft. In addition the sideslip produces a change in incidence of the tail-rotor blades, so that the tail rotor acts like a vertical fin providing 'weathercock' stability.

8.3.5 Yawing disturbance

A disturbance in yaw causes a change of incidence at the tail rotor and so again produces a fin damping effect, additional to that of the actual aircraft fin. Overall, however, basic directional stability tends to be poor because of degradation by upstream flow separations and wake effects.

8.3.6 General conclusion

It is seen from the above descriptions that longitudinal static stability characteristics are significantly different from, and more complex than, those of a fixed-wing aircraft, whilst lateral characteristics of the two types of aircraft are similar, although the forces and moments arise in different ways.

8.4 Dynamic stability

8.4.1 Analytical process

The mathematical treatment of dynamic stability given by Bramwell follows the lines of the standard treatment for fixed-wing aircraft. Wind axes are used, with the X -axis parallel to the flight path, and the stability derivatives ultimately are fully non-dimensionalized.

The classical format is useful because it is basic in character and displays essential comparisons prominently. The most notable distinction which emerges is that whereas with a fixed-wing aircraft, the stability quartic equation splits into two quadratics, leading to a simple physical interpretation of the motion, with the helicopter this unfortunately is not so, and as a consequence the calculation of roots becomes a more complicated process.

Industrial procedures for the helicopter tend to be on rather different lines. The analysis is generally made with reference to body axes, with origin at the CG. In this way the X -axis remains forward relative to the airframe, whatever the direction of flight or of relative airflow. The classical linearization of small perturbations is still applicable in principle, the necessary inclusion of initial-condition velocity components along the body axes representing only a minor complication. Force and moment contributions from main rotor, tail rotor, airframe and fixed tail surface are collected along each body axis, as functions of flow parameters, control angles and flapping coefficients and are then differentiated with respect to each independent variable in turn. Modern computational techniques provide ready solutions to the polynomials. Full non-dimensionalization of the derivatives is less useful than for fixed-wing aircraft and a preferred alternative is to ‘normalize’ the force and moment derivatives in terms of the helicopter weight and moment of inertia respectively.

8.4.2 Special case of hover

In hovering flight the uncoupled longitudinal and lateral motions break down further. Longitudinal motion resolves into an uncoupled vertical velocity mode and an oscillatory mode coupling forward velocity and pitch attitude. In a similar manner, lateral motion breaks down into an uncoupled yaw mode and an oscillatory mode coupling lateral velocity and roll attitude. Both of these coupled modes are dynamically unstable. The physical nature of the longitudinal oscillation is illustrated in Fig. 8.5 and can be described as follows.

Suppose the hovering helicopter to experience a small forward velocity as at (a). Incremental flapping creates a nose-up disc tilt, which results in a nose-up pitching moment on the aircraft. This is as described in Section 8.3.2, (the important overall qualification being that there is no significant aircraft drag force). A nose-up

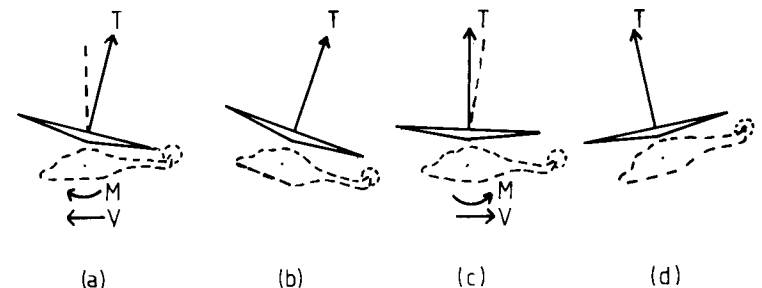


Fig. 8.5 Longitudinal dynamic instability in hover.

attitude develops and the backward-inclined thrust opposes the forward motion and eventually arrests it, as at (b). The disc tilt and rotor moment have now been reduced to zero. A backward swing commences, in which the disc tilts forward, exerting a nose-down moment, as at (c). A nose-down attitude develops and the backward movement is ultimately arrested, as at (d). The helicopter then accelerates forward under the influence of the forward inclination of thrust and returns to the situation at (a). Mathematical analysis shows, and experience confirms, that the motion is dynamically unstable, the amplitude increasing steadily if the aircraft is left to itself.

This longitudinal divergent mode and its lateral-directional counterpart constitute a fundamental problem of hovering dynamics. They require constant attention by the pilot, though since both are usually of low frequency, some degree of instability can generally be allowed. It remains the situation, however, that ‘hands-off’ hovering is not possible unless a helicopter is provided with an appropriate degree of artificial stability.

8.5 Hingeless rotor

A hingeless rotor flaps in similar manner to an articulated rotor and both the rotor forces and the flapping derivatives are little different between the two. Terms expressing hub moments, however, are increased severalfold with the hingeless rotor so that, as has been said, compared with the 3% to 4% hinge offset of an articulated rotor, the effective offset of a hingeless rotor is likely to be 12% to 16% or even higher. This increased stiffness has an

adverse effect on longitudinal static stability; in particular the pitch instability at high speed is much more severe (Fig. 8.4). A forward CG position is an alleviating factor, but in practice the CG position is dominated by role considerations. The horizontal tailplane can be designed to play a significant part. Not only is the stabilizing influence a direct function of tailplane size but also the angular setting to the fuselage affects the pitching moment balance in trim and can be used to minimize hub moment over the critical part of the operational flight envelope. Despite this, however, the stability degradation in high-speed flight normally remains a dominant feature.

8.6 Control

Control characteristics refer to a helicopter's ability to respond to control inputs and so move from one flight condition to another. The inputs are made, as has been seen, by applying pitch angles to the rotor blades so as to generate the appropriate forces and moments. On the main rotor the angles are made up of the collective pitch θ_0 and the longitudinal and lateral cyclic pitch angles B_1 and A_1 as introduced in Chapter 4. The tail rotor conventionally has only collective pitch variation, determined by the thrust required for yawing moment balance.

A word is required here about rate damping. When the helicopter experiences a rate of pitch, the rotor blades are subjected to gyroscopic forces proportional to that rate. A nose-up rotation induces a download on an advancing blade, leading to nose-down tilt of the rotor disc. The associated offset of the thrust vector from the aircraft CG and the direct rotor moment are both in the sense opposing the helicopter rotation and constitute a damping effect or stabilising feature. A similar argument applies to the gyroscopic effects of a rate of roll.

Adequacy of control is formally assessed in two ways, by *control power* and *control sensitivity*. Control power refers to the maximum moment that can be generated. Normalizing this in terms of aircraft moment of inertia, the measure becomes one of initial acceleration produced per unit displacement of the cyclic control stick. Control sensitivity recognizes the importance of a correlation between control power and the damping of the resultant motion; the ratio can be expressed as angular velocity per unit stick displacement. High

control sensitivity means that control power is large relative to damping, so that a large angular velocity is reached before the damping moment stabilizes the motion.

The large effective offset of a hingeless rotor conveys both increased control power and greater inherent damping, resulting in shorter time constants and crisper response to control inputs. Basic flying characteristics in the hover and at low forward speeds are normally improved by this, because the more immediate response is valuable to the pilot for overcoming the unstable oscillatory behaviour described in Section 8.4.2.

A mathematical treatment of helicopter response is given by Bramwell (pp. 231–249) and illustrated by typical results for a number of different control inputs. His results for the normal acceleration produced by a sudden increase of longitudinal cyclic pitch (B_1) in forward-level flight at advance ratio 0.3 are reproduced in Fig. 8.6. We note the more rapid response of the hingeless rotor compared with the articulated rotor, a response which the equations show to be divergent in the absence of a tailplane. Fitting a tailplane reduces the response rates and in both cases appears to stabilize them after three or four seconds.

Roll response in hover is another important flying quality, particularly in relation to manoeuvring near the ground. In an appropriate example, Bramwell shows the hingeless helicopter reaching a constant rate of roll within less than a second, while the articulated version takes three or four seconds to do so. For a given degree of cyclic pitch, the final roll rates are the same, because the control

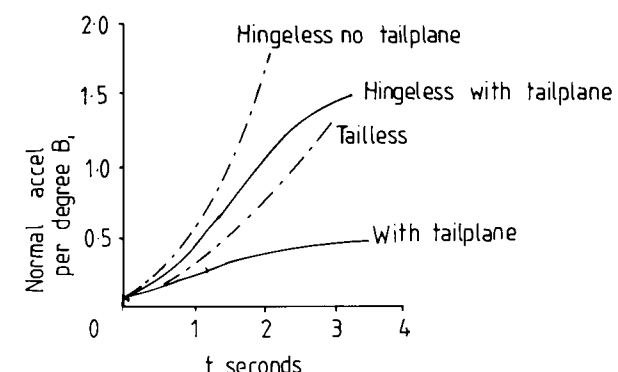


Fig. 8.6 Calculated rotor response to B_1 (after Bramwell).

power and roll damping differ in roughly the same proportion in the two aircraft.

Rotor response characteristics can be described more or less uniquely in terms of a single non-dimensional parameter, the *stiffness number* S , defined as

$$S = (\lambda^2 - 1)/n \quad (8.1)$$

This expresses the ratio of elastic to aerodynamic flapping moments on the blade. λ is the blade natural flapping frequency, having the value 1.0 for zero blade offset and related generally to the percentage offset e by:

$$\lambda^2 = -\frac{1 + \frac{1}{2}e}{1 - e} \quad (8.2)$$

Thus a 4% offset yields a value $\lambda = 1.03$; for hingeless rotors the λ values are generally in the range 1.09 to 1.15. In Equation (8.1), n is a normalizing inertia number. Some basic rotor characteristics are shown as functions of stiffness number in Fig. 8.7. Taking the four parts of the diagram in turn, the following comments can be made.

- (a) Rotors have until now made use of only relatively restricted parts of the inertia/stiffness plane.
- (b) In the amount of disc tilt produced on a fixed hovering rotor per degree of cyclic pitch, articulated and the 'softer' hingeless rotors are practically identical.
- (c) On the phase lag between cyclic pitch application and blade flapping, we observe the standard 90° for an articulated rotor with zero hinge offset, decreasing with increase of off-set, real or effective, to 15°–20° lower for a hingeless rotor.
- (d) For the low stiffness numbers of articulated rotors, the principal component of moment about the aircraft CG is likely to be that produced by thrust vector tilt. Hingeless rotors, however, produce moments mainly by stiffness; their high hub moment gives good control for manoeuvring but needs to be minimized for steady flight, in order to restrict as much as possible hub load fluctuations and vibratory input to the helicopter.

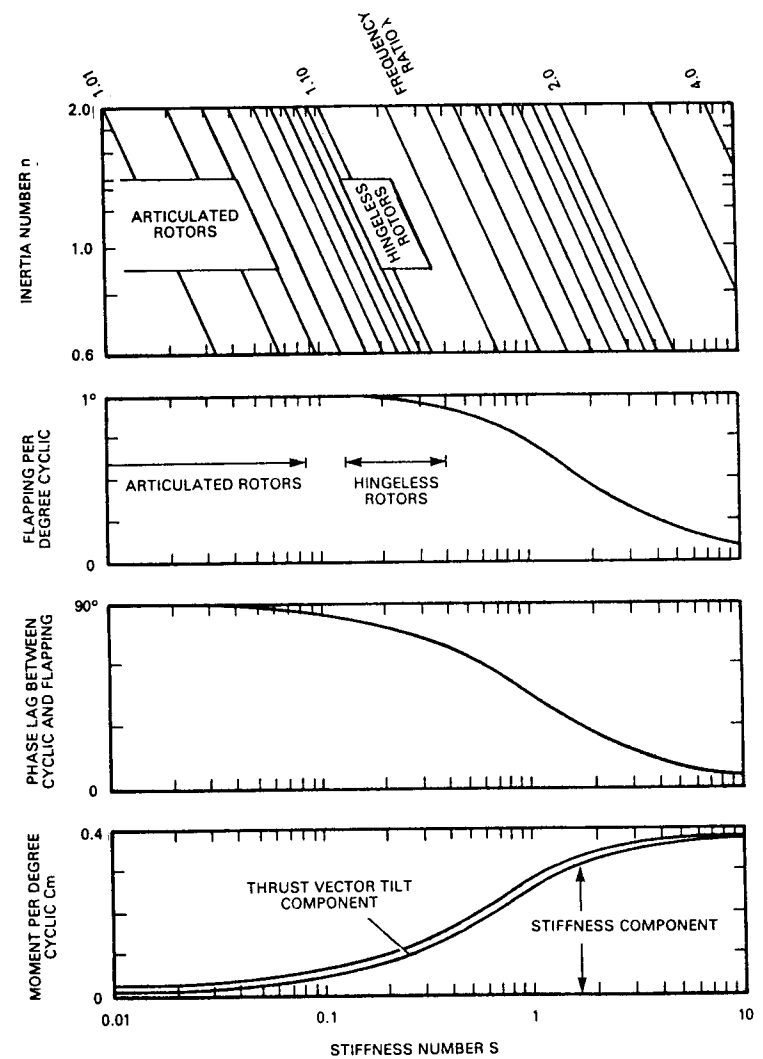


Fig. 8.7 Rotor characteristics in terms of stiffness number.

8.7 Autostabilization

In order to make the helicopter a viable operational aircraft, shortcomings in stability and control characteristics generally have to be made good by use of automatic flight control systems. The complexity of such systems, providing stability augmentation, long-

term datum-holding autopilot functions, automatically executed manoeuvres and so on, depends upon the mission task, the failure survivability requirements and of course on the characteristics of the basic helicopter.

Autostabilization is the response to what is perhaps the commonest situation, that in which inadequate basic stability is combined with ample control power. The helicopter is basically flyable but in the absence of automatic aids, continuous correction by the pilot would be required — a tiring process and in some conditions (such as flying on instruments) potentially dangerous. The corrective is to utilize some of the available control power to generate moments proportional to a given motion variable and thereby correct the motion. An automatic signal is superimposed on the pilot's manual input, without directly affecting it. No signal feeds back to the controls; the pilot merely experiences the changed flying character.

Autostabilizing systems have in the past used mechanical devices integral to the rotor; typical of these are the Bell Stabilizer Bar and the Lockheed Control Gyro. Alternatively, devices may be electro-mechanical, operating on attitude or rate signals from helicopter motion sensors. Electric or electronic systems are the more flexible and multipurpose. An example is the *attitude hold* system, which returns the helicopter always to the attitude commanded, even in the disturbing environments such as gusty air. Naturally, the more the stability is augmented in this way, the greater is the attention that has to be paid to augmenting the control power remaining to the pilot. The balance is often achieved by giving the pilot direct control over the attitude datum commanded. The design of a particular system is governed by the degree of augmentation desired and the total control power available.

References

- 1 Hohenemser, K. (1939) 'Dynamic stability of a helicopter with hinged rotor blades'. *NACA Tech. Memo. 907*.
- 2 Sissingh, G.J. (1946) 'Contributions to the dynamic stability of rotary wing aircraft with articulated blades'. *Air Materiel Command Trans. F-TS-690-RE*.

Index

Bold type indicates main entries. Pages following an item should also be consulted.

- actuator disc, **5**, 16, 34, 51
- advance ratio μ , **37**, 40, 55, 66, 87, 88, 105
- aerodynamic moment, 64
- angle of incidence (attack), **24**, 57, 71, 74, 79, **84**, 123
- articulation, **2**, **40**, 80, 127
- attitude hold, 132
- autorotation, **1**, **14**
- autostabilization, **2**, **131**
- azimuth angle, **37**, 49, 53, 72, 88
- balance of forces, **63**, **117**
of moments, **117**, 119, 120
- Beddoes, T.S., **74**, 94
- Bell Stabilizer Bar, 132
- Bennett, J.A.J., **63**, 69
- Bennett, W.E., 22
- best range speed, 103, 114, 116
- blade
 - advancing, **37**, 45, 71, 76, 89, 105
 - boundary layer, 74
 - camber, 71
 - centrifugal force, 23, 42, **64**
 - dynamic stall, 74
 - element theory, **16**, **23**
 - feathering, **40**, 44, 49
 - flapping **38**, 42, 49
 - lead-lag, 40
 - loading, **16**, **17**
 - mean lift coefficient, 31
 - oscillation, 74
 - pitch, collective, **44**, 128
 - cyclic, **44**, 128
- pitching moment, 72
- pitching moment break, 74
- retreating, **37**, 45, 71, 76, 89, 105
- section design, **71**, 107
- stall, **2**, **8**, **71**, 74, 76, 105, 113
- tip shapes, 76
- twist, **27**, 29, 60, 65
- wake, **16**, 54
- Bramwell, A.S., **3**, 34, 42, 60, 65, 122, 125, 129
- Brotherhood, P., 13
- Carta, F.O., **74**, 94
- castles, 13
- ceiling, 102
- Cheesman, I.C., 22
- Cierva, Juan de la, **2**, **38**
- Clark, D.R., **20**, 22
- climb
 - in forward flight, 102
 - vertical, **9**, **97**
- coaxial rotor, 2
- cockpit view, 46
- collective pitch, *see* blade
- compound helicopter, 2
- compressibility drag, **71**, 76
- coning angle, **43**, 68
- control, **44**, **128**
 - plane, **45**
- cyclic pitch, *see* blade
- deflectors, 86
- descent, 11
- direct head moment, **118**, 120

disc loading, 7, 91
 disturbance motions, 122
 dynamic stability, *see* stability
 dynamic stall, *see* blade
 eddy flow
 helicopter fuselage, 83
 rotor, 12
 endurance, 103
 engine nacelle drag, 79
 performance, 90
 Farren, W.S., 74, 94
 feathering hinge, 40
 motion, *see* blade
 figure-of-eight diagram, 71, 87
 fixed-wing aircraft, 1, 52, 70, 76,
 83, 95, 111, 113, 125
 flapping coefficients, 43, 64, 68
 equation, 42, 64
 hinge, 38
 motion, *see* blade
 Fourier series, 43, 46
 Froude, 5
 fuselage shape parameters, 79,
 82
 gas turbine engine, 7, 70, 90
 Gessow, A., 13
 Glauert, H., 5, 22, 51, 53, 69
 glide distance, 103
 Goldstein, S., 20, 110, 116
 Gray, R.B., 19, 22
 Gustafson, 13
 Haines, A.B., 112, 116
 Ham, N.D., 74, 94
 Hefner, R.A., 21, 22
 helicopter types, 2
 H force, 60
 high altitude operation, 113
 higher harmonic control,
 example, 87
 hingeless rotor, 41, 80, 118, 124,
 127, 129

hinge offset, 41, 118
 Hoerner, S.F., 110, 116
 Hohenemser, K., 122, 132
 horizontal tailplane, 118, 123,
 129
 ideal twist, 29
 incompressible flow, 5
 induced power, 7, 21, 32, 53, 62,
 97
 velocity, 7, 13, 21, 28, 51
 inflow angle, 23
 factor, 7, 25
 inner vortex sheet, 19
 Johnson, Wayne, 3, 25, 61, 65,
 74, 94
 Jones, J.P., 1, 17, 22, 94
 Keys, C.N., 3, 79, 99, 106, 107,
 116
 Knight, M., 21, 22
 Landgrebe, A.J., 19, 22
 landing gear drag, 78, 111
 lateral cyclic, 46
 lateral (sideways) tilt, 43
 lead-lag hinge, 40
 Leiper, A.C., 20, 22
 level speed, 103
 Lilienthal, Otto, 1
 Lockheed Control Gyro, 132
 lock number, 65
 longitudinal (backward) tilt, 43
 longitudinal cyclic, 46
 Lowe, B.G., 94
 Lowson, M.V., 108, 116
 Mangler, K.W., 53, 69
 mass conservation, 5
 McCroskey, W.J., 74, 94
 momentum theory
 forward flight, 51
 vertical flight, 5
 Morel, T., 83, 94

NACA 0012 blade, 71, 75
 no-feathering axis, 47, 49
 plane, 47, 49
 non-uniform inflow, 28, 53
 offset hinge, *see* hinge offset
 optimum speeds, 103
 parachute analogy, 15
 Philippe, J.J., 76, 94
 piston engine, 7, 70
 pitch angle, *see* blade
 bearing, 40
 Pitkin, B., 117
 power (coefficient), 7, 8, 26, 32,
 61, 96, 113
 charts, 100
 induced, 7, 10, 32, 53, 61, 99
 parasite, 62, 99, 104
 profile, 8, 32, 62, 99
 Prandtl, L., 34
 Pronty, R.W., 99, 116
 range, 103, 114
 Rankine, 5
 rate damping, 128
 really-low-drag helicopter, 108
 rear-fuselage upsweep, 83
 reversed flow, 38
 roll-balanced lift, 40
 rotor blade area, 89
 blades, number of, 93
 control, 44
 design, 88
 radius, 90
 solidity, 25, 58, 90
 tip speed, 23, 89
 rotorhead drag, 79
 Saunders, G.H., 44, 50
 second harmonic, 44, 87
 Seddon, J., 83, 94
 separated flow, 12, 80, 83
 shaft normal plane, 46
 Sheehy, T.W., 80, 94
 side-by-side rotor, 2
 Sikorsky, Igor, 2
 Siss Singh, G.J., 122, 132
 Smith, R.V., 113
 specification, 95
 Squire, H.B., 53, 69
 stability
 dynamic, 125
 static and general, 121, 122
 Stepniewski, W.Z., 3, 63, 107,
 109
 Stewart, W., 87
 streamline flow, 85
 streamtube, 5, 34
 swashplate, 45
 tail rotor, 2, 97, 102, 111, 120,
 125
 tandem rotors, 2
 Theodorsen, 20
 thrust (coefficient), 1, 5, 7, 14,
 24, 27, 51, 58, 66, 88, 97
 envelope, 105
 tilt rotor, 2
 tilt wing, 2
 tip loss, 34
 path axis, 47
 plane, 44, 47
 vortex, 11, 16, 20
 torque (coefficient), 24, 61
 transmission, 3, 9, 97, 99
 Trebble, W.J.G., 94
 trim, 62, 117
 turbulent wake state, 12
 twist, *see* blade
 vertical fin, 118, 125
 vertical flight, 9, 11, 23
 vibration, 16
 vortex ring state, 11
 theory, 21
 wake, 16
 wake analysis, 20, *see also* blade
 free, 20

INDEX

- prescribed, 20
Wheatley, 34
Wiesner, R., 79, 94, 106, 116
- Wilby, P.G., 72, 76, 94
windmill brake state, 12
world speed record, 107